Injectable Bioactive Gelatin-Hyaluronan-Calcium Phosphate (GH-CP) and Its Osteogenic Potential for Flapless Guided Bone Regeneration (GBR)

Injectable Bioactive Gelatin-Hyaluronan-Calcium Phosphate (GH-CP) and Its Osteogenic Potential for Flapless Guided Bone Regeneration (GBR)

A Thesis Presented by :

Young Kwang Kim, DMD, DMSc (Candidate)

To

The Faculty of Medicine

in partial fulfillment of the requirements for the degree of

Doctor of Medial Sciences

Research Mentor:

Myron Spector, PhD

Professor of Orthopedic Surgery,

Brigham and Women′s Hospital, Harvard Medical School

Harvard School of Dental Medicine

Boston, Massachusetts

May 2019

Dedication

To my genuine passion for more knowledge and creativity.

To the sacrifices that my parents have made on my behalf.

To my one and only love, Sol, with her care, support, and patience.

To the Lord my God with his holy presence.

Acknowledgments

This thesis project could not have been achieved without the endless support and guidance from the following scholars and individuals whom I would like to express my greatest and sincere appreciation.

First, I would like to thank my research mentor, Dr. Myron Spector, for his excellent supervision throughout this thesis research project. Since the very first conversation with Dr. Spector in one of the rooms at Harvard, my passion for bone tissue engineering in the field of guided bone regeneration has become bigger, all of which ultimately led me to apply for changing my degree from the master of medical science (MMSc) to the doctor of medical science (DMSc). Your support, guidance, encouragement, wisdom, and leadership have hugely influenced and shaped my perspective for what being a respectful academician can be like. Besides academia, I still remember the moment when you said that "treat your woman with all your best" as tightly holding your beloved. You also showed me how being a true gentleman is like.

To all of my thesis examiners and committees, Dr. Shigemi Nagai, Dr. Jeffrey Michael Karp, Dr. Francesca Gori, Dr. Yefu Li, Dr. Bernard Friedland, and Dr. German O. Gallucci - thank you all for your commitment, valuable time, and great guidance throughout my thesis project. Presenting my research in front of you have been truly amazing and unforgettable moments. Looking up with your academic achievements and on-going activities, you will be my primary role models as I am going to begin a new journey as a career academician.

To my program director of the Advanced Graduate Education in Prosthodontics at Harvard, Dr. Sang J. Lee - thank you for selecting me as your very first student upon starting the program and for always believing in my sincere passion towards Prosthodontics. You portrayed such heavy roles of being a leader with dedication, responsibility, and diplomacy. No matter what happens, you are and will be my father figure in the field of Prosthodontics throughout my upcoming professional career.

To my primary clinical attending, Dr. Jason D. Lee - I can confidently say that most of my clinical concepts and skills have been taught by you. I could not have imagined going through my Prosthodontics residency without you. Your excellent clinical and documentation skills have truly motivated me to challenge my limitations, and to set my standards always high. Your humbleness and integrity have significantly influenced my growth throughout this program.

To Jae Young Kim - thank you for motivating and influencing me in the field of basic science and Prosthodontics.

To Wanting Niu, Christopher Love, and Hwan Drew Kim - thank you for kindly teaching and instructing me how to run the experiments for my research project. As a clinician, your help has absolutely supported my research experience and achievements.

To dear my fellow Prosthodontics colleagues, thank you for choosing your specialty, the same as mine. Spending hours in our lab together and always striving for providing the best to our patients, I feel confident that we have chosen the right specialty. We represent our program, and I feel proud of you becoming my life-long colleagues.

To my parents and two sisters for their support, love, and daily prayers.

To my beloved, Sol Hannah Lee - you taught me what unconditional love means. Thank you for believing in my love towards you and loving me with your whole heart. Thank you for never letting me give up. You are the most beautiful woman I have ever seen in my life.

Lastly, but not least, I glorify my Lord Father God for allowing me to continue on my path in which I have a genuine passion and fascination.

April 4th 2019

Sitting at my desk inside the closet

Boston, Massachusetts

*For this investigative work, I also appreciate such financial support by the Department of Veterans Affairs, donation of calcium phosphate particles by Geistlich Biomaterials (Geistlich, Switzerland), and gelatins by the Institute of Bioengineering and Nanotechnology and the Agency for Science, Technology and Research (A*STAR) in Singapore.*

Table of Contents

Abbreviations

Guided bone regeneration (GBR)

Bone tissue engineering (BTE)

Calcium phosphate (CP)

Gelatin-hydroxyphenylpropionic acid (Gtn-HPA)

Hyaluronic acid-tyramine (HA-Tyr)

Gelatin-Hyaluronan-Calcium Phosphate (GH-CP)

Horseradish peroxidase (HRP)

Hydrogen peroxide (H_2O_2)

Bone marrow-derived mesenchymal stem cells (bMSCs)

Osteocalcin (OCN)

Osteopontin (OPN)

Alizarin Red S (ARS)

α-smooth muscle actin (α-SMA)

Enzyme-linked immunosorbent assay (ELISA)

Recombinant platelet-derived growth factor-BB (rhPDGF-BB)

Recombinant fibroblast growth factor-2(rhFGF-2)

Cone beam computed tomography (CBCT)

Mucoperiosteal flap tension mimicking torquer (MFTMT)

Abstract

Injectable Bioactive Gelatin-Hyaluronan-Calcium Phosphate (GH-CP) and Its Osteogenic Potential for Flapless Guided Bone Regeneration (GBR)

DMSc candidate: Young Kwang Kim, DMD

Submitted to the Faculty of Medicine on May 2019 in partial fulfillment of the requirements for the degree of Doctor of Medical Sciences in Harvard School of Dental Medicine

In this contemporary era of minimally invasive surgery, injectable biomaterial scaffolds have shown their strategic potential in bone tissue engineering (BTE). Completely injectable hydrogel substratum with micro-sized bone graft particulates through a needle-shape orifice permits a new paradigm of flapless guided bone regeneration (GBR) utilizing a tunneled subperiosteal pouch concept. Although several biopolymers and their BTE applications have emerged, there is still a need for a clinically applicable delivery system; a systematic characterization of physicochemical properties; a mechanistic understanding of osteogenic cells within this biopolymer complex; and implementation of chemoattractants, all of which to construct a foundational framework for future *in vivo* investigations.

The first objective of this thesis is to design and to establish a novel injectable dual-syringe auto-mix system for providing a clinically relevant *in situ* cross-linking biopolymer hydrogel infused with osteoconductive particles. A combination of gelatin-hydroxyphenyl propionic acid (Gtn-HPA or G gel), hyaluronic acid-tyramine (HA-Tyr or H gel), the covalent cross-linking modulators of horseradish peroxidase and hydrogen peroxide, and calcium phosphate particles with different sizes (~250μm, ~175μm, and ~100μm) were investigated, with respect to content distribution, storage/compressive modulus, and swelling/expansion ratios. Another objective was to evaluate the behavior of bone marrow-derived mesenchymal stem cells (bMSCs) in the gel, including: cellular viability and morphology; proliferation (Ki67); contractility (α-smooth muscle actin, α-SMA); differentiation (osteocalcin/osteopontin, OCN/OPN); and mineralization (Alizarin Red S, ARS, staining). This work included an assessment of the chemotactic and osteogenic roles of bMSCs via incorporating rhPDGF-BB and rhFGF-2. Additionally, a translational cone beam computed tomography (CBCT) volumetric experiment of GBR in an *ex vivo* model was employed to investigate the structural integrity of the graft-host union.

Our dual-syringe auto-mix system of Gelatin-Hyaluronan-Calcium Phosphate (GH-CP) achieved an immediate *in situ* cross-linking with microscopically well-dispersed CP particles. This mechanically fine-tunable GH-CP demonstrated higher storage and compressive modulus, and reduced swelling and expansion ratios, compared to gelatin (G) and gelatin-hyaluronan (GH) gels. For viability, G and GH gels revealed highly favorable state, while H gel showed inferiority. Each gel illustrated different morphological traits of bMSCs on the G gel as mostly elongated; the H gel as mostly rounded; and the GH gel as half mixed. With no apparent differences among the three gel groups, α-SMA showed a prominent expression compared to Ki67 levels. Interestingly, GH-CP gel, as expressed with both intra- and extra-cellularly, resulted in a greater osteogenic potential of OCN/OPN levels and ARS staining compared to G and GH gels. It was also demonstrated that pre-soaking of CP particles with the chemoattractants, rhPDGF-BB/rhFGF-2, results in attachment of bMSCs, with the possibility of contact osteogenesis. The culture medium also exhibited notable effects on this *in vitro* differentiation capability. Along with the aforementioned cellular outcomes, our *ex vivo* volumetric CBCT analysis also revealed structural integrity of GH-CP over the conventional calcium phosphate. Consequently, these findings provide *in vitro* physicochemical and osteogenic support for GH-CP to be utilized in such flapless GBR surgical arena with its further potentials in incorporating diverse pharmacotherapeutics.

Thesis mentor: Myron Spector, PhD
Title: Professor of Orthopedic Surgery (Biomaterials), Harvard Medical School
Senior Lecturer, Massachusetts Institute of Technology
Director, Tissue Engineering and Regenerative Medicine Lab, VA Boston Healthcare System

Keywords : gelatin, hyaluronan, hydrogel, calcium phosphate, osteogenesis, guided bone regeneration

Chapter 1 - Introduction

Minimally invasive surgery has become a current trend in medicine. Particularly, in the field of soft and hard tissue augmentation, minimal mucoperiosteal access [1] and tunneling approach of periosteum detachment [2] have been widely utilized by many clinicians due to a myriad of benefits such as less swelling, fast healing, and fully intact surrounding mucoperiosteal architecture. This such closed environment allows maximal potential in stem cell nourishment, neovascularization, and therefore better osteogenesis.

Guided bone regeneration (GBR), which has been originated from guided tissue regeneration (GTR), shares the same bioengineering concept of blocking the infiltration of epithelial and fibroblastic cells to the defect site via a barrier membrane during the endosteal or periosteal wound healing. Since the stability of host-graft union is one of the most critical components in augmentation success [3], various efforts have been applied such as mixing [4] or layering [5] different graft materials in a hope of achieving structural integrity. For these conventional GBR methods, periosteal releasing incisions with multiple mattress sutures are necessary to achieve sufficient flap tissue release and structural integrity for primary wound closure. Subsequently, sub-periosteal pouch concept utilizing an internal tunneling detachment of periosteum [2, 6] without raising any flaps has become popular through getting the structural integrity from fully intact surrounding mucoperiosteal tension with no auxiliary stabilizing sutures nor barrier membranes. These aforementioned tunneling concepts utilize recombinant platelet-derived growth factor-BB (rhPDGF-BB) for its chemotactic recruitment, proliferation, and differentiation of periosteal stem cells as well as inducible osteogenic progenitor cells. PDGF-BB, as one of the most abundant chemoattractants in the platelet-rich plasma (PRP), is now approved by the US Food and Drug Administration with beta-tricalcium phosphate as a product called Gem 21S (BioMimetic Therapeutics), yet it is still a cement-type delivering method. A wide array of calcium phosphate (CP) bone graft substitute materials in particulate form are currently being employed in the clinic to facilitate bone regeneration in many types of oral and maxillofacial defects. Unmet applications of such materials are the treatments of incompletely-contained defects and defects in patients with a condition that impairs bone formation. As of now, there are no such truly injectable bone graft materials through a needle-like orifice.

As mentioned briefly, chemoattractants have been also shown to enhance the attraction, mitogenesis, and differentiation of pluripotent stem cells. In the field of GBR, bone conditioned medium (BCM) [7, 8], containing a cocktail of released chemoattractants from autogenous bone chips, has been characterized and employed as a pre-soaking substratum for bone graft application. However, due to relatively fast physiologic dissolving or dissipation of the provisional matrix during wound healing, the efficacy of this pre-soaking application as combined moieties is questionable.

Our proposed solution is to employ a gelatin-hyaluronan (Gtn-HA)-based matrix as the binder for the CP particles. The novel feature of the Gtn and HA that we are employing — Gtn conjugated with hydroxyphenyl propionic acid (HPA) and HA-conjugated with tyramine (Tyr) — is that they undergo covalent cross-linking *in vivo* after being injected in a liquid form. The benefits of Gtn-HA (GH) mixture are: 1) it enables the use of CP particles of a smaller diameter than normally employed, providing for a truly injectable material; 2) it retains the particles at the implant site until new bone has bridged the particles; and 3) it serves as an effective delivery vehicle for osteogenic agents such as chemoattracting growth factors and stem cells, thus improving the quality of osteogenesis.

The overall goal of this thesis is to develop a clinically, mechanically, and cellularly favorable injection system of CP particles-infused hydrogel with chemoattractants through a needle-like orifice, along with covalent cross-linkers which can fine-tune the gelation speed and structural stiffness. Each component of different gel complexes, osteoconductive CP particles, and osteoinductive growth factors (Fig. 1-1) have been sequentially added for the purpose of formulating experimental groups to investigate individual component's roles separately. Goat bone-marrow derived stem cells (bMSCs) are utilized for the investigative purpose of osteogenic differentiation, although it may or may not be incorporated as an osteogenic factor within the gel composite system for the future possible application with further stem cell technology.

Chapter 2 illustrates the background, foundational knowledge, and the motivation of this thesis.

Chapter 3 characterizes a comprehensive process of developing a dual-syringe auto-mix injectable system for gelatin-hyaluronan-calcium phosphate (GH-CP). Physicochemical properties have been investigated to outline the gelation time, storage modulus, compression strength, elastic modulus, and swelling/expansion ratios of each gel group.

Chapter 4 examines the cellular viability of bone marrow-derived mesenchymal stem cells (bMSCs) and its osteogenic proliferation (Ki67), contractility (α-smooth muscle actin, α-SMA), differentiation (osteocalcin/osteopontin, OCN/OPN), and mineralization (Alizarin Red S, ARS, staining) within GH-CP.

Chapter 5 assesses the potential migrative and osteogenic roles of chemoattractants (recombinant platelet-derived growth factor-BB or rhPDGF-BB; and recombinant fibroblast growth factor-2 or rhFGF-2) on GH-CP, in addition to validating a current clinical concept of pre-soaking for the bone graft particulates.

Chapter 6 directly compares the volumetric deformation of GH-CP with conventional CP under a physiologic mucoperiosteal tension of primary wound closure via a new cone beam computed tomography (CBCT) methodology.

Chapter 7 elaborates the possible limitations and future directions from this thesis.

Chapter 8 outlines the conclusive statements from attained results and insights of this thesis.

Chapter 9 lists figures and tables.

Chapter 10 is a collection of references.

Chapter 2 - Background and motivation

2.1. Principles of osteogenesis

Upon the tremendous increase of utilizing endosseous implants in dentistry, adjunct bone augmentations have gained its popularity in the oral-maxillofacial regions [9]. Autogenous bone graft has been a golden standard [10] due to its safety from any potential disease transmission [11]. **Osteogenesis** is defined as such condition of containing osteoprogenitor cells directly from host bone or grafting material [12], and only applicable with autogenous bone graft [12] as of now. **Osteoinduction** describes the signaling induction cascade of undifferentiated pluripotent stem cells getting differentiated into osteoblast-like cells through the presence of chemoattractants or signaling molecules [9]. Although human platelet-rich plasma (PRP) contains a cocktail of various growth factors [13], recombinant platelet-derived growth factor-BB (i.e. rhPDGF-BB) is by far the only FDA-approved chemoattractant in dental market [14], yet other growth factors have been actively investigated in the field of research science. Through such an osteoinductive signal cascade, the graft-host union is known to proceed into a process of endochondral ossification [11]. **Osteoconduction** means that implanted scaffolds, whether endosseous fixtures or bone graft materials, attracts a chemotactic migration of osteogenic cells followed by neovascularization through the extracellular fluid and non-collagenous proteins within the provisional peri-implant blood clot matrix [15]. By definition, bone formation is not possible through only osteoconductive modality [16].

Similar to any type of physiologic mechanisms, endosseous or periosteal wound healing process occurs with several steps as inflammation, proliferation, and maturation, sequentially. Davies *et al* have described a specific cascade of *de novo* bone formation with constructive steps [17] as 1) osteogenic cells excreting collagen-free bone matrix proteins such as osteopontin and bone sialoprotein; 2) these organic matrices initiating calcium phosphate nucleation for further mineralization; 3) crystallization of elongated calcium phosphates followed by assembly of collagen fibers; 4) each collagen fibril's calcification process amongst collagen free calcified layers with non-collagen proteins. As the implant surface textures have been improved from hydrophobic to hydrophilic, immediate chemotactic attachment of osteogenic cells has been feasible before *de novo* bone formation, as establishing different elaborative terminologies like contact/distance osteogenesis, or CO/DO [18]; CO describes osteogenesis from the implanted material's surface, whereas DO begins its osteogenesis from the surrounding bone surface

towards the implanted material's surface. DO occurs with machined surface fixtures or within less vascular cortical bones, while CO likely happens with modern hydrophilic implants or within marrow-rich cancellous bones.

2.2. Bone graft materials

The golden standard autogenous bone graft has been recapitulated due to its donor site morbidity, limited volumetric quantity, risks of iatrogenic complications, and high resorption rate [19] through the consideration of other grafting material options.

As an initial alternative, the allograft is introduced via getting harvested from the same species [20], along with its numerous configurations and forms [3]. **Fresh-frozen allograft (FFA)** is acquired from a same-species donor going through a total hip replacement or through a cadaveric source, which provides better incorporation with neovascularization [21] and physiologic resorption [22]. However, FFA has been avoided by the majority of clinicians due to its potential risk of disease transmission, particularly, the immunosuppression issues [23]. As a result, **freeze-dried bone allograft (FDBA)** has been available with its convenient storage property [3] and more reliable safety status as alleviating the risk of potential disease transmission or immune reactions [24]. However, freeze-drying characterization process destroys the bone cells and denatures the remnant organic matrix within the graft, eliminating its osteoinductive trait, and therefore becoming only osteoconductive [20]. This drying process also decreases the physical rigidity of the graft and less vascularizing, compared to autogenous bone grafts [21]. **Demineralized freeze-dried bone allograft (DFDBA)**, via chemical treatment of hydrochloric acid, enhances both osteoinductive and osteoconductive potentials, with more exposure of bone morphogenic proteins and copious collagen matrix, respectively [25]. A reported study states that DFDBA produces more new bone formation in the sub-sinusal space, compared to anorganic xenograft [26], yet a major disadvantage of DFDBA is structural integrity and difficult handling, as well as still existing possible disease transmission [20]. Some reported investigations insist that there is no significant superiority of DFDBA [27] but rather describe it as nothing more than weak osteoconductive material [28].

Xenograft, harvested from a different species [12], are either coral, porcine or bovine-derived [29]. Bovine hydroxyapatite is the most heavily and widely investigated xenograft due to its excellent osteoconductivity [30], with its three commercially available forms as 1) unsintered with organic matrix; 2) unsintered and deproteinized; 3) sintered and deproteinized (Osteograf-

NTM, CeraMed Co, Denver, CO & Endobon™ Merck Co, Darmstadt, Germany) [31]. Out of these three products, the unsintered and deproteinized form (Bio-Oss®, Geistlich Biomaterials, Geistlich, Switzerland) is the most widely utilized bovine hydroxyapatite due to its less crystalline and small structural sizes with its better resorptive and incorporative properties on the host tissues. Removed organic matrix via the deproteinization secures its biocompatibility with the minimal immune response [32]. However, some studies declare the inferiority of bovine hydroxyapatite [33] with minimal new bone formation [34] due to lack of proper physiologic resorption [35–37].

Alloplast has a completely synthetic production capability and favorable osteoconductivity [20], with its derivatives as calcium phosphate and calcium sulfate cement. Alloplasts get sintered through high temperature while gaining its crystalline structures [20]. Most common alloplastic ceramics are synthetic hydroxyapatite, which has slow resorption rates due to high crystalline structures, and β-tricalcium phosphates [11] which has good osteoconductivity [38] but relatively fast resorption rate [39].

Above all, since all of the currently available bone graft particulates have pros and cons, a combinational therapeutic approach is getting its attention amongst clinicians and researchers as a new trend of bone graft modality.

2.3. Guided bone regeneration (GBR)

In the field of implant dentistry, GBR technique, which is derived from guided tissue regeneration (GTR), has emerged with its bioengineering concept as blocking the ingrowth of infiltrating epithelial cells or fibroblastic cells from the exposed connective tissue towards the osteogenic site before proliferating osteoprogenitor cells undergoing osteogenesis (Dahlin, *et al.,* 1989), through biocompatible barrier membranes [40]. Besides the role of blocking, barrier membranes also serve as maintaining the volumetric space with structural integrity, which is one of the most critical factors in bone augmentation success [3]. At a real surgical arena of ridge augmentation, especially with surrounding movable musculoskeletal apparatus, barrier membrane itself may not necessarily provide a sufficient structural support. Therefore, the utilization of bone graft materials to prevent volumetric collapse has been established in the name of GBR [41].

Further rigidity of bone-graft union is achieved by various technique-sensitive surgical methods such as relieving incisions and multiple sutures for idealizing tissue tension and

stabilization, respectively. To improve such structural integrity and osteogenic potential, autogenous bone chips are first layered to the defect site followed by covering with more rigid anorganic bovine bone minerals [5], which is known as 'sandwich technique.' Urban *et al* have invented so-called 'sausage technique' via mixing these osteogenic and fast-resorptive autogenous bone chips with deproteinized bovine hydroxyapatites as 1:1 ratio, along with tacking screws to nicely intact resorbable collagen membrane on the cortical bone surface [4]. Some clinicians even utilize the application of protein sealant to the grafted union for better structural integrity, yet it has been shown to retard new bone formation [42].

Following the current minimally invasive surgical trend in medicine, a tunneling technique (i.e. without any flap opening) of mucogingival surgical procedures has gained its popularity amongst clinicians due to less swelling and fast healing [1]. Hard tissue augmentation with incorporation of rhPDGF-BB has also been attempted via this tunneling technique and shown predictable osteogenic regeneration outcomes both clinically, radiographically, and histologically [2, 6].

Along with this supportive evidence of already established surgical techniques and concepts of tunneling route, our thesis proposes a flapless GBR technique where a clinician can access through a small access hole above the mucogingival junction with selectively detaching the intact periosteum to create a subperiosteal pouch (Fig. 3-1B & Fig. 6-5A). Then, if it becomes possible to inject the bone graft materials through a needle shape orifice, a simple injection directly on top of the keratinized tissue of alveolar mucosa can complete the ridge augmentation GBR procedure in few seconds with no utilization of flaps or sutures. This innovative delivery system may not be limited to the field of GBR of pre-edentulous ridge augmentation, but also expand its potential applications in various other clinical scenarios such as tissue repositioning recession treatments, periodontal defects, peri-implantitis, socket preservation, immediate placement, sub-sinusal augmentation, etc.

2.4. Bone tissue engineering (BTE)

As of now, there is no currently merchandised product of purely injectable bone graft materials enabling its transfer through a needle-shape orifice. This so-called thixotropic injection is technically only possible with micro-sized bone graft particulates as being dispersed in such viscoelastic substratum. Currently available injectable products in the market are either through a syringe-size orifice plunging system with conventional graft particulates (Bio-Oss Pen®,

Geistlich Biomaterials, Geistlich, Switzerland) or only protein infused gels (Emdogain®, Straumann, Switzerland). Combinational therapeutic modality seems challenging in its merchandising since the FDA approval process evaluates each component separately along with unequal regulations amongst different countries. Recombinant platelet-derived growth factor-BB (rhPDGF-BB), along with β-tricalcium phosphate as a paste mixing modality (GEM 21S, BioMimetic Therapeutics), is by far the only FDA-approved combinational bone grafting product tailored in a periodontal defect, yet it is still not injectable.

As GEM 21S has emerged to the field of BTE, utilization of chemoattractant has gotten its attention in GBR as well. Particularly, within the tunneled subperiosteal pouch, bone graft materials with GEM 21S has excluded conventional barrier membranes [2] to recruit inducible osteoprogenitor cells and periosteal-derived mesenchymal stem cells (MSCs) from the periosteum. Periosteal-derived MSCs are known with greater osteogenic potential compared to bone-marrow-derived MSCs [43, 44], which builds a foundational rationale towards predictable subperiosteal pouch flapless GBR concept (See 2.3.).

Bone conditioned medium (BCM) [7, 8], containing the released chemoattractant from autogenous bone chips, has been introduced and applied as a pre-soaking modality in recent BTE of implant dentistry. However, due to relatively fast physiologic dissolving or dissipation of the provisional matrix during wound healing, the efficacy of this pre-soaking application as combined moieties is unknown.

Unlike clinical merchandise products, in the field of research science, various combinational BTE injectable materials have been actively investigated. Particularly, hydrogels mixed with hydroxyapatites (HAs) have enhanced the mechanical strength as well as mineralization [47]. Nano-HA/glyco chitosan/hyaluronic acid composite cement has shown its injectability [51]. An alginate-based scaffold with β-tricalcium phosphate beads has also demonstrated its novel injectable applicability in BTE followed by successful subcutaneous *in vivo* osteogenic differentiation [49]. Gelatin-based microparticles infused with hydrogel, formulating N-isopropylacrylamide/gelatin microparticle-composite, have enhanced bony bridging and mineralization with maximized surface area contact [46]. A methoxy polyethylene glycol-b-polycaprolactone block copolymer based injectable hydrogel has also shown a favorable osteogenic expressions of osteonectin, osteopontin, and osteocalcin [45]. A citric acid-based bioinert PEG maleate citrate/HA composite has shown its *in situ* cross-linking trait [50]. Another calcium silicate infused alginate has shown its favorable osteogenic adhesion,

proliferation, and differentiation, followed by angiogenesis as well [52]. A thermosensitive sol-gel-sol copolymer infused with collagen and nanohydroxyapatite has also been developed [48]. Physical interactions of thermosensitive chitosan-base hydrogel with β-tricalcium phosphate has also been demonstrated [53]. A recent study has combined two scaffolds as HA and gelatin microspheres inside alginate [54].

As illustrated above, many particles infused hydrogel systems have been investigated and successfully demonstrated its injectability, yet incorporation of chemoattractant in such systems has been rarely studied. Further, in spite of these studies' reported osteogenic differentiation with bone markers and level differences, distributional analysis of expressions within gel complex have been missing. Therefore, this thesis has focused more on the migration potential of infused cells inside gel complexes in the hope of investigating its directional cues in osteogenesis (Chapter 5).

Chapter 3 - Injectable dual-syringe model for gelatin-hyaluronan-calcium phosphate (GH-CP)

3.1. Introduction

In a supreme coalescence of the modern surgical trend in minimal invasiveness and the excellent improvement in material science, hydrogels have emerged in the field of bone tissue engineering (BTE) for the last few decades. These viscoelastic biopolymer gels are injectable through a syringe into a defect site, followed by undergoing either *in situ* gelation or polymerization throughout molecular ionic or covalent interactions in the aqueous precursor. This cross-linking chemical process allows the gels to become sufficiently flowable, enabling firm adherence to the irregular defect sites, which creates a desirable architectural union for tissue regeneration in both biological and physical point of view. Within their high water-content matrix, hydrogels have a superior permeability status with organic fuels such as oxygen, nutrients, and other critical metabolites, setting a preferred cellular environment for its proliferation, migration, and differentiation. In the field of bone tissue engineering (BTE), many currently available gel systems incorporated with high concentrations of osteoconductive scaffolds (mostly calcium phosphates) exist as more like cement, not as a truly injectable substratum due to its primary concern of mechanical stability.

3.2. Objective, hypothesis, aims, and rationale

The **objective** of the investigative work illustrated in this chapter is to establish an injectable dual-syringe auto-mix system for gelatin-hyaluronan-calcium phosphate (GH-CP) with favorable clinical handling properties (i.e., flowability and immediate gelation). Specifically, incorporation of gelatin-hydroxyphenyl propionic acid (Gtn-HPA), hyaluronic acid-tyramine (HA-Tyr), and calcium phosphates are analyzed via testing three different sequential gel combinations as:

1. Gelatin group: “G”
2. Gelatin-hyaluronan group: “GH”
3. Gelatin-hyaluronan-calcium phosphate group: “GH-CP”

Our **primary hypothesis** is that immediate gelation with a well-distribution of intra-gel contents coming out of a dual-syringe auto-mix system is repeatably achievable regardless of

particle sizes, orifice tip sizes, as well as different gel combinations. A **second hypothesis** is that the addition of CP particles formulates more favorable physical properties on GH-CP gel for a clinical GBR environment.

The **specific aims** are to: 1) reveal the gelation time and storage modulus of the three gel groups; 2) determine the compression strength and modulus of elasticity of the three gel groups; 3) assess the swelling and expansion ratio of the three gel groups.

Different sizes of CP particles (~250μm, ~175μm, and ~100μm) are initially investigated to primarily idealize the microscopic view for the experimental status of next chapters. The physical characteristics of the gel groups are based on rheological behavior (gelation time and shear storage modulus), mechanical properties (compressive modulus), swelling and expansion ratio. These parameters portray a comparative outline of gel compositions upon specific tissue engineering applications at a surgical arena. The maximum intra-oral flap tension in primary wound closure of the mucoperiosteal flaps, which is on the range of .15~.2N [55] or approximately 2500 pascals under the diameter of 8mm, has been referenced as a clinical comparative component.

This chapter's study guides to a direct comparison between three types of gel compositions via subsequent additions of different materials with its final heterogenous combined group as GH-CP. During the pilot optimization experiments, in spite of biologically favorable aspects of Gtn-HPA, calcium phosphate sedimentation phenomenon, leading to a clogging issue at the tip of a pipette, was observed with Gtn-HPA even with increased wt. % (Fig. 3-3 A & B). This incident led to our initial insight of utilizing HA-Tyr as a pre-gelated carrier medium, successfully dissipating CP particles before cross-linking (Fig. 3-8 B). Simultaneously, designing a dual-syringe auto-mix model system was initiated, followed by prototype developments (Fig. 3-4 A~D). This study is the very first to develop a dual-syringe auto-mix model system for gelatin-hyaluronan gel combinations mixed with osteoconductive CP particles in terms of product development, enabling a complete injectability through a needle shape orifice. This study is also the first to fine-tune the distribution in such ideal microscopic view of the ingredients of gel composites. Lastly, it is the first study in delineating the mechanical profile of GH-CP via the sequential addition of components for creating the experimental groups.

3.3. Materials and methods

3.3.1. Development of the injectable dual-syringe auto-mix system for immediate gelation

3.3.1.1. Gelatin-hydroxyphenyl propionic (Gtn-HPA) acid hydrogel

Gelatin conjugated with HPA was donated by the Institute of Bioengineering and Nanotechnology (Singapore). Initially, Gtn-HPA conjugates were manufactured by a general carbodimide/active ester-mediated coupling reaction [56, 57]. The portion of amine groups of gelatin within HPA, referred to as a degree of conjugation, was circumscribed by the standard 2,4,6-trinitrobenzene sulfonic acid (TNBS) process [58] to be 90%.

3.3.1.2. Hyaluronic acid-Tyramine (HA-Tyr) hydrogel

Synthesis of HA-Tyr conjugates was done as illustrated previously and the substitution degree, referring the number of tyramine molecules per 100 repeating units of HA, was six as determined by 1H NMR [59, 60].

3.3.1.3. Covalent cross-linking

Applying horseradish peroxidase (HRP; stock concentration as 25 unit/mL; Wako Chemical USA, Richmond, VA, USA) and H_2O_2 (stock concentration as 9.7M; Sigma- Aldrich) as the vital reaction enzymes, both Gtn-HPA and HA-Tyr conjugates become covalently cross-linked throughout the moieties of oxidative reaction.

3.3.1.4. Calcium phosphate particles

Pre-filtered different sizes (~100μm, ~175μm, and ~250μm) of calcium phosphate particles were donated for this particular study (Geistlich Pharma, Wolhusen, Switzerland) (Fig. 3-2). 10% (w/v) of CP particles was used for all of the gel castings due to its optimal mechanical, degradation, and cell proliferation properties within the gel composite [61].

3.3.1.5. Dual-syringe auto-mix system

To initiate an immediate cross-linking gelation process right before coming out of the tip, a double-barrel dual syringe system was designed (Fig. 3-4 A). Several prototypes were initially trialed to come up with the ideal distribution of components into each barrel syringe (Fig. 3-4 B~D), followed by fine-tuning the concentrations of HRP and H_2O_2 (Fig. 3-4 E~H) to compose favorable structural integrity and gelation speed of GH-CP. Lyophilized Gtn–HPA and HA-Tyr

were dissolved in phosphate-buffered solution (PBS) at a concentration of 8 wt% and 4 wt% accordingly, followed by loading on each syringe of the system. Prior to loading both gels into the dual-syringe auto-mix system, thermal gelation of the gels was completed inside the warm 37°C incubator for 1 hour. Along with pre-measured 10mg of CP particles, a volume of 20 µL of HRP (giving a final target concentration of 0.5 unit/mL) was stored in one side of the syringes consisting 500µL of HA-Tyr. 10µL of H_2O_2 is stored in another syringe containing 500µL of Gtn-HPA, giving a final target concentration of 6.8mM. Immediate cross-linking was initiated as those two gels getting thoroughly mixed while flowing out through the dual-syringe auto-mix tip (Fig. 3-8 C). For any cell containing gels, the gel preparations were done in culture medium.

3.3.2. Indirect gel cast fabrication

Indirect gel casts were fabricated through a syringe molds preparation method (Fig. 3-8 D). 75% reagent alcohol wiped parafilm was cut into 1.5cm x 1.5cm pieces and stored in a dish in the cell culture hood overnight with UV light on. Syringe sections were also soaked with 75% reagent alcohol for 30 minutes, followed by rinsing with sterile H_2O and natural drying in the cell culture room. Then, one side of the syringe section was sealed with 1.5cm x 1.5cm parafilm as a mold. Cross-linking gelation was completed within this tube at 21°C, followed by careful removal to be used for specific experiments. The expected total volume of this casted cylinder gel was approximately 250µL with 8-9mm diameter and 3-4mm height.

3.3.3. Rheology testing

A TA instruments AR-G2 rheometer using parallel plate geometry (20mm diameter) was used to get rheological measurements (Fig. 3-9 A). A linear viscoelastic regime of the gelled materials was maintained along with the aforementioned set-up conditions. Evaporation was avoided by applying a layer of silicone oil. All measurements were recorded at 37°C in the oscillation mode with a constant strain of 1% and a frequency of 1 Hz (Fig. 3-9 B).

3.3.4. Unconfined compression testing

A Zwick/Roell Z2.5 static materials tester (Zwick GmbH & Co., Ulm, Germany) and integrated testing software (testXpert, Zwick) were used for the purpose of unconfined compression test. Soluble gel volumes of 250µL were cast in 32-well plates to create samples

6mm in diameter and 3-4mm in thickness. Before compression testing, the gels were cross-linked and swelled in PBS for 1 hour.

Compression tests were conducted at a fixed strain rate of 0.5%/s to the highest strain of 10%, and back to 0, using a 20N load cell (Part No. BTC-LC0020N.P01, Zwick) with a sampling frequency of 2Hz at 37°C (Fig. 3-10 A). The diameter of the cast samples was measured with digital calipers. For some samples, Teflon tapes were utilized to prevent adhesion of the samples to the machine. The elastic modulus of compression was decided by the slope of the true stress-strain curve within the linear regime of the material, which is within 0~15% (Figure 3-10 E).

3.3.5. Swelling ratio

Indirect gel casts (250μL, 8-9mm diameter, and 3-4mm height) were stored in PBS for 7 days at 37°C for allowing swelling. Tweezers were utilized for a gentle scooping motion to protect the gels' structures. The weight of freshly made gels and swollen gels were recorded as W_0 and W_1, respectively. The swelling ratio was derived using the following equation:

$$Swelling\ Ratio = | W_0 - W_1 | / W_0 * 100\%$$

3.3.6. Expansion ratio

The volume of 250μL gels was cast through dispensing to the bottom of cryotubes to maximize the surrounding structural frame as consistent as possible amongst experimental groups (Fig. 3-12 A), followed by filling 500μL of PBS on top of the cross-linked gels for 7 days for maximizing its water absorption at 37°C. The shape of the casted gels was in hemisphere shape due to the base of cryotube's design. An impression of vinyl polysiloxane (VPS) (Fig. 3-12 B) was first made and became an initial reference volume (E_0) for the calculation. The rest of the experimental cast gels were carefully scooped out from each cryotube, followed by diameter measurements to calculate the expanded volume (E_1) (Fig. 3-12 B). The volume of hemisphere and expansion ratio were derived using the following equation:

$$\text{Hemisphere volume (E)} = (2 / 3)\ \pi\ r^3$$

$$Expansion\ ratio = E_1/E_0 * 100\%$$

3.3.7. Statistics

Data in this chapter are described as mean ± standard deviation, standard error, or min & max. Statistical significance was examined by unpaired t-test, or one- / two-way analysis of variance (ANOVA). In such cases of significance in ANOVA, Tukey's post-hoc multiple comparison tests were run with a significance criterion of $p < 0.05$ using GraphPad Prism 7 (GraphPad Software, Inc., CA, USA).

3.4. Results

3.4.1. Pre-gelation sedimentation of CP particles

All sizes of calcium phosphate (CP) particles (~100μm, ~175μm, and ~250μm) demonstrated a sedimentation phenomenon within Gtn-HPA 12%, 8 wt%, 4 wt%, and 2 wt% (Fig. 3-3 A), causing a clogging issue at the pipette tip or injection tip (Fig. 3-3 B).

Using 10mg of CP particles dispersed in pre-gelated 500μL of Gtn-HPA or HA-Tyr, it was observed that once 1/10 of CP particles sink vertically, as C/G becoming less than 0.9 (Fig. 3-3 B), injection became impossible through a 1mL pipette tip due to clogging. Considering that, in a realistic clinical setting, the approximate minimum time necessary for adequately positioning and aiming the tip towards the defect is around 2-3 seconds, an inclusion criterion (yes or no) of C/G being greater than 0.9 at the time point of 3 seconds was created. It turned out that all of Gtn-HPA 8 wt% was ‘no’, while all of HA-Tyr 4% was ‘yes’ (n=6) (Fig. 3-3 C).

CP particles in Gtn-HPA 8 wt% and HA-Tyr 4 wt% completely sedimented after 49.71 ± 2.296 seconds and 221.4 ± 5.756 seconds (n=7, mean ± S.E.), respectively (Fig. 3-5 A & B).

3.4.2. Immediate gelation of GH-CP with ideal microscopic distribution of CP particles and bMSCs

All sizes of calcium phosphate (CP) particles (~250μm, ~175μm, and ~100μm) were able to get dispensed out of either an auto-mix tip or 1mL pipette tip, followed by *in situ* immediate gelation process. All of the sizes of CP particles within the cross-linked gel matrices were well-dispersed. Different magnification levels of (1X, 10X, and 30X) microscopic views were utilized to visualize and compare the magnitude of gap distances between CP particles (Fig. 3-6).

Then, different tip sizes of the dual-syringe auto-mix model (small orifice diameter = 900μm; large orifice diameter = 2mm) with 175μm CP particles and bone-marrow derived

mesenchymal stem cells (bMSCs) were investigated to compare the inter-particle and inter-cellular distances of cross-linked GH-CP, which turned out to be statistically non-significant (n=4, p-value > 0.05). All of the contents in GH-CP were visually well-distributed (Fig. 3-7 A & B) throughout the microscope. Two-factor ANOVA showed no significant effect of different orifices of auto-mix tips (i.e., small and large orifice) on the distribution of contents within the gel (i.e. CP particles and bMSCs) (P = 0.3194). Inter-cellular distance and inter-particle distances through a small orifice auto-mix tip were 65.2 ± 11.6μm and 57.5 ± 14.3μm (n=4, mean ± S.D.), respectively, while through a large orifice auto-mix tip, they were 63.8 ± 10.4μm and 66.7 ± 13.6μm (n=4, mean ± S.D.), respectively (Fig. 3-7 C).

3.4.3. Rheological behavior of gels

Oscillation rheometer, measuring the storage (G') and loss moduli (G") in terms of shear strain, was utilized to examine the dynamic cross-linking process of gelatin (G), gelatin-hyaluronan (GH), and gelatin-hyaluronan-calcium phosphate (GH-CP) gel combinations, as well as different calcium phosphate (CP) particles (~250μm, ~175μm, and ~100μm) with GH gel as an initial experiment. The rheological experiment method is a standardized way to analyze such thixotropic or viscoelastic materials like hydrogels. G' is, most of the times, used as expressing the level of stiffness of the testing material. Typically, a graphical crossover of G' and G" is a way to estimate the gelation rate. However, in this experiment, due to high [HRP], the gelation cross-linking was completed in few seconds, and thereby, the crossover was already passed at the start of time recording inside the rheometer.

3.4.3.1. Fine-tuning gels as increasing [HRP] and [H_2O_2]

To achieve a favorable clinical modality in GBR (i.e., fast gelation and durable stiffness), [HRP] and [H_2O_2] were fine-tuned throughout incremental increase with multiple pilot experiments. The initial starting concentrations were referenced from the previous study of our neural procedural application [62], followed by fine-tuned customization for this study's purpose.

By increasing [HRP] from .1U/mL to .5U/mL, the cross-linking graph became steeper (Figure 3-9 D), representing a faster gelation rate. Using a linear regression model, the increase of gelation rate was successfully demonstrated with statistical significance (p = 0.0057). The primary metric obtained from the rheological testing was G' at 3.6 min, reaching the plateau of completed cross-linking % (Figure 3-9 D).

By increasing [H_2O_2] from 1.2mM to 6.8mM, G' at 3.6 min had around two-fold of increase (n=6, p=.0047), suggesting higher cross-linking density (Figure 3-9 E).

3.4.3.2. Rheological behavior on different diameters of CP particles

One-factor ANOVA revealed no significant effect of different CP diameters on G' at 3.6 min (P = 0.9746). G' at 3.6 min of gelatin gel with CP sizes of 100μm, 175μm, and 250μm were 8607 ± 4304 Pa, 8369 ± 816 Pa, and 9002 ± 2118 Pa, respectively (n=3, mean ± S.D.) (Figure 3-9 F).

3.4.3.3. Rheological behavior on different gel combinations

An increase in G' at 3.6 min was observed among different gel groups (G, GH, and GH-CP), along with a statistical significance in one-factor ANOVA (p = 0.0008). Tukey's post-hoc test showed statistically significant differences between G and GH ($p < 0.05$), as well as GH and GH-CP ($p < 0.001$). Average mean values of G' at 3.6 min in G, GH, and GH-CP were 3521 ± 1162 Pa, 7569 ± 2662 Pa, and 8659 ± 2195 Pa (n=6, mean ± S.D.), respectively (Figure 3-9 G).

3.4.4. Compression testing

Unconfined compression testing was run as a different modality to assess mechanical stiffness of gel groups. Full cross-linking was secured via storing the gels in PBS for 1 hour, prior to compression testing. All of the gel groups demonstrated both elastic and plastic behavior, illustrating a variation between the nominal and true curves in stress-strain plots (Figure 3-10 D).

Upon compression, a diversion of approximately 5% was found in the nominal and true stress-strain curves, portraying that hydrogels consist of both elastic and plastic ingredients (Figure 3-10 E). For this chapter's analysis, it was assumed that all of the gel groups were elastic, followed by a calculation of the compression modulus (E) from the range of 0-15% of strain fraction from the true stress-strain curve, as producing R2 value as greater than 0.95 (Figure 3-10 E).

3.4.4.1. Compressive behavior on different diameters of CP particles

One-factor ANOVA revealed no significant effect of different CP diameters on E (P = 0.5106). E values of GH gel with CP sizes of 100μm, 175μm, and 250μm were 13502 ± 7995 Pa, 20915 ± 5503 Pa, and 15984 ± 8710 Pa, respectively (n=3, mean ± S.D.) (Figure 3-10 F).

3.4.4.2. Compression behavior on different gel combinations

A sequential increase in E was observed among different gel groups (G < GH < GH-CP), along with a statistical significance in one-factor ANOVA ($p = 0.0007$). Tukey's post-hoc test showed statistically significant differences between G and GH-CP ($p < 0.001$), as well as GH and GH-CP ($p < 0.05$). Average mean values of G' at 3.6 min in G, GH, and GH-CP were 5542 ± 2955 Pa, 9797 ± 2271 Pa, and 16800 ± 7294 Pa (n=6, mean ± S.D.), respectively (Figure 3-10 G).

3.4.5. Swelling ratio

The swelling ratio of different gel groups, stored in PBS for 7 days at 37°C, was analyzed. One-factor ANOVA showed no significant effect of different CP diameters on the swelling ratio ($P = 0.3202$). The swelling ratio of GH gel with CP sizes of 100μm, 175μm, and 250μm was 44.25 ± 8.173 %, 28.63 ± 5.306 %, and 39.84 ± 15.03 % (n=3, mean ± S.D.), respectively (Figure 3-11 A).

A statistical significance of the swelling ratio was found among different gel groups (G, GH, and GH-CP), according to one-factor ANOVA ($p = 0.0016$). Tukey's post-hoc test showed statistically significant differences between G and GH ($p < 0.01$), as well as GH and GH-CP ($p < 0.05$). Average mean values of the swelling ratio in G, GH, and GH-CP were 32.29 ± 11.07 %, 53.19 ± 8.153 %, and 38.53 ± 10.68 % (n=6, mean ± S.D.), respectively (Figure 3-11 B).

3.4.6. Expansion ratio

The expansion ratio of different gel groups, stored in PBS for 7 days at 37°C, was examined for its clinical correlation of GBR surgery. A statistical significance of the expansion ratio was observed among different gel groups (G, GH, and GH-CP), according to one-factor ANOVA ($p = 0.0003$). Tukey's post-hoc test showed statistically significant differences between G and GH ($p < 0.001$), G and GH-CP ($p < 0.05$), as well as GH and GH-CP ($p < 0.05$). Average mean values of the expansion ratio in G, GH, and GH-CP were 19.30 ± 11.70 %, 138.7 ± 47.01 %, and 80.03 ± 39.62 % (n=6, mean ± S.D.), respectively (Figure 3-12 C).

3.5. Discussion

In this chapter, three different gel groups (G, GH, GH-CP) were analyzed and assessed based on numerous physical metrics and configuration criteria. The eventual intention for this investigation of hydrogels is to accomplish future *in vivo* application. With a goal of developing a new potential and completely injectable bone grafting substratum in flapless GBR environment, characterizations of these gels were investigated through rheological and mechanical behavior (cross-linking speed and modulus), swelling and expansion properties.

3.5.1. Gtn-HPA serves as a biologically proven basic infrastructure

Due to its biologically favorable and injectable merits, many hydrogel biopolymer modalities have emerged in the field of bone tissue engineering [61, 63, 64]. Out of many kinds, physically cross-linked hydrogels are deficient of structural strength and integrity, whereas chemically cross-linked hydrogels are more superior with their covalently bonded polymerization architectures to create greater mechanical stiffness and strength. This firm chemical backbone enables a sturdy resistance to enzymatic degradation with multi-linked collagen fibrils and molecules together [65]. In the field of neurology, previously reported work from our lab has introduced Gtn-HPA as tunable biopolymer scaffold matrices where controlling the permeability, proliferation, migration, and differentiation of human mesenchymal stem cells (hMSCs) becomes possible [62]. This feasibility of mechanical adjustment originates from its oxidative coupling of HPA moieties via enzymatic catalysts of H_2O_2 and HRP with their roles in regulating the abundance of formulating cross-links (Fig. 3-9 E) and modulating the gelation speed (Fig. 3-9 D), respectively. HRP, which causes no damaging effects on cellular activity and metabolism [66], begins the chemical reaction at physiological temperature and pH, along with its tunability from varying the concentrations [56, 67].

The phenols of HPA bonds through C-C linkage between the aromatic ring's ortho-carbons or C-O linkage formed by the phenolic oxygen and ortho-carbon [68]. Gelatin consists of matrix metalloprotease (MMP)-sensitive chains, which can be catabolized by MMP releasing endothelial cells [69]. Since other proteases [70] can also degrade gelatin, Gtn-HPA biopolymer can be biodegradable in physiologic condition.

3.5.2. HA-Tyr disperses CP particles to accommodate sedimentation phenomenon

In the particle-infused matrices, a sedimentation property determines shelf stability and prevents the random orientation of particles after being adhered to the defect, which may have been viewed as causing unpredictable osteoconduction [71]. However, sedimented CP particles in post-gelated matrices may spatially limit for new mineral depositions due to its low resorption rates [36], compared to the biopolymer hydrogels with relatively faster physiologic degradation; hydroxyapatite is also known to be non-resorbable [72] in the body. Creation of rooms amongst particles with hydrophilic carrier has been turned out having more osteoconductive effect [73]. As well, in a heavily sedimented zone of CP particles, vascularization anastomosis enriching to the graft core may be compromised [74, 75]. In a pre-gelation medium, sedimentation becomes even more problematic due to clogging issue (Fig. 3-3 B), preventing proper ejection out of the syringe.

In the early pilot phase of our experiment, due to the sedimentation issue (Fig. 3-5 A), HA-Tyr was chosen for an auxiliary gel medium to carry CP particles due to its greater viscosity than Gtn-HPA while sharing the same chemical cross-linkers (Fig. 3-5 B). HA-Tyr was also developed by Kurisawa and his co-workers [59] for chondrogenesis as another well-established biopolymer system [64]. Particularly, HA-Tyr hydrogels have a distinguished effect on the spatial arrangement of inter-polymer cells, therefore, followed by systematic matrix biosynthesis and cartilage regeneration [76], turning out to be an appropriate gel substratum for our dual-syringe auto-mix injection system.

3.5.3. Consolidation of Gtn-HPA and HA-Tyr, formulating Gtn-HA (GH), creates a bioinert porous covalent mesh framework

Combining these two phenol containing polymers (gelatin and hyaluronan), along with HRP and H_2O_2, enhances covalent cross-linking to yield a porous polymerized framework (Fig. 3-8 A). Addition of HA-Tyr to Gtn-HPA seems raising both shear storage modulus (Fig 3-9 G) and compression modulus (Fig 3-10 G). Besides Gtn-HPA's osteogenic potential (See 3.5.1.), the hyaluronic acid (HA) is also known for its osteostimulative effect *in vitro* [77] and changing its concentration level affects mesenchymal cellular condensation [78]. Complete gelation occurs over time, allowing these two backbones of polymers phasing independently to the point where a discrete domain anisotropically formulates pores within the polymerized gel composite [79].

This pore formulation may be crucial for cellular attachment, migration, and differentiation within the gel matrices system [80].

3.5.4. The addition of CP particles profits both mechanical and biological traits of GH-CP.

Aiming for matching up with the surrounding anatomical environment, bone tissue engineering necessitates a mechanical strength, in which most of the current hydrogel systems are lacking. Accordingly, many techniques and strategies of increasing structural durability have been investigated and proposed such as increasing crosslinkers, monomer content, filler/fibers addition, or even pre-embedding cells to form functional tissues prior to implantation [81, 82]. An excessive level of H_2O_2 provokes potential cellular death and limited gelation process, which has been supported by many other investigations [83–85]. Elevated H_2O_2 even constricts pore diameter [60] of gel systems, which may diminish cellular cohesiveness. Besides, creating hydrogels too viscous for the purpose of improving structural integrity may potentiate the syringe system less injectable, and therefore clinically unfavorable.

Hence, for our model, structural strength is enhanced with the addition of micro-sized CP particles (~100μm, ~175μm, and ~250μm) added to GH gel biopolymers. Positively charged polymers attract negatively charged units such as carbonate and phosphate [86], as well as potential chemoattractants [87] (Chapter 5). Vice versa, negatively charged carboxyl groups join with calcium ions, directing mineral nucleation and propagation [88, 89]. CP-bearing matrices strengthens mechanical properties [61] and also improve the osteogenic differentiation of hMSCs through adenosine signaling [90] (Chapter 4). Our pilot experiments showed that 40 w/v% CP demonstrated an unfavorable condition of proper injection, in which other studies also support that it creates such a solid-like performance in the hydrogel [91]. Consequently, for our system of GH-CP, 10 w/v% CP was utilized due to its pre-established investigation of a superior mechanical trait, drug delivery, swelling, and ideal degradation rate, followed by refined cell proliferation [61]. 10 w/v% CP also produced an excellent condition of microscopic view for the rest of further experiments in terms of component distribution (Fig. 3-6).

3.5.5. The dual-syringe auto-mix system enables homogenetic mixing in immediate gelation setting.

Utilization of hydrogel biopolymers brings several benefits as: 1) facilitating injection; 2) *in situ* implantation; 3) preventing dispersion of particles. Particularly, fabricating a cross-linked

cast with well-dissipated particles is critical to maximize the spatial efficiency of contact osteogenesis for new mineral depositions. The process of mixing plays a significant role in dictating hydrogel's homogeneity and mechanical strength [92, 93]. Inconsistent mixing often produces inhomogeneous regions [94], which ultimately affects cell behavior [95, 96]. During the optimization phase, the addition of HA-Tyr to our modality has spontaneously brought an insight into developing the dual-syringe auto-mix system (Fig. 3-4 A~D), with an auto-mix tip (Fig. 3-8 C), turning out to be an excellent armamentarium for homogenetic mixing in gelation and persistent mechanical stability. Throughout this dual-syringe auto-mix system, it has been possible to fabricate GH-CP being well-dispersed with CP particles, ideally optimized for the following experiments in the next chapters (Fig. 3-6). Furthermore, the utilization of different orifice sizes of auto-mix tips has no significant difference in the orientation of spread out CP particles and bMSCs (Fig. 3-7 C), which opens up its applicability to a wide array of clinical situations (i.e., subperiosteal closed-flap tunneling approach, open-flap bone augmentation or socket preservation environment, etc).

3.5.6. Rheological behavior of cross-linking GH-CP is favorable in guided bone regeneration.

Since immediate physical dynamics of the cross-linking hydrogels is pivotal both in mechanical and biological viewpoint, *in situ* rheology was evaluated. The adjustability of gelation time by [HRP] and the stiffness strength by [H_2O_2] [97] directed us to begin with fine-tuning GH-CP (Fig. 3-9 D) up to the point where complete cross-linking is achieved within 1 min after the ejection through a dual syringe auto-mix tip. This so-called "maturation time" is essential in a way that the gelation process should be slow enough to fully adapt to the irregular shapes of defects and, at the same time, fast enough to generate such cross-linked gels with well-dissipated CP particles inside. Clinically speaking, the shorter, the better for both clinicians and patients in terms of maximizing efficiency and comfort. Overall, adjustable gelation time also means more flexibility at a surgical arena; for instance, different anatomical regions and defect shapes of surgical sites may require various levels of gelation time. For our modality, [H_2O_2] is also fine-adjusted in a way to achieve greater G' (Fig. 3-9 E) to set the initial reference as high as possible within the acceptable range of our pilot study experiments. Manipulatable modulus also indicates a more favorable GBR surgical procedure in terms of retaining the graft materials *in situ*.

Looking at its aforementioned properties, rheological behavior of GH-CP seems highly correlated with one of the basic augmentation rationales, the stability of graft-host union [3]. The different diameter of CP particles seems to have no influence on G' (Fig. 3-9 F), meaning that variations of the syringe packages may be merchandized depending on the defect sizes or resorption preferences customized for each clinician's specific treatment plan of procedures (i.e. endosseous implant placements, loading prosthesis, etc). On the other hand, the storage modulus (G') of the matrices increases as combining two gels together, and even more significantly with the addition of CP particles (Fig. 3-9 G). In a clinical setting, besides enhancing contact osteogenesis [18] with added CP particles as osteoconductive scaffolds, this elevation of storage modulus offers structurally firm initial architecture where technique-sensitive adjunct procedures such as stabilizing mattress sutures or barrier membranes may no longer be necessary, reducing the surgical complexity drastically.

Further, increasing the storage modulus of gels has been shown to up-regulate the expression of osteogenic differentiation levels (ALP and RUNX2) of hMSCs [98]. This reference proposes a positive insight that adding CP particles, as increasing the storage modulus, into our biopolymer matrices will improve the osteogenic potential, which will be further investigated in the next chapters.

3.5.7. Compressive behavior of cross-linked GH-CP is favorable in guided bone regeneration.

One of the greatest interests of current bone tissue engineering (BTE) research is to level the mechanical properties of surrounding bony structures [99]. Due to its insufficient mechanical properties and infeasibility in a load-bearing situation, hydrogels are often illustrated as greatly limited in BTE. This common perception may be misleading because all of the currently available bone graft substitutes are not indeed load bearing [100]. Especially, in GBR, since the grafting site tends to locate on the outer alveolar mucosa regions, which is way out of the functional range, load-bearing at the surgical site is not quite possible, unless the patient intentionally rubs the treatment site. Rather, tissue tensions from the macroscopic masticatory ligaments and muscles all the way to the microscopic periosteal connective tissue attachment apparatus may be more meaningful to further investigate, because bone healing mechanism is tightly related with the local mechanical changes [101].

The beginning portion in stress-strain curves of Gtn-HPA recorded during unconfined compression testing displayed abrupt reduction in slope after the unloading curve (Fig. 3-10 E).

This sudden drop indicates that there exists slight adhesive attraction forces between the cross-linked sample and the platens, revealing the adhesiveness of post-gelated biopolymers. This means that the incremental administration of the hydrogels may be clinically possible whenever needed. Moreover, this adhesive property may imply a tissue-friendly stabilization of the cross-linked gels; in other words, when the hydrogel is cross-linked within a minimally invasive tunneling approach, its surrounding intaglio soft tissues around the subperiosteal pouch can tightly grasp the cross-linked hydrogel, creating supplemental retention and resistance of further stabilized graft-host union.

Addition of hydroxyapatite to gelatin has been shown to significantly increase the compressive strength [102]. In our study, the compression modulus (E) of the matrices got also increased with the addition of CP particles; the stiffness of GH-CP was about 3-fold higher than G and about 2-fold higher than GH (Fig. 3-10 G). This elevation of E clearly explicates the significance and importance of incorporating CP particles to strengthen further structural integrity of the biopolymer gel system. However, similar to the rheology test, CP particle sizes are not correlated (Fig. 3-10 F) with the E, meaning that utilization of different particle sizes for customized clinical procedures and purposes may be implemented accordingly.

3.5.8. Correlational analysis between rheological and compressive tests deliver meticulous material insights of GH-CP.

It is well known that for such semi-flexible biopolymers, the compressive modulus (E) is approximately equal to 3-fold the storage modulus (G') [103]. In our studies, we found that E (Fig. 3-10 G) was approximately double the G' (Fig. 3-9 G) on every gel group. This difference portrays that GH-CP gel and other hydrogel groups are unable to exist as totally incompressible material. Additionally, the divergent nominal and true stress-strain curves (Fig. 3-10 D), along with the hysteresis on the loading/unloading graph (Fig. 3-10 E), shows that GH-CP gel and other hydrogel groups cannot exist as purely elastic material either. Most importantly, a constant pattern of increasing modulus (G < GH < GH-CP) is correlated in both rheological (Fig. 3-9 G) and compression testing (Fig. 3-10 G), supporting the consistency of our experiment with minimized critical errors, along with a meticulous understanding of the dynamic mechanisms of GH-CP. To discover further insight into material behavior of GH-CP, other additional mechanical examination of viscoelastic analysis may be helpful.

A high-level of correlation about increased modulus by adding HA-Tyr and CP particles on both rheological and compression tests institutes strong reliability of our data. Two different covalent polymerization reactions of Gtn-HPA/HA-Tyr backbones (Fig. 3-8 A) may give more robust collagen strings coiling up together, compared to Gtn-HPA only, which is shown with the consistent graphical increase after the addition of HA-Tyr. Adding CP particles into this Gtn-HA gel composite may fill out the interstitial heterogenic spaces, further strengthening the mechanical properties of GH-CP. In addition, as Reddy *et al*'s theoretical experiment shows that positively charged calcium ions interact with negatively charged aromatic groups [104], it is also possible that, for our system, calcium ions released from CP particles within GH-CP gel matrices may interact with free reactive sites of the aromatic groups of -HPA and -Tyr, building a more rigid architecture of the gel composites, in which Neffe *et al* drew similar insights with different gel groups [105].

3.5.9. Addition of CP particles on GH gel alleviates its swelling and expansion properties.

An elevated swelling ratio indicates efficient permeability towards active nutrient and waste exchange. In other words, a hydrogel with a high swelling ratio may expedite more active transportation of biological nutrients and wastes, as well as water molecules, which may also potentiate more infiltrating vessel formations within the gel system. However, too much swelling may also cause a poor GBR prognosis via tissue dehiscence during the periosteal wound healing phase. Hydrogels engulfed with oversaturating water molecules may also diminish mechanical properties. Subsequently, a well-balanced equilibrium between improved mechanical properties and the swelling ratio is necessary to establish a harmonized effect of structural integrity and permeability.

For the swelling and volumetric expansion test, because of the initial woven bone formation occurring at around 7 days [106] under the normal physiological periosteal wound healing process, cross-linked GH-CP and other gel groups were stored in PBS for 7 days, to maximize its water absorption within our most subperiosteal mimicking *in vitro* set-up. Similar to mechanical testing, CP diameters showed no statistical significance on swelling ratio (Fig. 3-11 A) amongst groups. This finding also potentiates the incorporation of different particle sizes within GH-CP gel as providing customization of bone grafting procedures (i.e. volumatric maintenance for an extended pontic site or new bone regeneration), and predictable clinical outcomes.

Both of the swelling and expansion ratios show consistent correlational pattern amongst each gel group, yet the order of increase is different (G < GH-CP < GH) from the previous results of mechanical testing. First, both swelling and expansion ratio of GH group was significantly greater than the G groups (Fig. 3-11 B & Fig. 3-12 C). This observation can be explained with a potential increase of pore sizes in heterogenic GH gel, compared to homogenous G gel, because decreased pore size is correlated with decreased swelling potential [107].

Interestingly, upon the addition of CP particles to the GH gel, both swelling and expansion demonstrated a statistically significant decline, which can be explained with exceeding bonding interactions from calcium ions with aromatic polymer groups. The greater interaction linking many polymeric strands transforms into a stringy mesh, followed by a reduction in the swelling ratio [91]. CP particles, simply positioning themselves within heterogenic interstitial spaces between -HPA and -Tyr moieties, may have also just reduced physical room allowing further water absorption and therefore less permeability.

The graphical magnitude of differences seems more amplified in the expansion test, compared to the swelling test, which is simply due to their mathematical equation differences. The swelling test used the subtracted difference, while the expansion test used the whole post-swollen volume as numerator values in the calculation.

3.6. Summary

Physical testing of three different hydrogel groups (G, GH, GH-CP gels) was examined for its potential application in guided bone regeneration (GBR) setting. A dual-syringe auto-mix model, yielding an immediate *in situ* covalent cross-linking through an auto-mix tip, was designed and optimized in a way to spread CP particles evenly both in pre- and post-cross-linked hydrogels. Microscopic view of CP particles in GH-CP was also idealized for further *in vitro* experiments. In-depth characterization of each gel was conducted for the rheological and compressive properties, swelling/expansion ratios, and CP particles influence when consolidated in the gels. Both rheological and compressive behaviors of cross-linked GH-CP increased as adding HA-Tyr and CP particles. Interestingly, swelling and expansion ratios were increased with combining HA-Tyr but alleviated with CP particles addition. These findings from this chapter convey the merits of GH-CP in its potential application for flapless subperiosteal GBR, as well as scientific motivations and foundations towards the next investigative chapters.

Chapter 4 - *In vitro* osteogenic potential of bone marrow-derived mesenchymal stem cells (bMSCs) in GH-CP

4.1. Introduction

The positive benefits provided by gelatin-hyaluronan calcium phosphate (GH-CP) gel such as facilitating injection or implantation and preventing dispersion, as well as improving mechanical properties (see Chapter 3), is somewhat offset by the adverse effect that the very presence of the matrix has in excluding fibrin clot from forming in the interstices among the particles. This coagulated fibrin clot serves as a provisional scaffold that permits the favorable physiological environment of migrated hematopoietic stem cells within the interstitial pore spaces among the particles. It is essential, then, that the biopolymer binder of the particles, replacing the function of the fibrin clot, be permissive of cell proliferation, migration, and differentiation. In a realm of orthopedic and surgical implant dentistry, where *de novo* bone formation is quintessential, researchers have attempted mixing calcium phosphates as osteoconductive scaffolds within different kinds of biopolymers. However, thorough investigations at a cellular level and understanding their mechanisms are still lacking.

4.2. Objective, hypothesis, aims, and rationale

The **objective** of the investigative work illustrated in this chapter is to examine the cellular viability of bone marrow-derived mesenchymal stem cells (bMSCs) and its osteogenic proliferation, differentiation, and mineralization within GH-CP.

For the cellular viability testing, the initial cellular background is investigated with three individual gel groups as:

1. Gelatin group: “G”
2. Hyaluronan group: "H"
3. Gelatin-hyaluronan group: “GH”

For the osteogenic differentiation, same as chapter 3, the incorporation of gelatin-hydroxyphenyl propionic acid (Gtn-HPA), Hyaluronic acid-tyramine (HA-Tyr), and CP particles are analyzed via testing three different sequential gel combinations as:

1. Gelatin group: “G”
2. Gelatin-hyaluronan group: “GH”

3. Gelatin-hyaluronan-calcium phosphate group: “GH-CP”

Our **primary hypothesis** is that bMSCs are viable in all gel groups. **A second hypothesis** is that the addition of CP exhibits more osteogenic potential compared to other gel groups.

The **specific aims** are to: 1) determine the viability (%) of bMSCs in the different gel groups (G, H, GH) with morphological analysis; 2) evaluate the behavior of bone marrow-derived mesenchymal stem cells (bMSCs) in the gel, including: cellular proliferation (Ki67); contractility (α-smooth muscle actin, α-SMA); differentiation (osteocalcin/osteopontin, OCN/OPN); and mineralization (Alizarin Red S, ARS, staining).

In spite of previous references [59, 60, 62] with verified biopolymers' cytotoxicity, because of our increased w/v% for its specific purpose of the bone tissue engineering (BTE), the viability test was first performed to establish a basic foundational understanding of our testing gel groups at a cellular level. Considering obtained information of different mechanical properties (See Chapter 3), morphological analysis of bMSCs was also assessed to understand its correlation.

Due to technical challenges, very few studies have been investigated to quantify the osteogenic differentiation of bMSCs in hydrogels, especially when incorporated with CP particles. Our pilot experiments of immunofluorescence were initially attempted with the same dimensions of gel casts from the previous mechanical testing and resulted in a significant image scattering under the confocal microscope, possibly from multi-layered CP particles. Therefore, the volume of gel casts was re-optimized in terms of a thinner layer achieving acceptable immunofluorescence and ideal microscopic optical visualization.

This chapter's study leads to a systematic understanding of the behaviors of osteoblast-like cells differentiated from bMSCs within GH-CP. This study is the first investigative work, trying to outline the sequence of cellular cascades in *de novo* bone formation within CP particles infused biopolymers. This study is the first utilizing Alizarin Red S (ARS) under the confocal fluorescence for the calcified deposits within CP particles incorporated hydrogels.

4.3. Materials and methods

4.3.1. Isolation and culture of goat bone marrow-derived mesenchymal stem cells (bMSCs)

The iliac crest of adult 2-3 years old female Spanish caprine (45 kg) was utilized for extracting bone marrow aspirates, followed by transferring to sterile tubes containing cold phosphate-buffered saline (PBS)/1 mM ethylenediamine tetraacetic acid (EDTA). Cell isolation technique was based on the protocol validated by Friedenstein *et al*. [108].

The medium, trypsin, and PBS were warmed in 37°C water bath. Then, the medium was removed via vacuum pipette, followed by rinsing with PBS. Trypsin was then added and stored in an incubator for 5 minutes. After a microscopic verification of cell detachment and floating, the medium was added to inactivate the trypsin. Centrifuging at 1500 rpm for 10 minutes was run to establish the cell pellet at the bottom of the tube. After vacuuming the medium, cells were resuspended and counted accordingly, targeting 100,000 cells/mL in the experimental samples.

After cleaning the hemacytometer and coverslip with 70% alcohol, 100µL of the sample from the cell suspension was diluted with trypan blue as 1:2 dilution ratio. After mixing, 15µL of was suspended through a micropipette tip, as being loaded into the hemacytometer under the coverslip by capillary action. Under the 10x microscopic view, cell counting (clear cells as viable; stained cells as dead) proceeded in each of the four corner and central squares. Only the top and left lines were counted, excluding the ones on the bottom or right lines of each square, to prevent any recounting.

4.3.2. Direct gel cast fabrication

Direct gel casts were fabricated using the same dual syringe system (Fig. 3-8), through a dispensary to the experimental dish wells, with a volume of 120µL. Before the experiment, each element of the dual syringe system (i.e., double barrel syringe & CP particles) was stored in the fume hood with UV light for one week, prior to incorporating with bMSCs within the gel. All of the cross-linking gelation experiments were completed in the cell culture hood at 21°C, followed by storing them at 37°C in an incubator with routinely replaced culturing mediums for the necessary duration of time on each experiment.

4.3.3. Osteogenic differentiation of bMSCs

The pluripotency of bMSCs by osteogenic and adipogenic differentiation was confirmed by prior works [109] from our lab. Adherent bMSCs infused cross-linked gel groups were cultured in the osteogenic medium for 28 days (i.e., first 5 days in expansion medium, followed

by the rest of days in osteogenic medium) to induce osteogenic differentiation at 37°C in an incubator. For the baseline control group, gel groups were cultured only in the expansion medium for the same duration of time. The expansion medium consisted of: Dulbecco's modified Eagle's medium-low glucose (DMEM-LG, Invitrogen, Karlsruhe, Germany) supplemented with 10% fetal bovine serum (FBS), and the osteogenic medium consisted of: Dulbecco's modified Eagle's medium-low glucose (DMEM-LG, Invitrogen, Karlsruhe, Germany) supplemented with 10% FBS, 0.05mM ascorbic acid phosphate (Wako Chemicals), 100 nM dexamethasone (Sigma), and 10mM β-glycerophosphate (Santa Cruz Biotechnology, Santa Cruz, CA) [110]. Previous pilot experiments demonstrated that 3-day intervals of replacing the culturing medium were acceptable in terms of cell viability.

4.3.4. Cell viability

Live/Dead® Viability/Cytotoxicity Assay (Molecular Probes, Inc.) was utilized for measuring cell viability. 4 μM ethidium homodimer (EthD-1) and 2 μM calcein-AM of LG-DMEM solution was used for incubating cell-seeded gels.

The direct cast gels (100μL) were loaded, via a dual syringe model, on to a 24 well plate (n=6) in the cell culture fume hood at 21°C, followed by dispensing 300μL of expansion medium on each well. These gel groups were stored at 37°C in an incubator for 24 hours.

After the utilization of Live/dead® viability cytotoxicity kit, the well plate with gel groups was carried onto the confocal microscope and inspected under a fluorescent microscope. Four sections of each gel were randomly selected on a total of 6 samples in each group for analysis. EthD-1 was used to stain dead cells and calcein-AM was used to stain live cells (Fig. 4-1 A). Image J software (NIH, Bethesda, MD) was used for percentage quantification analysis and cell morphology observation.

4.3.5. Immunocytochemistry and immunofluorescence (ICC/IF)

For direct gel cell cultures, a standard protocol of ICC on the monolayer culture slides was modified via extending its duration, which was previously optimized by our lab. For direct thin gel culture of cells in control and osteogenic media, the media was removed and the gels were fixed in 500μL of 4% paraformaldehyde (PFA) for 2 hours at room temperature. After washing with 500μL of PBS, they were then permeabilized in 300μL of 0.1% Triton-X 100 (Sigma) for 1 hour at 4°C. The gel cultures of cells were again washed in PBS followed by

quenching of endogenous peroxidase activity with 5-6 drops of a peroxidase blocking reagent (Envision Plus+ System-HRP (AEC), Dako, Carpinteria, CA) at 21°C overnight. Non-specific binding was blocked by protein block serum-free (Dako). Gel cell cultures were incubated with primary antibodies overnight at 4°C. Monoclonal anti-Osteocalcin (OCN) mouse antibody (Abcam) was used at a dilution of 1:200. Monoclonal anti-Osteopontin (OPN) rabbit antibody (Abcam) was used at a dilution of 1:1000. Monoclonal anti-α-smooth muscle mouse antibody (Abcam) was used at a dilution of 1:400. Monoclonal anti-Ki67 rabbit antibody (Abcam) was used at a dilution of 1:1000. Negative controls were incubated with stock negative control mouse IgG fraction (Dako) at the same dilution instead of the primary antibody. After two times of washing with of 500μL PBS by a duration of 2 hours each, another 500μL PBS was used for washing and stored at 4°C with foil overnight. Then, after removing PBS, 250μL of combined secondary detection antibodies, Alexa 488 (Green - emission wavelength) and Cy 3 (Red - emission wavelength) diluted to 1:300 each were used and stored at 4°C with foil overnight. After one wash with 0.05% Tween® 20 and another wash with PBS for 2 hours each, DAPI was applied and stored at 4°C with foil for 8 hours. Then, right before confocal imaging, DAPI was replaced with PBS.

Quantitatively analysis was drawn either by comparing total cell-counting (Ki67) or mean gray values (OCN/OPN) in the Image J software (NIH, Bethesda, MD). Particularly, for the mean gray values analysis, four microscopic view positions were randomly chosen out of a single gel sample. On each selected microscopic view, four regions of interests (ROIs) with a diameter of 100μm were selected originating from the most visually fluorescent areas. These values were then averaged out for the rest of six samples (n=6) on each experimental group.

4.3.6. Mineralization analysis

The media of cell-infused gel groups were removed, and the gels were fixed in 500μL of 4% paraformaldehyde (PFA) for 2 hours at room temperature. After washing with 500μL of PBS, Alizarin Red Solution (ARS) (Sigma-Aldrich) was used to detect calcium depositions within the gel cultures, referencing the basic mechanism that calcium forms an Alizarin Red S-calcium complex in a chelation process, and the end product is birefringent [111]. 300μL of ARS was applied for each gel culture for 30 minutes. Then continuous PBS wash replacement per day was performed for three weeks to remove as much remnant ARS pigments of the gels with maximal architectural preservation prior to both optical and confocal microscopic image analysis.

Along with the typical ARS analysis method under the optical microscopy, confocal analysis of ARS was also investigated with its result of high relevance. Few studies [112, 113] also support confocal analysis of ARS. For the quantitative analysis, the mean gray values analysis along with four microscopic view positions were randomly chosen out of a single gel sample. On each selected image of microscopic view, four regions of interests (ROIs) with a diameter of 100μm were selected originating from the most visually fluorescent areas of the visible cell's center position (Fig. 4-5 C) to calculate the mean gray values in the Image J software (NIH, Bethesda, MD). ROIs touching CP particles were excluded from the analysis, due to the fact that these are pre-existing calcium sources in the gels. These averaged values were then averaged out for the rest of six samples (n=6) on each experimental group.

4.3.7. Statistics

Data in this chapter are described as mean ± standard deviation, standard error, or min & max. Statistical significance was examined by unpaired t-test, or one- / two-way analysis of variance (ANOVA). In such cases of significance in ANOVA, Tukey's or Bonferroni-Sidak's post-hoc multiple comparison tests were run with a significance criterion of $p < 0.05$ using GraphPad Prism 7 (GraphPad Software, Inc., CA, USA).

4.4. Results

4.4.1. Cell viability

G, H, and GH gels, infused with bMSCs, were assessed for cell viability. Cell viability of H gel group showed a decline, compared to the other gel groups, with a statistical significance in one-way ANOVA ($p < 0.0001$). Tukey's post-hoc test showed statistically significant differences between G and H ($P < 0.0001$), as well as H and GH ($P < 0.0001$). Average mean values of cell viability in G, H, and GH were 90.47 ± 3.81 %, 58.20 ± 4.08 %, 87.72 ± 4.42 % (n=6, mean ± S.D.), respectively (Fig. 4-1 B).

4.4.2. Cell morphology

The cytoplasmic morphology of bMSCs, approximately 10-20μm in length, appeared variable throughout the gel groups. Therefore, the shapes were categorized as either rounded or elongated (Fig. 4-1 C). Two-factor ANOVA demonstrated a statistical significance of varying

gel groups and morphologies on the cell proportions (%) ($p < 0.0001$). Bonferroni-Sidak's post-hoc test showed that a statistically significant elongated shape of bMSCs in G gel ($p < 0.001$) and rounded shapes of bMSCs in H gel ($p < 0.0001$). Meanwhile, GH gel consisted of a well-distributed ratio of round and elongated shapes of bMSCs. Average mean % ratios of rounded: elongated forms of bMSCs are 39.7 ± 1.8%: 60.3 ± 1.8% in G, 93.2 ± 2.2%: 6.7 ± 2.2% in H, and 50.3 ± 3.8%: 49.7 ± 3.8% in GH (n=6, mean ± SEM.) (Fig 4-1 A & C).

4.4.3. α-SMA expression

All bMSCs in G, GH, GH-CP gels were stained in α-smooth muscle actin (α-SMA), representing high contractile activity [114]. DAPI staining of nuclei well coincides with the positions of α-SMA. Cytoplasmic staining of α-SMA was in 15-25μm in length, slightly larger than the nuclei staining of DAPI (n=6) (Fig. 4-3 A).

4.4.4. Ki67 expression

Some bMSCs in G, GH, GH-CP gels were stained in Ki67, representing cell proliferation [115]. Ki67 fluorescence was expressed in dotted points, as a ranged diameter of 3-5μm (Fig. 4-3 A) and expressed in between proliferating bMSCs (Fig. 4-4 A). Therefore, cell counting method was chosen for the methodology of quantitative analysis.

One-factor ANOVA revealed no statistically significant effect of different gel groups on total Ki67 counting ($P = 0.42$). Mean values of Ki67 counting of G, GH, GH-CP gels were 82.25 ± 20.98, 95.00 ± 28.01, 104.5 ± 19.02, respectively (n=6, mean ± S.D.) (Fig. 4-4 B).

4.4.5. Osteogenic differentiation (OCN/OPN expression)

Osteocalcin (OCN), or bone gamma-carboxyglutamic acid-containing (gla) protein, is the most richly expressed non-collagenous protein and produced by osteoblasts in bone [116]. Due to its high affinity to calcium and hydroxyapatite [117], OCN is one of the most widely utilized bone markers. Notably, OCN is more intimately related to the deposition of osteoid, rather than to composition of mineralized bone [118, 119].

Osteopontin (OPN), also known as bone sialoprotein I (BSP-1 or BNSP), is a non-collagenous glycoprotein, which is acidic molecular composition with its cell- and hydroxyapatite-affinity properties [120]., is also commonly utilized as an osteoblast differentiation marker [121].

In our experiment, both OCN and OPN were expressed amongst different gel groups with a progressively increasing pattern of fluorescence (G < GH < GH-CP). Both intra- and extra-cellular OCN/OPN expressions were observed in GH and GH-CP gels, compared to mostly intra-cellular expression in G group (Fig 4-3 A). Further, OCN seemed more evident than OCP in all of the three gel groups (Fig 4-3 B).

Two-factor ANOVA demonstrated statistical significances of mean gray values on different gel groups ($P = 0.0003$) and in between OCN and OPN ($P < 0.0001$). Bonferroni-Sidak's post-hoc test showed that the mean gray values of OCN in G gel was less than GH gel ($p < 0.05$), as well as than GH-CP gel ($p < 0.05$) (Fig 4-3 B). The mean gray values of OPN in G gel showed the same declining pattern, compared to GH gel and to GH-CP gel ($p < 0.05$). The difference between OCN and OPN expression levels showed a statistically significance in all of G gel ($p < 0.01$), GH gel ($p < 0.0001$), and GH-CP gel ($p < 0.001$). Mean gray values of OCN/OPN in G, GH, and GH-CP are $1.570 \pm .175$ / 0.011 ± 0.0001, $2.516 \pm .203$ / $.348 \pm .118$, and $2.752 \pm .272$ / $1.076 \pm .363$, respectively (n=6, mean ± SEM.).

4.4.6. De novo bone formation

4.4.6.1. A hypothetical cascade of de novo bone formation of bMSCs in GH-CP in vitro

While culturing GH-CP gel with the osteogenic medium (see 4.3.3.) for 28 days, the changing dynamics of bMSCs, blended with CP particles and GH hydrogel, was observed under the optical microscopy with a magnification of 30x.

Then, the following findings of potential *de novo* bone formation were remarked in a chronological manner. When bMSCs were cultured in expansion medium (DMEM-LG + 10% FBS) for the first 5 days, cytoplasmic morphology of bMSCs was in a circular shape (Fig. 4-2 A). After changing to osteogenic medium (see 4.3.3.), cytoplasmic stretching was observed in bMSCs (Fig. 4-2 B). Within a few days, these elongated cells seemed beginning to interconnect each other through forming net-like trajectory lines together within the gel matrix (Fig. 4-2 C). Throughout the week 1 to 2, spreading bMSCs were more observed on the surface of CP particles in terms of docking (Fig. 4-2 D) and adherence (Fig. 4-2 E), followed by the initial sign of osteoid depositions from the differentiating osteogenic cells via contact and distance osteogenesis (Fig. 4-2 F). Through week 2 to 4, cells became more dispersed and diffused into the gel matrix or collagen fibrils from *de novo* bone formations (Fig. 4.2 G and H). Along with

other upcoming results in this chapter, "cling osteogenesis" theory is termed as a conceptual osteogenic cascade mechanism (Fig. 4-2 I), to formulate the osteoid/calcified-bone boundary (OCBB). Detailed elaboration of this concept is reviewed in the upcoming discussion of this chapter.

4.4.6.2. Alizarin Red S (ARS) staining for mineralization

Alizarin Red S (ARS) staining, also known as Turkey Red or Mordant Red 11, is an organic compound, which stains free calcium ions or calcium-containing parenchymas or compositions [111]. In our study, after the 28 days of osteogenic differentiating culture, since visually detectable *de novo* bone formations within the gel groups were observed (Fig. 4-2), ARS staining was utilized for the verification of mineralizations within the gels. After three weeks of continuous daily washing with PBS (see 4.3.6.), both optical and confocal microscopic analysis was processed. Grossly, all of the gel groups seemed to contain slightly left-over ARS staining dyes as transparent red color gel matrices, while the pre-existing calcium phosphate particles and calcified collagen compartments from the osteogenesis were stained as darker deposits (Fig. 4-5 A). These dark stains were easily detectable in GH-CP gels, while G and GH gels were not distinguishable each other in a gross view. Notably, GH-CP with osteogenic medium (Ost) showed a demarcated visual difference, compared to GH-CP with expansion medium (Exp), in terms of having more heavily stained dark CP particles, as well as much more abundant dark osteoid-like residues within the gel matrices (Fig. 4-5 B), which was verified with magnified (X30) views with curtain-like dark stains near CP particles and within the gel matrices. Bright field views under the same magnification also supported a consistency of difference between two groups (Exp. vs Ost.) of GH-CP in terms of having more prominent dark mineralized depositions in the matrices and near CP particles. Interestingly, GH-CP gels of both Exp. and Ost. showed less visually detectable cells in gel matrices. Through confocal microscopy with green emission, ARS staining was detected at the tracing of dark stains under the optical microscopy. These confocal findings in GH-CP were confirmed with a supplementary quantitative analysis, as depicted in Fig. 4-6. A consistent length of the line was drawn from a highly fluorescent cell to the outermost surface of the pre-existing CP particle. Then, these straight lines were divided in half to allocate a middle dissecting line for inter-distant segmentation (Fig. 4-6 A), followed by graphical analysis of the gray values in each zone of segmented points (Fig. 4-6 B). Then, the

average mean gray values within 50 pixels of the same location in the middle segmented point were compared, which showed a statistically significant difference ($p < 0.001$) (Fig. 4-6 C).

In G and GH gels, bMSCs were kept in its original sizes in Exp. (15-20μm length) and enlarged as elongated with inconsistently spread-out shapes in Ost. (50~70μm length). Dark stained osteoid-like residues were also expressed in G and GH gel matrices, although they seemed less significant compared to GH-CP gel. Confocal microscopy with green emission, as locating at the exact same spot of a bright field view image, also expressed florescence of ARS as the curtain-like dark stains in G and GH gels (Fig. 4-5 A).

As explained in 4.3.6., four randomly chosen images of the mean gray values (100μm diameter) of the region of interests (ROIs) were averaged out on every 6 samples of gels. The mean gray value pattern demonstrated no changes in Exp. on all groups of gels, compared to a progressive increase pattern in Ost. in gel groups (G < GH < GH-CP). Two-factor ANOVA showed a statistical significance of the mean gray values on different gel groups ($p = 0.0095$) and on culturing mediums ($p = 0.0057$). Bonferroni-Sidak's post-hoc test revealed that GH-CP (Ost.) showed a statistically significant increase, compared to G (Ost.) ($p < 0.01$) and to GH (Ost.) ($p < 0.01$) (Fig. 4-5. D). ARS fluorescence's mean gray values of Exp./Ost. in G, GH, and GH-CP are 1.172 ± 0.202 / 1.044 ± 0.195, 1.065 ± 0.165 / 2.136 ± 0.228, and 1.294 ± 0.097 / 4.834 ± 1.367, respectively (n=6, mean ± SEM.).

4.5. Discussion

After the previous chapter's findings on the mechanical properties, in this chapter, cellular and biological aspects of GH-CP were highlighted. Goat bone marrow-derived mesenchymal stem cells (bMSCs) were properly isolated (See 4.3.1.) and injected through a dual-syringe auto-mix model system (See 3.4.2.) as being fused inside the cross-linked GH-CP in a thin direct cast. Initially, cellular foundations of viability and morphology analysis were established in each hydrogel (G, H, and GH) environment, without incorporating CP particles. Then, immunocytochemistry and immunofluorescence (ICC/IF) of α-SMA, Ki67, OCN/OPN, and ARS staining were examined, with gel groups as G, GH, and GH-CP, to understand the dynamics of osteogenic differentiation, along with thoughtful insights.

4.5.1. Sub-periosteal pouch concept potentiates its synergetic collaboration with injectable GH-CP, enabling flapless guided bone regeneration.

A minimally invasive trend has greatly influenced surgical dentistry, flourishing many innovative techniques [1, 122, 123]. In our study, a sub-periosteal pouch concept of flapless GBR is proposed (Fig. 3-1 B), which can be created via pinhole access under the mucogingival junction, followed by internally detaching periosteum through a tunneling instrument. Then, an injectable GH-CP can be squirted through a keratinized alveolar tissue into the subperiosteal pouch through a needle-shape orifice or narrow tip. After the full cross-linking *in situ*, because the penetrated tissue access is minimal, no flaps nor suturing may be necessary. Instead, *in situ* blood clotting may be sufficient enough to achieve primary wound closure. This sub-periosteal pouch concept can: 1) maximize the patient's comfort; 2) reduce surgical duration; 3) retain the structural integrity of the graft-host union via a tension of completely enclosed alveolar tissues; 4) allow faster healing with a completely closed wound environment; 5) increase the osteogenic potential through periosteum-derived mesenchymal stem cells. This novel surgical technique mimics the sub-sinusal space, one of the most osteogenically favorable oral and maxilla-facial spaces.

4.5.2. Gtn-HA (GH) generates a favorable niche for bMSCs in terms of cell viability.

Our experiments revealed that bMSCs were viable as being fused within mechanically tunable hydrogels, withstanding the simultaneous chemical cross-linking process, and persisting its viability for 24 hours (see 4.4.1.) and 28 days (see 4.4.5.) after encapsulation. In spite of obvious cytotoxicity of HRP and H_2O_2, 90% of cells were viable through both pre-gelated Gtn-HPA gel (Fig. 3-8 A) and post-gelated G and GH. This means that minimal concentration of H_2O_2 in pre-gelated Gtn-HPA has insignificant influence on the survival of dissipated bMSCs, as well as that HRP and H_2O_2 were rapidly depleted after going through the dual-syringe auto-mix tip.

In spite of reported favorability of HA gel [76, 124], in our study, it showed a drastic decrease of cell viability, compared to G and GH (Fig. 4-1 B). This phenomenon could be due to high w/v% of gel, increasing its stiffness, which is reported to decrease cell proliferation [125]. Besides, Hyaluronan, a multifunctional glycosaminoglycan, is reported as having low cell settlement properties [126] and the architectural foundation of the peri-cellular matrix, which promotes cell detachment and rounding [127]. A little volume of the thin cast of a cross-linked

gel may have also provided an insufficient niche for survival of bMSCs in HA gel. In our dual syringe model, bMSCs were initially dispensed in Gtn-HPA within the pre-gelation syringe. Interestingly, combination of HA-Tyr with Gtn-HPA, forming GH gel, has exhibited improved cell viability, getting over 90% again (Fig. 4-1 B). This improvement can be due to the fact that heterogeneity in GH may have created more permeable, porous, and favorable environment for cells [79]. As a result, for the next following osteogenic experiments, experimental groups of G, GH, and GH-CP were utilized.

4.5.3. The inter-matrix dynamic architecture of gels and integrin incorporation is a decisive factor in adherence, morphology, and contractility of bMSCs.

Our study demonstrates various shapes of cytoplasmic phenotypes in submerged bMSCs inside different gel groups as G gel with mostly elongated cells, H gel with mostly rounded cells, and GH gel with both of cell types in half ratios (Fig. 4-1 A and C). Although MSCs tend to express more adherent characteristics compared to hematopoietic stem and progenitor cells (HSPCs) [128], different appearances of bMSCs in our study lead us to thoughtful insights into adherence, morphology, and contractility of MSCs.

Interconnection is a central bioengineering factor on any dynamic arrangements of organisms or organelles. At a cellular level, the initial phase of interconnection of MSCs springs with the adherence to the extracellular matrix (ECM) system for its further survival and proper function [129]. For flourishing this biomimetic and adhesive matrix environment in bone tissue engineering, several methods have been suggested in such ways of surface treatment, material patterning, or utilizing natural biomaterials [130]. As demonstrated in our study, elongated or spreading cells are observed microscopically (Fig. 4-1 A), which represents its fibrillar matrix adherence structure in the form of matrix disruption [131]. This microscopically adhered mesh system later serves as a critical role of shredding the cross-linked biopolymers for the ultimate full physiological resorption, which may be essential for making space of neovascularization and therefore, new bone formation.

Cell-matrix interaction gets initiated by cell-adherence mechanism, as operated with so-called integrins [129], which regulate the signaling cascade of transmembrane attachment on the cytoskeleton. The gel (i.e., denatured collagen) contains β1 integrin receptors [132] for its favorable cell attachment mechanism, while natural collagen fibers react with a different mechanism [133] as operating functional responses. Linking these integrins and ECM proteins to

the actin cytoskeleton, focal adhesions (FAs) fine-tune the adhesion capability [134]. Plus, converting the gel status by heating even switches its integrin specificity [135]. These merits of findings suggest the existence of different integrin receptor expressions amongst our different gel groups in a way that G or GH gel is more favorable than H gel.

In our previous study, mixing two different gels Gtn-HPA and HA-Tyr together appears increasing the physical stiffness and porosity together (See 3.5.3.). Usually, viscous substratum limits cell motions [136], turning to possibly more constricted round shapes due to high stiffness, which is supported by a reported study saying that cells cultured on soft medium display more spreading properties compared to more elastic medium [137]. However, a different study states that stiffer matrices indeed assist in increasing cell spreading to promote the osteogenesis [138]. Therefore, rather than the stiffness of matrices alone, cell morphology seems depended on the correlation with integrin expressions and other interdisciplinary factors such as actin filaments.

By definition, actin filaments are cellular infrastructure system for transmitting the force coming from contacting with surrounding substratum [139], which is often expressed with α-SMA levels indicating its potential to osteogenic differentiation [114]. Cell spreading appearance within the substrate can portray the intensification of actomyosin contractility ultimately leading to osteogenic differentiation [140]. This actomyosin protein network allows the cells to feel such mechano-perception via contractile forces upon its adherence to the substrate [134]. In a molecular level, non-muscle myosin-II, which is an actin crosslinking protein as producing filaments, become phosphorylated and exert forces to the matrix, which can then pushback from a resistant matrix causing its positive feedback onto cytoskeletal actin filaments [141]. Our ICC/IF study demonstrates a great level of α-SMA expression on all gel groups of G, GH, and GH-CP (Fig. 4-3 A), meaning that bMSCs within all of our gel groups are capable of osteogenic differentiation, probably due to its stiff 3D gel environment [142].

4.5.4. The proliferation (Ki67) potential of bMSCs does not seem to be different among the three gel groups.

The proliferation (Ki67) of bMSCs seemed less significantly expressed (Fig. 4-3 A) than other markers like DAPI and α-SMA on all of the gel groups (G, GH, GH-CP) in terms of size and distribution, probably because of the time point of fixation and staining at 28 days, where most of the cell proliferation was completed, as well as due to generally stiffer gel groups. Most of the reported studies state that stiffer hydrogel environment causes less proliferation of MSCs

[57, 143]. Nevertheless, for our study, Ki67 expression levels were mostly observed in between dividing cells (Fig. 4-4 A). As explained previously (See 4.4.4.), cell counting method was utilized to quantitatively compare possible differences amongst groups, which turned out to be non-significant (Fig. 4-4 B), meaning that addition of HA-Tyr to Gtn-HPA or CP particles to GH gel do not significantly affect their proliferation property. As mentioned before, it is also possible that our experimental observation window was too late to detect any potential differences in Ki67's proliferation rate level amongst different gel groups in terms of timeline.

4.5.5. Osteogenic potential increases with gel combination and calcium phosphate addition.

4.5.5.1. Elevated OCN and OPN levels, formulating OCN-OPN complexes, can induce a positive feedback mechanism towards osteogenic differentiation.

During a late stage of osteogenic lineage, osteoblasts produce OCN proteins [144], which serve as a terminating signal upon the maturation of bone matrix (a.k.a, mineralization inhibitor) [116]. On the other hands, OPN is involved in a relatively early phase of osteogenic lineage [145], as being enriched on the mineralized tissues with its primary function of provoking the early signaling anchoring cascades of ligand-receptor interactions [146]. These interactive anchorages from OPN are involved with cells like osteoblasts or osteoclasts [120], executing such interactive osteoblast-osteoclast coupling [147] as a pivotal process in bone metabolism and growth. OPN is shown to upregulate other osteoblast differentiation markers [148], as well as to regulate periodontitis progression via the NF-κB pathway [149], all of which confirms its orchestrating role in cell adherence.

Interestingly, in spite of its primary role as mineralization inhibition, the OCN gene can positively interact with Runx2, inducing the osteoblast-specific gene transcription pathways both *in vitro* and *in vivo* [150]. Investigative works of this synergetic role of OCN with other markers have founded *in vitro* discovery of rapidly formulating high-affinity OCN-OPN complexes [151], which may exist with merged expression and protein binding properties even after being bound to the surface of hydroxyapatites, becoming the building blocks of calcium frameworks in osteogenesis. A recently reported study also support the synergetic effect of OCN and OPN in bone regeneration via enhancing the osteogenic potential of MSCs [152].

In our study, both immunofluorescence expression level of OCN/OPN (4-3 A and B) and mineralization of ARS staining (4-5 A and D) showed the same expression pattern in an

increasing order of G < GH < GH-CP. This observation describes the upregulated osteogenesis upon the combination of two different gels as well as the addition of CP particles. By observing the traces of interconnecting MSCs within GH gel (Fig. 4-2 C and D) and elevated OPN expression level in GH and GH-CP gels, it is reasonable to state that the interactive cellular adherence becomes more intense as combining two gels (i.e. Gtn-HA) and the CP addition, possibly due to heterogenetic porosity (See 3.5.3.) and improved mechanical strength (See 3.5.6. and 3.5.7.), respectively.

4.5.5.2. Stiffness of GH-CP can drive the cell fate of infused bMSCs into osteogenic lineages.

Stiffness or elasticity of matrices dictates the cell fate of MSCs [153, 154]. To elaborate, substratum bearing high-affinity, low-affinity (highly dense), and low-affinity (less dense) peptide cores promote MSCs into osteogenesis, myogenesis, and neurogenesis, respectively [155]. Substratum with osteoid-like stiffness (10 to 40 kPa) leads into osteogenic differentiation, whereas softer matrices (10 kPa) into myogenic differentiation [156]. By adding CP particles, our GH-CP falls into the osteogenic range of stiffness with its compressive modulus as 16.8 kPa (Fig. 3-10 G), along with higher OCN/OPN expression (Fig 4-3) and mineralization (Fig 4-5) levels. As elaborated previously (See 4.5.3.), higher stiffness also advocates actin-myosin assembly with contractile forces, as expressing stress fibers [157], for its positive influence on osteogenic differentiation.

In our study, mechanical property increases as in order of G < GH < GH-CP, due to its heterogenic covalent matrices of mesh framework (See 3.5.3.) and CP particle's physicochemical interaction (See 3.5.4.) within GH gel. Such elevated mechanical stiffness of cross-linked biopolymers boosts the osteogenesis of MSCs via endochondral ossification process [158]. In spite of relatively small expression, notably, our G and GH gels without CP particles also demonstrate OCN/OPN expression and mineralization (Fig. 4-3 and 4-5), meaning that our gel framework modulus is stiff enough for initiating osteogenesis by itself. A reported study states that different biopolymer stiffness also expresses different bone protein levels [159], which may explain our findings of elevated expression of osteogenic differentiation with increased modulus.

4.5.5.3. Mineral ions released from CP particles within GH-CP can promote osteogenic differentiation of bMSCs.

Reported studies state that matrix-bound CP minerals get formulated within CP infused gel composite with a dissolution of released calcium and phosphate ions, achieving the equilibrium [160, 161] in the matrix system. Our study also demonstrates the observation of more significantly displayed osteoid/calcified-bone boundary (OCBB) (Fig. 4-2 I) upon the addition of CP particles, compared to a small fraction in mineralization within G and GH gels (Fig. 4-5 A and D). This demonstration of the osteogenic differentiation and mineralization without any osteoinductive components within the gel matrices, as well as the observable osteogenic difference between GH and GH-CP, clearly indicates that the released mineral ions from CP particles play a key role in terms of signaling osteogenic lineages. This mechanism has already been figured out by Shih and co-workers [90] in such that extracellular phosphate ions get transferred through sodium-phosphate symporter SLC20a1 into the cytoplasm, followed by going through mitochondria for ATP synthesis and secretion. Then, this extracellular ATP gets metabolized into adenosine which returns back to the cell to induce osteogenic differentiation through the A2b adenosine receptor. Clearly, our results of upregulated *de novo* bone formation in GH-CP gel (Fig. 4-5 A and D), compared to G and GH gels, support the aforementioned anabolic mechanism of released mineral ions. Gross views of GH-CP (Ost.) shows evident new bone formations both around CP particles and within the gel.

4.5.6. Heterogeneous interpenetrating gap striation (HIGS) theory

In our study, non-collagenous bone markers (osteocalcin and osteopontin) were expressed in all of the gel groups of G, GH, and GH-CP (See 4.5.5.1.), yet its distribution pattern in each group seemed unique. In G gel, the fluorescence of OCN/OPN was mostly restricted as intra-cellularly. On the other hands, the fluorescence was both extra- and intra-cellularly expressed in GH and GH-CP gels, yet more spread-out appearance was observed in GH-CP gel (Fig. 4-3 A). Under the optical microscope, this extra-cellular fluorescence followed the trajectory pattern of interconnecting lines (Fig. 4-2 C and D), which looked like 'crack-like' lines. The mean gray values of OCN/OPN expression was also increased in order of G < GH < GH-CP (Fig 4-3 B). These consistent differences became more significant, as no fluorescence was observed with the control group stained with negative control mouse IgG fraction. Interestingly, under the optical bright field and confocal views, mineralization pattern demonstrated the same

kind of distribution pattern; mineralization fluorescence of ARS staining seemed intra-cellularly expressed on every gel group under the Exp. medium. Ost:G gel group also expressed ARS fluorescence intra-cellularly. Ost:GH and Ost:GH-CP gels clearly showed the same appearance of spread-out distribution in mineralization, as following the 'crack-like' lines (Fig. 4-5 A).

Other reported studies describe this 'crack-like' lines with different terms such as capillary structure [162] or sprouting [163], with their common interpretation of an etiological factor in possible inhomogeneity of the gel [164]. This concept is also well-supported by our findings in such a way of demonstrating more of these 'crack-like' appearances in GH and GH-CP gels, compared to G gel. Plus, because we do not really observe these 'crack-like' lines in all of the gel groups with Exp. medium (Fig. 4-2 A and Fig. 4-5 A), it is also possible that MSCs undergoing the osteogenic differentiation with increased transmembrane activities of transporting phosphate ions, ATP, adenosine (See 4.5.5.3.) may have created more gel deformation tracings around the differentiating cells. In a reported observation study, hMSCs turned out to congregate in the structurally softest, or most degraded, region of the gel [95], which may explain the fluorescence and cellular aggregation phenomenon in our GH and GH-CP gels (Fig. 4-3 A) within its possible irregularity of gel consistency around the 'crack-like' lines.

Another interesting explanation of the enigma in our results can be exosomes. Intracellularly, during the osteogenic differentiation, matrix vesicles with calcium and phosphate ions are produced in the mitochondria and excreted extracellularly targeting to deposit within the collagen fibrils [165]. During this process, the exosomes with bioactive molecules originated from Golgi apparatus and endoplasmic reticulum, budding to the plasma membrane as a multi-vesicular body (MVB), spreading extracellularly [166]. This Golgi system completes the glycosylation of pro-collagen as packaging them to granules to the cell membrane before the final secretion [167]. Because these exosomes usually contain proteins, miRNA, and mRNA [168], it is reasonable to assume that our non-collagenous bone proteins of OCN and OPN may have also packaged within these exosomes. The size of each exosome is usually around 50nm, which is approximately 20 to 100 fold smaller than the average fluorescent OCN/OPN dots (around 1 to 5μm diameter) in our results. The bigger sizes and shapes of fluorescence can be explained with the possible formation of OCN-OPN complexes (See 4.5.5.1.) with its high affinity since the fluorescence is expressed in non-uniform patterns (small/medium dots, spread-out, aggregated, etc).

Similar to the exosomes, matrix vesicles (MVs) get originated from the plasma membrane of osteogenic cells and seen at the initial phase of mineral formation, before matrix mineralization [169]. MVs consist of its parental phospholipids with calcium channel proteins, called annexins [170], which is in hexameric architecture for transporting calcium ions [171] and with type III sodium-dependent phosphate transporter for carrying phosphate ions, all of which becomes apatite formation within MVs [172]. In our results, Exp. medium groups, as well as G gel of both Exp. and Ost., clearly demonstrate mineralization expressed intra-cellularly, portraying non-secreted MVs with calcium and phosphate ions. Observing the mineralization being expressed extra-cellularly in GH and GH-CP gels under the Ost. medium, following the 'crack-line' appearances, it probably illustrates secreted MVs outside the cells during the osteogenic differentiation. Interestingly, MVs do not bind to denatured collagens or gelatins [173] but to type II and X collagen [170] or just collagens [173]. Because of this characteristic, calcium/phosphate ion-containing MVs may have hardly propelled out of the cells but instead stuck intra-cellularly in the monolithic G gel groups. Vice versa, these MVs may have found its extracellular pathways relatively easily in between the porous heterogeneity of GH and GH-CP gels.

This existence of porosity in heterogenic GH gel (See 3.5.3.) may have created the aforementioned 'crack-like' lines within the gels, in which a new theoretical terminology, **heterogeneous interpenetrating gap striation (HIGS)**, can be introduced. It is then assumed that excreted exosomes with non-collagenous bone proteins (OCN/OPN) and matrix vesicles with calcium/phosphate ions may get trapped within this conceptual interstitial spaces of HIGS. This entrapment may facilitate creating OCN-OPN complexes which positively enhance osteogenic differentiation (See. 4.5.5.1.). Then, MCs with inner calcium/phosphate ions surrounded by its phospholipids may initiate its own nucleation of nanocrystals, as shown in the extracellular mineralization of our gels (Fig. 4-5). A larger size of fluorescent expressions can be explained with a reported study exhibiting the aggregation of osteoinductive or differentiation factors [174]. According to our data, we propose that HIGS is formulated through: 1) inhomogeneity of mixing different gel types; 2) proximal deformation of gels surrounding an active osteogenic cell; and 3) progressive entrapment of exosomes and MVs, creating a physical spatial gap, positively influencing the osteogenic differentiation.

4.5.7. "Cling Osteogenesis" theory: simultaneous contact and distance osteogenesis

In bone tissue engineering, numerous methods have been engaged to provoke *de novo* bone formation in non-mineralized hydrogels [175]. Particularly, the addition of inorganic or calcium phosphate particles has been incorporated and observed producing subsequent well-integrated mineralization with surrounding tissues, yet the sequential mechanism has not yet been introduced. A classic investigation of new bone formation from implanted calcified cartilage [176] potentiates a possible simultaneously active *de novo* bone formation within GH-CP.

Throughout our results, we propose a theoretical concept, called **"cling osteogenesis"** (Fig. 4-8), as a new bone tissue engineering perspective. This terminology describes a simultaneous *de novo* bone formation of contact and distance osteogenesis, followed by ultimate interconnection through "cling zone" as a bridging moiety. **Distance osteogenesis (DO)**, first termed in describing a phenomenon of peri-implant bone formation from the pre-existing bone towards the implant surface [177], is used as a description of osteogenic differentiation at HIGS (See 4.5.6.) comprised of exosomes with non-collagenous bone proteins and matrix vesicles containing hydroxyapatites. **Contact osteogenesis (CO)** is also a term originally describing peri-implant endosseous healing in such a way that osteogenic cells initiate its first *de novo* bone formation from the implant surface [178]. Similarly, in our concept of "cling osteogenesis," CO is used to represent such osteogenic anabolism originating from the surface of CP particles. Because DO and CO co-occur in multiple areas within the gel substratum, the interconnecting zones where CO and DO get adjoined together is termed as "cling zone," where a dynamic gel deformation from actively proliferating osteogenic cells may occur, and therefore attracting more cells, exosomes, and matrix vesicles. These aggregated residues may cause tractional forces as initiating gel deformation in a spread-out spongy fashion (Fig. 4-2 C), becoming a potentially beneficial source of neovascularization and providing room for new bone formation.

bMSCs differentiate into osteoblast-like cells after up-taking extracellular phosphate ions (See 4.5.5.3.), followed by releasing osteoid matrix [179] via exosomes and matrix vesicles (See 4.5.6.) to the regions at CO and DO simultaneously. These matrices of osteoid moieties, comprised of collagen fibrils, proteoglycans, and non-collagenous proteins, are known to get larger and thicker through mineralization of apatite formations [180]. This enlargement advocates the continuous growth of calcium phosphate nucleation from both CO and DO. Further, these crystalized minerals can accumulate between fibrillar spaces but also within the

fibrils themselves [181], supporting the initiation of DO within embedded hydroxyapatites of aggregated matrix vesicles at HIGS. Within the heterogenic biopolymers of GH-CP, these CP nucleation residues may have strengthened its physicochemical strength (See Chapter 3) due to the fact that positively charged polymers attract negatively charged units such as carbonate and phosphate [86], while negatively charged carboxyl groups join with calcium ions, directing mineral nucleation and propagation [88, 89]. Since the stiffness of osseous structures is dictated not by the mineral density but by the orientation of apatite crystallization [182], this theoretical cling osteogenesis of interconnecting *de novo* bone formations within C.O. and D.O. may further progressively improve its stiffness of this graft architecture in terms of providing densely formulated fibrillation as a multi-directional mesh net framework.

4.6. Summary

Viability testing of different gel groups (G, H, GH gels) was performed to assess the cytotoxicity of each biopolymer substratum, followed by the morphology analysis of bone marrow-derived mesenchymal stem cells (bMSCs). Then, different gel combinations (G, GH, GH-CP gels) were grouped to evaluate proliferation (Ki67); contractility (α-smooth muscle actin, α-SMA); differentiation (osteocalcin/osteopontin, OCN/OPN); and mineralization (Alizarin Red S, ARS, staining). For viability, G and GH gels revealed a highly favorable state, while H gel showed inferiority. Each gel illustrated different morphological traits of bMSCs on the G gel as mostly elongated; the H gel as mostly rounded; and the GH gel as half mixed. With no apparent differences among the three gel groups, α-SMA showed a prominent expression compared to Ki67 levels. Interestingly, GH-CP gel, as expressed with both intra- and extra-cellularly, resulted in a greater osteogenic potential of OCN/OPN levels and ARS staining compared to G and GH gels. From these observations, heterogeneous interpenetrating gap striation (HIGS) and cling osteogenesis theories were termed and introduced.

Chapter 5 - In vitro evaluation of chemoattractants (rhPDGF-BB/rhFGF-2) on GH-CP

5.1. Introduction

To understand the osteogenesis in cell-matrix medium, investigations in the proliferation and differentiation of bMSCs have been studied in previous chapters. In a real clinical application of GH-CP, whether injecting it with stem cells or not, migration of osteogenic cells within the gel matrices becomes pivotal in terms of establishing a deep penetration into the core and adhering onto the surface of CP particles for contact osteogenesis. Our lab's previous reported study discovered that incorporating chemoattractants with the gels induces the attraction and migration of MSCs into the gel system [62]. In normal physiology during the periosteal wound healing, platelet-rich plasma (PRP) fused in the clot with abundant natural growth factors and platelets provokes so-called chemotactic cues, yet this provisional matrix dissolves away fast in our body. Consequently, in recent bone graft science, numerous studies have recently attempted incorporating chemoattractants on the bone graft substitutes, via a process of pre-coating in bone conditioned medium [7, 183]. However, understanding the release rate of these chemoattractants from the graft-host union *in vivo* is realistically challenging, yet we know that the natural provisional matrices get physiologically dissolved away in a couple of days. Therefore, whether utilizing these extra clinical steps of pre-soaking chemoattractants delivers a clinically relevant significance remains as questionable.

5.2. Objective, hypothesis, aims, and rationale

The **objective** of the investigative work illustrated in this chapter is to evaluate the release, migration, and osteogenic potentials of chemoattractants (platelet-derived growth factor-BB or PDGF-BB; and fibroblast growth factor-2 or FGF-2) on GH-CP, as well as to validate a current surgical concept of pre-soaking chemoattractants on the bone graft particulates.

The release potential of chemoattractants from GH-CP is investigated via testing four different gel groups as:

1. G + chemoattractants group: “G+GFs"
2. GH + chemoattractants group: "GH+GFs"
3. GH-CP + chemoattractants mixed in the gel group: "GH-CP+GFs"
4. GH-CP + chemoattractants pre-soaked on the CP: "GH-CP+GFs (pre-soaked)"

The migration and osteogenic differentiation of bMSCs are analyzed via testing four different gel groups as:

1. GH-CP
2. GH + chemoattractants group: "GH+GFs"
3. GH-CP + chemoattractants mixed in the gel group: "GH-CP+GFs"
4. GH-CP + chemoattractants pre-soaked on the CP: "GH-CP+GFs (pre-soaked)"

Our **primary hypothesis** is that incorporating the chemoattractants in GH-CP improves its migrative potential and osteogenic differentiation. A **second hypothesis** is that pre-soaking the CP particles with chemoattractants contributes as a more favorable modality of bone tissue engineering (BTE) in terms of sustained release potential and chemotaxis of bMSCs.

The **specific aims** are to: 1) measure the total release (%) of rhPDGF-BB/rhFGF-2 from the different gel groups [G+GFs, GH+GFs, GH-CP+GFs, and GH-CP+GFs (pre-soaked)]; 2) quantitatively analyze the migration of bMSCs in different gel groups [GH-CP, GH+GFs, GH-CP+GFs, and GH-CP+GFs (pre-soaked)]; 3) assess the osteogenic differentiation of gel groups in regards to spatial distribution.

Along with previous findings on the heterogeneity of GH (See 4.5.4. and 4.5.6.) and the influence of CP addition (See 3.5.4. and 3.5.9.) on GH-CP, as well as the major clinical enigma of pre-soaking effect, it becomes logical to question the progressively releasing phenomenon of chemoattractants from the cross-linked gels. This investigation will allow us to learn the sustainability of chemoattractants within different gel combinations, outlining foundational guideline for this modality's future clinical application. Chemoattractants of this chapter (rhPDGF-BB/rhFGF-2) have been selected due to the fact that one of the most abundant platelet-derived growth factors is PDGF-BB [13], and FGF-2 is a popularly utilized cell modulator [184]. Particularly, many reported studies have demonstrated the synergetic effectiveness of PDGF-BB/FGF-2 on the growth of MSCs [185–188]. In spite of the currently available platelet-rich plasma (PRP) utilization, this chapter has rather focused more on investigating the behaviors of MSCs and the influence of pre-soaking chemoattractants on CP particles, as well as their dynamic influence on the osteogenic differentiation, via using only two growth factors. Prior to *in vivo* trial in the near future, incorporation of PRP may be our next trajectory experiment.

This chapter has explored various new *in vitro* experimental methodologies. This chapter is the first study recording a live-cell monitoring on the early migration of bMSCs within cross-linked cell infused gel/particle composites, along with novel quantification criteria outlining the cell velocity, acceleration, and randomness behavior. This chapter is the first investigative work looking at whether the addition of CP particles inside gel matrices plays a role in preventing the growth factor release. This chapter is the very first study designing the proof-of-concept that pre-soaked bone graft particulates with chemoattractants may draw the chemotaxis of osteogenic cells.

5.3. Materials and methods

The same laboratory techniques of culturing bMSCs (See 4.3.1.), gel cast fabrication (See 4.3.2.), culturing mediums/replacement protocol (See 4.3.3.), and ICC/IF (See 4.3.5.) from Chapter 4 were utilized for this chapter. However, during the pilot experiments of live-cell monitoring within the 17-hours recording window, under the same *in vitro* setting in Chapter 3 and 4 of gels (i.e. [HRP] as 0.5U/mL and [H_2O_2] as 6.8mM), detectable cell migration was not observed. Then, our next pilot experiments were run with less stiff concentrations of [HRP] as 0.1U/mL and [H_2O_2] as 1.2mM, from the previously reported investigation in our lab (Fig. 3-9 D and E); consequently, we successfully demonstrated the observable migration of bMSCs. Therefore, for this chapter's experiments, to understand the correlation of pre-soaking chemoattractants, the gel concentrations of [HRP] as .1U/mL and [H_2O_2] as 1.2mM were utilized while keeping other experimental methods and materials as the same.

5.3.1. Enzyme-linked immunosorbent assay (ELISA) to detect released chemoattractants (rhPDGF-BB/rhFGF-2)

To explore the release potential from different gel groups, through our pre-established dual-syringe auto-mix injection system (See 3.3.1.), chemoattractants of recombinant human PDGF-BB (PeproTech Inc.) and recombinant human FGF-2 (PeproTech Inc.) were incorporated into the gel fabrication process of different gel groups as G+GFs, GH+GFs, GH-CP+GFs, and GH-CP+GFs (pre-soaked). For this consolidation, the stock solutions of rhPDGF-BB/rhFGF-2 (i.e., 10μg/mL each) were diluted 50 times into the final cast gel with its target concentration of 200ng/mL each. Therefore, for the dual-syringe auto-mix system with a total volume 1.5mL, 30μL of each rhPDGF-BB and rhFGF-2 were loaded to the pre-gelating syringe side of Gtn-

HPA, followed by an immediate cross-linking through an auto-mix tip with its verified mixing capability (See 3.5.5.). For this experiment purpose, rhPDGF-BB and rhFGF-2 were grouped separately in a way to fabricate two different sets of gel casts, and to investigate each growth-factor's individual behavior in GH-CP. Each drop of injection was incrementally dispensed on a total of six cryotubes as a serial loading until emptying all of the volumes from the syringe, allocating each tube with an approximately 230μL volume of cast gel. Then, 1mL of PBS was put inside each tube at 37°C for 7 days, along with daily collection of the PBS with released rhPDGF-BB/rhFGF-2. Starting on the first day, 500μL of the solution was collected before refilling another 500μL of PBS on each gel group, and this collection process continued for 7 days. The total time duration of 7 days was chosen because it is the most activated, chemotactic, migrative phase of MSCs in periosteal wound healing, where the initial sign of woven bone formation appears [189].

Released rhPDGF-BB/rhFGF-2 were detected by using a human PDGF/FGF-basic standard ABTS ELISA development kits. Rabbit Anti-Human PDGF-BB/FGF + 2.5mg D-mannitol were diluted with PBS to a concentration of 1.0μg/mL and captured on a 96-well ELISA plate (Costar® Assay plate, coming, Kennebunk ME, USA) overnight at room temperature. After washing one time with 0.05% Tween-20 in PBS and two times with PBS, the plate was blocked with 300μL of 1% BSA in PBS for 2 hours at room temperature. After washing with the same aforementioned steps, 100μL of standard solutions (sequentially diluted PDGF-BB standard from 1000pg/mL and FGF-basic from 4000pg/mL) and samples were immediately added and incubated at room temperature for 2 hours. After washing steps, detection antibody was diluted to 0.25ug/mL and added with 100μL per well at room temperature for 2 hours. After another washing steps, Avidin-HRP conjugate was diluted of 1:2000 and added with 100μL per well at room temperature for 30 minutes. Then, after the last washing steps, 100μL of ABTS liquid substrate was added per well and immediately incubated at a 37°C warm room as foiled. The color change was read using Gen5™ plate reader (Biotek®, Winooski, VT, USA).

5.3.2. Live-cell imaging

For this experiment, direct gel casts (See 4.3.2.) were fabricated incorporated with chemoattractants in groups of GH-CP, GH+GFs, GH-CP+GFs, and GH-CP+GFs (pre-soaked). Prior to injection of gel groups, agarose gel was pre-layered under each well. Then, 30μL of each

rhPDGF-BB and rhFGF-2 (50X dilution) were pre-dispensed into each syringe of a dual-syringe auto-mix model with a total volume of 1.5mL with an approximate volume of 120μL on each sample. Incremental injection method (See 5.3.1.) was also utilized for this experiment to achieve as dispersed growth-factors as possible within each cross-linked gel samples. Our pilot experiments demonstrated that ideal observation time-point of cell migration within the recording duration of 17 hours is around 40 hours after the gel fabrication. Accordingly, fabricated gel casts were stored in the expansion medium at 37°C for two days, prior to recording the live-cell monitoring using Nikon Eclipse Ti-E with HUBC Inverted Phase Contrast Fluorescent Microscope (Cambridge Scientific Corp., MA, USA). During the recording of 17 hours, with image capturing every 10 minutes, the plate with MSCs infused gels was kept in a physiologic state, inside a full enclosure system (InVivo Scientific LLC., MA, USA), achieving a closed loop heating system to keep the sterile gaseous condition and auto-equilibrating humidification system, all of which balanced the intaglio condition of gas to 37°C and 95% humidity. Then, utilizing the Image J software (NIH, Bethesda, MD), cellular migration was investigated in terms of quantifying the velocity, acceleration, and randomness of direction.

5.3.2.1. Randomness behavior quantification

Besides typical velocity or acceleration analysis, a new innovative quantitative analysis of migrating bMSCs was designed for randomness behavior quantification. Each migration tracing of every gel group (Fig. 5-4 A) from Image J Software was analyzed. For this unique analysis, to filter out any potential type I errors, the inclusion criteria of counting randomness incident were created in such ways that: 1) changing degree should be less than 90 degrees; 2) the length of the migration segment should be greater than 10μm (Fig. 5-4 B).

5.3.3. Osteogenic differentiation (distributional OCN/OPN expression)

The same protocols were followed for the thin gel fabrication (See 5.3.2.) to make the same experimental groups of GH-CP, GH+GFs, GH-CP+GFs, and GH-CP+GFs (pre-soaked). Then, the same osteogenic differentiation protocol (See 4.3.3.) was performed for 28 days, followed by the fixation and staining protocols for ICC/IF of osteocalcin (OCN) and osteopontin (OPN) (See 4.3.5.).

Notably, to depict potentially different OCN/OPN fluorescence distribution in reference to CP particles, different segments of locations were categorized as: 1) Calcium phosphate

particles (CP); 2) Osteoid/calcified-bone boundary (OCBB); and 3) Gel (Fig. 5-8 B). Then, as pre-established in the previous chapter (See 4.3.5.), four regions of interests (ROIs) with a diameter of 100μm were selected originating from the most visually fluorescent areas in each location of the aforementioned categories. For further analysis, ROI of calcium (ROI-C), representing combined CP and OCBB together, and ROI of gel (ROI-G) were categorized (Fig. 5-8 C), followed by selecting the four most florescent locations on each group. The sum of these four selected ROIs became either RID of ROI-C or ROI-G. Then, RawInDent (RID) was attained for the following computations as follow:

*RawInDent (RID) = MeanGrayValue * Pixels of selected region*
RID of ROI-C = Sum of RIDs of the four ROI-C selected regions
RID of ROI-G = Sum of RIDs of the four ROI-G selected regions

Total RID = (RID of ROI-C) + (RID of ROI-G)
*% RID of ROI-C = (RID of ROI-C) / Total RID * 100*

For this % RID of ROI-C, merged image files of OCN/OPN were used rather than separately for the ease of interpretation. Mean gray values, utilizing the same analyzing techniques from the previous chapter (See. 4.3.5.), was assessed to compare each gel group's OCN/OPN expression magnitudes (Fig. 5-8 E). Then, % RID of ROI-C of each gel groups containing CP particles were analyzed (Fig. 5-8 D) to understand the correlation between pre-soaking chemoattractants and fluorescence distribution near OCBB (n=6).

5.3.4. Statistics

Data in this chapter are described as mean ± standard deviation, standard error, or min & max. Statistical significance was examined by unpaired t-test, or one- / two-way analysis of variance (ANOVA). In such cases of significance in ANOVA, Tukey's or Fisher's PLSD post-hoc multiple comparison tests were run with a significance criterion of $p < 0.05$ using GraphPad Prism 7 (GraphPad Software, Inc., CA, USA).

5.4. Results

5.4.1. Comparison of released rhPDGF-BB/rhFGF-2

As explained in 5.3.1., collected samples with released rhPDGF-BB and rhFGF-2 were separately examined with ELISA experiment kits (Fig. 5-1 A). Consequently, total release (%) of rhPDGF-BB and rhFGF-2 were independently assessed for the gel groups of G+GFs, GH+GFs, GH-CP+GFs, and GH-CP+GFs (pre-soaked).

One-way ANOVA demonstrated a statistical significance ($p = 0.0004$) between total release (%) of rhPDGF-BB and different gel groups. Tukey's post-hoc test showed a statistically significant difference of GH-CP+GFs (pre-soaked) group on G+GFs group ($p < 0.05$), on GH+GFs group ($p < 0.001$), and on GH-CP+GFs ($p < 0.01$). Average mean values of total release in G+GFs, GH+GFs, GH-CP+GFs, and GH-CP+GFs (pre-soaked), are 7.17 ± 2.16%, 10.17 ± 0.74%, 8.82 ± 1.48%, and 3.90 ± 1.13%, respectively (n=6, mean ± S.D.), (Fig. 5-1 B).

However, one-way ANOVA revealed no statistical significance ($p = .4711$) between total release (%) of rhFGF-2 and different gel groups. Average mean values of total release in G+GFs, GH+GFs, GH-CP+GFs, and GH-CP+GFs (pre-soaked), are 22.14 ± 14.95%, 35.45 ± 24.16%, 21.80 ± 18.30%, 9.178 ± 10.60%, respectively (Fig. 5-1 C).

5.4.2. Migration analysis of bMSCs

Utilizing with Nikon Eclipse Ti-E with HUBC Inverted Phase Contrast Fluorescent Microscope (Cambridge Scientific Corp., MA, USA) and a full enclosure system (InVivo Scientific LLC., MA, USA), 17 hours of live-cell monitoring was recorded on each gel group of GH-CP, GH+GFs, GH-CP+GFs, and GH-CP+GFs (pre-soaked) (See 5.3.2.). Along with the Image J software, randomly selected cells were chosen for manual tracing analysis, which illustrated a clear difference amongst different gel groups visually (Fig. 5-2). This noticeable difference was further quantitatively analyzed.

5.4.2.1. Velocity

Tracings from each group displayed varying total distances (Fig. 5-3 A), and therefore different velocities (μm/min) from each cell group. One-factor ANOVA showed a statistically significant difference in velocity on different gel groups ($p < 0.0001$). Tukey's post-hoc test showed statistically significant differences ($p < 0.0001$) amongst all of the compared gels, except GH-CP and GH-CP+GFs (pre-soaked) ($p < 0.05$), which still showed a difference (Fig. 5-3 C). The average velocities of migrating bMSCs in GH-CP, GH+GFs, GH-CP+GFs, and GH-

CP+GFs (pre-soaked) were 0.052 ± 0.014μm/min, 0.359 ± 0.021μm/min, 0.235 ± 0.040μm/min, 0.097 ± 0.027μm/min (n=6, mean ± S.D.) (Fig. 5-3 C).

5.4.2.2. Acceleration

Because each image capturing of live-cell monitoring was done in every 10 minutes, via dividing each time point's velocity by 10 minutes, it was possible to spread acceleration distributions at each time point (Fig. 5-3 B). Qualitatively, the acceleration frequencies were in order from the most to the least as GH+GFs > GH-CP+GFs > GH-CP+GFs (pre-soaked) > GH-CP (Fig. 5-3 D). One-factor ANOVA showed a statistically significant difference in the average acceleration on different gel groups ($p < 0.0001$). Tukey's post-hoc test showed statistically significant differences ($p < 0.0001$) amongst all of the compared gels, except GH-CP and GH-CP+GFs (pre-soaked) ($p > 0.05$). The average accelerations of migrating bMSCs in GH-CP, GH+GFs, GH-CP+GFs, and GH-CP+GFs (pre-soaked) were 0.005373 ± 0.006286μm/min^2, 0.03735 ± 0.03834μm/min^2, 0.02439 ± 0.007393μm/min^2, 0.01009 ± 0.008305μm/min^2, respectively (n=6, mean ± S.D.) (Fig. 5-3 E).

5.4.2.3. Randomness behavior of bMSCs

As previously depicted, randomness behavior of bMSCs was quantified with a new innovative method (See 5.3.2.1.). Randomness incident turned out to reveal a statistical significance ($p < 0.0001$) amongst different gel groups. Tukey's post-hoc test showed statistically significant differences of GH-CP+GFs on GH-CP ($p < 0.001$), on GH+GFs ($p < 0.001$), and on GH-CP+GFs (pre-soaked) ($p < 0.001$). Average mean values of randomness incident in GH-CP, GH+GFs, GH-CP+GFs, and GH-CP+GFs (pre-soaked) were 0.6667 ± 0.5164, 0.3333 ± 0.5164, 2.833 ± 1.329, and 0.5000 ± 0.5477, respectively (n=6, mean ± S.D.) (Fig. 5-4 C).

5.4.2.4. Qualitative observations in the chemotaxis of bMSCs towards pre-soaked CP particles with rhPDGF-BB/rhFGF-2.

Throughout the live-cell monitoring experiment, bMSCs in GH-CP demonstrated several shreds of evidence in chemotactic migration within the surface of CP particles. bMSCs demonstrated acceleration, changing its morphology from circular (~15μm) to elongated linear (~45μm), as approaching towards the pre-soaked CP particles (Fig. 5-5). Then, once bMSC attaches on the surface of CP particle, it demonstrated its flexible cytoplasmic changes as

becoming cuboidal (~20μm) and adhered linear shape (~30μm) (Fig. 5-6). It was also demonstrated that already adhered bMSC migrating on the surface of CP particle with a much greater elongated shape (~50μm) (Fig. 5-7).

5.4.3. Distributional osteogenic (OCN/OPN) expression

Osteogenic differentiation with OCN/OPN expression in GH-CP was pre-established in the previous chapter (See 4.4.5.), along with its affirmation of *de novo* bone formation (See 4.4.6.). For this experiment, because of utilizing less stiff concentrations of HRP and H_2O_2 (See 5.3.), the migration phenomenon of cells was observed (See 5.4.2.4.), and therefore, a more thorough analysis was conducted (See 5.3.3.) to quantify the distributional aspects of OCN/OPN expressions.

5.4.3.1. OCN expression

Two-factor ANOVA showed a statistically significant difference of OCN expression level on different culturing mediums ($p < 0.0001$) and on different gel groups ($p = 0.0012$) (Fig. 5-8 E). The Fisher's PLSD post-hoc test demonstrated a statistically significant difference amongst Ost:GH-CP vs. Ost:GH-CP+GFs ($p = 0.0003$), Ost:GH-CP vs. Ost:GH-CP+GFs (pre-soaked) ($p < 0.0001$), Ost:GH+GFs vs. Ost:GH-CP+GFs ($p = 0.0046$), and Ost:GH+GFs vs. Ost:GH-CP+GFs (pre-soaked) ($p = 0.0008$). The average mean gray values of OCN in Exp:GH-CP, Exp:GH+GFs, Exp:GH-CP+GFs, and Exp:GH-CP+GFs (pre-soaked) are 1.02 ± 0.22, 0.53 ± 0.23, 1.23 ± 0.49, and 1.93 ± 0.31, respectively (n=6, mean ± SEM). Then, the average mean gray values of OCN in Ost:GH-CP, Ost:GH+GFs, Ost:GH-CP+GFs, and Ost:GH-CP+GFs (pre-soaked) are 2.91 ± 0.45, 4.54 ± 0.57, 9.11 ± 2.08, and 10.14 ± 1.81, respectively (n=6, mean ± SEM) (Fig. 5-8 E).

5.4.3.2. OPN expression

Two-factor ANOVA showed a statistically significant difference of OPN expression level on different culturing mediums ($p < 0.0001$) and on different gel groups ($p = 0.028$) (Fig. 5-8 E). The Fisher's PLSD post-hoc test demonstrated a statistically significant difference amongst Ost:GH-CP vs. Ost:GH-CP+GFs ($p = 0.012$), Ost:GH-CP vs. Ost:GH-CP+GFs (pre-soaked) ($p = 0.0009$), Ost:GH+GFs vs. Ost:GH-CP+GFs ($p = 0.084$), and Ost:GH+GFs vs. Ost:GH-CP+GFs (pre-soaked) ($p = 0.008$). The average mean gray values of OPN in Exp:GH-CP, Exp:GH+GFs,

Exp:GH-CP+GFs, and Exp:GH-CP+GFs (pre-soaked) are 0.82 ± 0.24, 0.61 ± 0.16, 1.15 ± 0.51, and 1.30 ± 0.46, respectively (n=6, mean ± SEM). Then, the average mean gray values of OPN in Ost:GH-CP, Ost:GH+GFs, Ost:GH-CP+GFs, and Ost:GH-CP+GFs (pre-soaked) are 1.95 ± 0.52, 3.34 ± 0.93, 6.05 ± 1.96, and 7.66 ± 1.88, respectively (n=6, mean ± SEM) (Fig. 5-8 E).

5.4.3.3. OCN vs OPN expression

Unpaired t-test with Welch's correction demonstrated that there was no statistically significant difference of OCN vs. OPN on Ost:GH-CP+GFs ($p = .3251$), as well as on Ost:GH-CP+GFs (pre-soaked) ($p = 3784$) (Fig. 5-8 E).

5.4.3.4. % RID of ROI-C

As explained previously (See 5.3.3.), % RID of ROI-C was calculated to measure how much OCN/OPN expression levels were located within the osteoid/calcified-bone boundary (OCBB) (Fig. 5-8 B and C), as opposed within the gel matrices.

One-factor ANOVA revealed a statistically significant effect of different gel groups on % RID of ROI-C ($p = 0.0312$). Tukey's post-hoc test showed statistically significant differences in % RID of ROI-C between GH-CP+GFs and GH-CP+GFs (pre-soaked) ($p < 0.05$). Average mean values of % RID of ROI-C in GH-CP, GH-CP+GFs, and GH-CP+GFs (pre-soaked) are 55.83 ± 24.42%, 54.50 ± 3.94%, and 77.33 ± 7.63%, respectively (n=6, mean ± S.D.).

5.5. Discussion

5.5.1. Chemoattractants are the engineering booster in cellular dynamics.

No doubt, the role of chemoattractants is pivotal in any cellular activities in living organisms. A target cell expresses such binding affinity for the chemoattractants to stimulate genetic expressions via a signaling pathway [190]. In a skeletal engineering perspective, recruitment of osteoblasts via released chemoattractants from the local resorption site dictates bone remodeling [191]. Ectopically embedded bone graft particulates are known to heal through a sequence of endochondral ossification, yet chemoattractant infused scaffolds appear to attract the inducible osteogenic cells from soft connective tissue, differentiating into mature osteoblasts [192]. This signaling property introduces a concept that recombinant chemoattractants may upregulate local stem cells in terms of further enhancing proliferation and differentiation through

the influx of more chemoattractants. Along with our lab's positive preliminary data [62] regarding chemotactic recruitment of bMSCs towards growth factor infused hydrogel, this chapter's study has incorporated the rhPDGF-BB/rhFGF-2 for assessing the chemotactic and osteogenic roles of bMSCs within our gel groups.

5.5.2. rhPDGF-BB and rhFGF-2 have their distinct roles but share a synergetic potential in osteogenesis.

One of the most intensely investigated chemoattractants is a platelet-derived growth factor-BB (PDGF-BB) which is found in the alpha granules within the clotted matrix of platelets and bone matrix [193] during the endosseous or periosteal wound healing. Upon the degranulation of platelet, numerous growth factors like PDGF-AA, PDGF-AB, PDGF-BB, VEGF, EGF, vitronectin get released. Out of these multiple isoforms, PDGF-BB is known as the universal due to its capacity to adhere to most receptor isotypes and its physiological potency [194]. PDGF-BB signals and orchestrates various cellular components such as extracellular matrix, PDGF-receptor presenting cells, endothelial cells, pericytes, mesenchymal stem cells. PDGF-BB adheres to the pericellular matrix via the C-terminus binding motif, while keeping its close proximity to vascular endothelial cells, and formulates a gradient of chemoattractants attracting pericytes [195] which bring new endothelial cells into the site [196]. These chemoattracted pericytes become active osteogenic cells [197]. PDGF-BB serves as a strong mitogen not only for pericytes but also for available activated MSCs [198], as well as modulates other osteogenic factors such as bone morphogenic proteins (BMPs) [199]. PDGF-BB also adjoin the infiltratively growing anastomotic vasculatures with PDGF-BB-expressing pericytes and MSCs, which creates a structural stabilization of the whole matrix union [195]. Further, the clinical usage of rhPDGF-BB has already been established [6], via its incorporation with β-tricalcium phosphate and approval by the US Food and Drug Administration (GEM 21S, BioMimetic Therapeutics) for treating periodontal defects [14].

Similarly, FGF-2 is also a strong mitogen for osteogenic cells [200] and within the bone matrix for controlling the bone remodeling [201], although FGF-2 is more known for inducing endothelial cell proliferation so as to accentuate tube-like trajectory formations [202]. FGF-2 (or bFGF) is known for activating the osteocalcin promoter [144], and FGF-2 infused hydroxyapatite granules has demonstrated proliferation and osteogenic differentiation [203]. Further, bMSCs on the hyaluronate-based polymer scaffold with FGF-2 notably improved

osteogenic expressions and mineralization. *In vivo* studies of administrating FGF both systemically and locally has significantly elevated bone composition and stimulated callus remodeling and endosseous wound healing [204]. Another *in vivo* rabbit skull defect model demonstrated the positive influence of FGF-2 towards bone formation [205]. It is also reported that even a one-time injection of rhFGF-2 has advanced osteogenesis in a distraction model of rabbit tibia [206]. A synergetic effect of FGF-2, when coadministered with BMP-2, has also been shown with increased mineralization [207].

As mentioned above, PDGF-BB and FGF-2 share many common resulting outcomes from signaling such as inducing angiogenesis [208], which is one of the most critical components in bone graft healing [3], although FGF-2 demonstrates a more potent effect on the angiogenesis than PDGF-BB [202]. Interestingly, a recently published study states that co-stimulation of PDGF-BB and FGF-2 has upregulated more additive mitogenic effect. Our study demonstrated a possibility that the addition of rhPDGF-BB and rhFGF-2 synergistically improves its migrative potential and osteogenic differentiation of bMSCs within gel polymers.

5.5.3. Covalently cross-linked status in hydrogels influences the adsorption of chemoattractants with variability.

Just like a provisional matrix of platelets during periosteal wound healing dissolves away in a couple of days, chemoattractants by themselves do not stay *in situ* any longer than that. Especially, exogenously infused rhPDGF-BB persists in a shorter period of time; a reported labeling study states that only 4% of the initial PDGF-BB gets remained at the site after only 96 hours [208]. When a solution of FGF is injected through *in vivo*, it has been shown that they instantly lose their functional capability through the diffusional spread and enzymatic inactivation [209]. To improve this natural dissipative phenomenon, an effort of lengthening the longevity of FGF-2 has been successfully attempted *in vitro* via incorporating a hydrogel, achieving three weeks of sustained release [210].

Protein adsorption and its release property depend on variable aspects of substratum such as charges, molecular morphology, crystallography, and porosity [211]. Hence, utilization of hydrogels for the purpose of the sustained release of incorporated proteins show predictable outcomes. The chemoattractants normally secure themselves within the extracellular matrix (ECM) binding with proteoglycans and fibronectin, and therefore, also adhere within the ECM-mimicking hydrogel matrices until the enzymatic breakdown of hydrogel structures [212], which

is the fundamental concept of sustained release. Particularly, gelatin (i.e. denatured collagen) with negatively charged acidic carboxyl groups (See 3.5.4.) is investigated to hold and carry FGF-2 through ionic bonding [87, 213]. A reported study also mentions that low water content is another factor of improving the release property, therefore its functional effect as well [214].

All of the gel groups in our experiment with rhPDGF-BB revealed much higher adsorption, having less than 10% as a total release in 28 days, compared to with rhFGF-2. This release potential difference may be explained with unequal average dimensional sizes with PDGF-BB as 35 KDa and FGF-2 as 17.2 kDa proteins [215]. The larger size of PDGF-BB could have simply had less likelihood of releasing out of the gel matrices. Another explanation can be binding affinity dynamics. The affinity of immobilized FGF-2 is shown to be low with vitronectin and/or fibronectin [215], whereas PDGF-BB with high affinity [216]. This different binding characteristic could have caused rhPDGF-BB with higher adsorption on our gels (Fig. 5-1 B), while FGF-2 showed a relatively fast release rate (Fig. 5-1 C). Most importantly, GH-CP+GFs (pre-soaked) gel group has upregulated the adsorption property statistically on rhPDGF-BB and grossly on rhFGF-2 (Fig. 5-1 B & C), which potentiates a possibility of even slower releasing capability from the bone graft union to maximize the prolonged *de novo* bone formation. Another interesting observation is with larger fluctuation in rhFGF-2 compared to rhPDGF-BB, referring to a more consistent binding affinity of rhPDGF-BB than rhFGF-2 within polymer matrices.

5.5.4. Incorporation of chemoattractants (rhPDGF-BB/rhFGF-2) promotes cellular migrative potential.

Our lab's preliminary data has already demonstrated such chemotactic attachment and migration of MSCs towards growth factor infused hydrogels [62] but have not yet investigated velocity, acceleration nor the pattern of direction. Typically, MSCs tend to migrate towards more greater stiffness [217], followed by their diverse differentiation potentials or cell fate upon the varying elasticity of surrounded substratum [218, 219] (See 4.5.5.2.), which is well correlated with the rationale of contact osteogenesis and our cling osteogenesis theory (See 4.5.7.). Simply, migrated MSCs may localize themselves onto stiff materials like surface of CP particles or HIGS (see 4.5.6.) and then differentiate into osteoblast-like cells, followed by the excretion of osteoid. In this chapter, 17 hours of live-cell monitoring (See 5.3.2.) has demonstrated distinguishing features of migrative patterns among different groups. From comparing GH-CP vs. GH-CP+GFs

gel, it is clear that addition of rhPDGF-BB/rh-FGF2 has enhanced both velocity (Fig. 5-3 C) and acceleration frequencies (Fig. 5-3 B & D) of bMSCs. Interestingly, OCN/OPN expressions have been also significantly more expressed upon the addition of rhPDGF-BB/rh-FGF-2 (Fig. 5-8 A & E). These findings may portray a favorable osteogenic differentiation with addition of chemoattractants due to improving migrative potential of bMSCs deep into the core of bone graft union or to the surface of CP particles, potentiating the simultaneous osteogenesis and neovascularization throughout the whole grafted space, instead of limiting on the superficial surface.

5.5.5. Addition of CP particles dissipates the directional cues of bMSCs but increases osteogenic differentiation.

The addition of CP particles has been shown to increase both mechanical properties (See 3.5.4.) and therefore osteogenic potential (See 4.5.5.) as well. In our study, incorporating growth factors has demonstrated its positive influence on cellular migrative potential (See 5.5.4.), which may enhance cellular penetration within the gel matrices for more spread-out osteogenesis. Interestingly, a reported study states that the influence of growth factors has been only observed with the soft substratum, whereas stiff substratum is sufficient enough to lead osteogenic differentiation by itself whether or not in the existence of growth factors [220], which emphasizes the key role of mechanical stiffness of gel polymers upon its osteogenic lineage.

In our results, the addition of CP particles (GH+GFs vs. GH-CP+GFs) has affected the directional cues of bMSCs becoming from unidirectional to multidirectional (Fig. 5-3 A). This observation is confirmed by another analysis of randomness quantification (Fig. 5-4 C), where incorporating CP particles in the gel polymers clearly makes bMSCs migrating in a more randomly fashion. This interesting cellular behavior may be due to affected elastic and compression modulus within the gel complex from added CP particles (See 3.5.4.), as simply creating mechanical irregularities for various cellular trajectory pathways. Plus, released mineral ions from CP particles (See 4.5.5.3.), along with aggregated bone matrix complexes within HIGS (See 4.5.6.), may have formulated both physical and ionic interconnections to scatter cellular direction. It is reasonable, then, to state that incorporated rhPDGF-BB/rhFGF-2 have affected bMSCs in both GH+GFs and GH-CP+GFs by looking at the similarly upregulated acceleration frequencies (Fig. 5-3 B & D). Nevertheless, looking at the different average values of velocity (Fig. 5-3 C) and acceleration (Fig. 5-3 E) between Ost:GH+GFs vs. Ost:GH-CP+GFs, the

dissipative role of CP particles upon cellular migration is reinforced. Although this affected cellular migration may seem to negatively affect the osteogenic differentiation, it has indeed expressed a higher level of OCN/OPN (Fig. 5-8 A & E). This finding can be correlated with a reported study revealing that cellular migration is an early fraction of osteogenesis, where the migrating potential disappears by the time MSCs begin differentiating for osteogenesis with increased adhesiveness [221]. These findings and insights give a comprehensive perception that infused CP particles seem to disrupt unidirectionally migrating bMSCs but at the same time intensifies osteogenic potential.

5.5.6. Pre-soaking CP particles in chemoattractants (rhPDGF-BB/rhFGF-2) upregulates its adsorption, chemotactic attachment of bMSCs, and therefore more contact osteogenesis.

Upon the platelet degranulation, pre-synthesized growth factors get secreted in 10 minutes, followed by its 90% secretion in the first hour [222]. Hence, bone conditioned media (BCM), which is a culture medium from autogenously harvested bone chips for 24 hours [223], has been introduced and shown its superior and predictable osteogenic efficiency in collagen barrier membrane [224] and bone graft particulates [8]. Recently, a possible synergistic TGF-β1/BMP-2 activity in BCM has been also demonstrated [225]. However, a rapidly dissolving property of the provisional clotted matrix gives a questionable efficacy of BCM in a real clinical environment.

Along with the demonstration of sustained release of chemoattractants in our gel groups (See 5.5.3.), pre-soaking CP particles has enhanced even slower release rate (Fig. 5-1 B) as less than 5% in 28 days. This outcome may have been due to micro- and macro-porosity of calcium phosphate particles, which provides such highly adsorptive surface features of adhering chemoattractive proteins. Interestingly, acceleration frequency seems concentrated in the middle of recording (Fig. 5-3 B), portraying the existence of possible tracking force from the CP particles towards bMSCs, so-called chemotaxis. Randomness quantification also illustrates that bMSCs become more uni-directional (Fig 5-4 C) towards rhPDGF-BB/rhFGF-2 pre-soaked CP particles during the live-cell monitoring (Fig. 5-5). Notably, the approaching bMSC changes its morphology from an ovoid shape (~8μm diameter) to a linear and elongated shape (~15μm diameter) (Fig. 5-5). Interestingly, once adhered on CP particle surface, bMSCs become larger in size (~25μm diameter) and still exhibits continuous dynamic contractility (Fig. 5-6) and migrating potential (Fig. 5-7) with its much more elongated shape (50~100μm). Infiltrating early

osteoprogenitor cells are similar to and indistinguishable from fibroblastic cells [226], although pre-osteoblastic cells have larger nuclei than fibroblastic precursors [227]. Less activated osteoblasts are known to be more elongated and flatter surface parallel to the bone surface, as well as the volume, in the forms called bone-lining cells [228]. This morphological dynamic well supports our results in this chapter that infiltrating bMSCs may accelerate with fibroblastic appearance until their adherence on CP surface where they become more elongated and larger getting ready for osteogenic differentiation. Particularly, GH-CP+GFs (pre-soaked) gel showed much more exaggerated osteoid/calcified-bone boundary (OCBB) (Fig. 5-8 B) along with highly intensified OCN/OPN expressions (Fig. 5-8 C). Osteogenic cells may have demonstrated a so-called agglomeration behavior through OCBB and even in gel substratum without CP particles (Fig. 5-3 A). Clustered osteoblasts are known to get together via tight junction [229] and communicate with gap junctions [230], all of which may have elevated osteogenic differentiation and osteoid depositions formulating OCBB (Fig. 5-8 B). Fascinatedly, % RID of ROI-C (See 5.3.3.) turns out to be greater in GH-CP+GFs (pre-soaked) than in GH-CP+GFs, which is a possible evidence of more contact osteogenesis. Whether or not more contact osteogenesis creates a difference in structural integrity should be further investigated in a possible next *in vivo* and *ex vivo* mechanical experiment.

5.6. Summary

The total release (%) of rhPDGF-BB/rhFGF-2 from the different gel groups [G+GFs, GH+GFs, GH-CP+GFs, and GH-CP+GFs (pre-soaked)] were measured to assess the adsorptiveness of chemoattractants in each gel group. Then, different gel groups [GH-CP, GH+GFs, GH-CP+GFs, and GH-CP+GFs (pre-soaked)] were evaluated to investigate the chemotactic and osteogenic roles of bMSCs via incorporating rhPDGF-BB and rhFGF-2. Incorporation of the chemoattractants, rhPDGF-BB/rhFGF-2, in GH-CP improved its migrative potential and osteogenic differentiation of bMSCs. It was also demonstrated that pre-soaking CP particles with the chemoattractants results in attachment of bMSCs, with the possibility of contact osteogenesis. The culture medium also exhibited notable effects on this *in vitro* differentiation capability.

Chapter 6 - *Ex vivo* volumetric cone beam computed tomography (CBCT) analysis and *in vivo* feasibility of GH-CP in GBR environment

6.1. Introduction

Previous chapters have successfully illustrated mechanical (Chapter 3), cellular (Chapter 4), and chemotactic (Chapter 5) aspects of GH-CP, enlightening its potential application as a next generation modality of bone tissue engineering (BTE). Along with these *in vitro* experiments, for its ultimate clinical application, translational studies are essential as a next trajectory step. Current *in vivo* animal models of BTE frequently necessitate histological analysis after euthanizing samples. Cone beam computed tomography (CBCT) scan has shown its potential in the implant dentistry market due to less radiographic exposure and better efficiency. However, very few studies have incorporated CBCT as a non-invasive analyzing armamentarium in BTE research, particularly, for the purpose of investigating cross-linked hydrogels. Further, in the field of guided bone regeneration (GBR), although many biological and cellular investigations have been reported, such biomechanical investigations as quantifying the structural integrity of the graft-host union in a physiologically mimicking condition have not yet been explored.

6.2. Objective, hypothesis, aims, and rationale

The **objective** of the investigative work illustrated in this chapter is to optimize a quantitative experimental design protocol for utilizing CBCT on *ex vivo* samples, as well as to evaluate the biomechanical volumetric changes of GH-CP in different GBR defect mimicking lesions (i.e. 1-wall or 3-wall defects) under the physiological setting.

This biomechanical investigation is a comparative analysis with two groups as:

1. Calcium phosphate only group: "CP"
2. Gelatin-hyaluronan calcium phosphate group: "GH-CP"

Our **primary hypothesis** is that GH-CP is more structurally resistant, compared to CP, under the condition of primary wound closure. **A second hypothesis** is that the one-wall defect is more prone to volumetric changes, compared to the three-wall defect in GBR environment.

The specific aims are to: 1) design a quantifiable *ex vivo* goat mandible model with GBR mimicking lesions; 2) calibrate the CBCT location and density setting using the software; 3)

build an *in vitro* device to generate force application, mimicking the primary wound closure tissue tension; 4) compare the volumetric deformations of two different graft groups (i.e. CP and GH-CP).

Although previous chapters of our study have assessed the mechanical and cellular foundations of GH-CP, a further translational interpretation is still necessary before its eventual clinical implementation. This study will allow us to directly compare the biomechanical rigidity of conventional bone graft particulates and GH-CP in GBR mimicking defects. This finding may not only support our previous outcomes of favorable physical and cellular aspects of GH-CP but also introduce a new surgical technique, along with a potential schematic of novel device.

This study consists of several newly established experimental designs and methods. This study is the first investigative work optimizing the repeatable position and density calibration of *ex vivo* bone samples using the CBCT, followed by utilizing implant surgical planning software CoDiagnostiX™. Further, to generate the same mucoperiosteal flap tension force, which is on the range of .15~.2N [55], a novel laboratory device, mucoperiosteal flap tension mimicking torquing (MFTMT) device, has been developed and employed for this chapter. Lastly, this chapter is the first study examining a structural deformation of grafted materials under the physiology-mimicking condition with different GBR defect lesions.

6.3. Materials and methods

6.3.1. Surgically extracted goat mandibular bone pieces

An adult 2-3 years old female Spanish caprine (45 kg) was euthanized during our lab's another IRB approved animal experiment, followed by harvesting the whole goat mandible via surgical dissection (Fig 6-1 A and B). The attained mandible bone was sectioned into multiple pieces (Fig 6-1 C) and dipped into 10% buffered formalin for ten days. After full dehydration in a fume hood for seven days, different volumetric sizes (Fig. 6-1 D) and types of GBR mimicking defects (Fig. 6-1 E) were created for pilot experiments and optimization.

6.3.2. CBCT calibration of position and density

The sectioned mandibular pieces with selected defect sizes and locations for *in vitro* biomechanical testing were optimized with Kodak 9000 Extraoral Imaging System CBCT in terms of finding its repeatable fixation jig position of ideal vertical and horizontal axis (Fig. 6-2

C) and voxel sizes (Fig. 6-2 A and B) in the software system for proper visualization of CP particles and GH gel. Once captured with CBCT, the Hounsfield units of the image were properly segmented to visualize our region of interest (Fig. 6-2 D), followed by alignment calibration in the software CoDiagnostiX™ (Fig. 6-2 E) for a proper display acquisition of cross-sectional images (Fig. 6-2 F).

6.3.3. Mucoperiosteal flap tension mimicking torquer (MFTMT) device

Mimicking the same physiological condition of mucoperiosteal flap tension as a novel laboratory device, mucoperiosteal flap tension mimicking torquer (MFTMT) device was developed and utilized (Fig. 6-3). Assemblies of MFTMT were composed of Straumann RC implant analog/RC screw, urethane dimethacrylate, condensation silicone putty, and nylon-based plastic paper with their functions as a connector, base plate/joining aid, stabilizer, and tissue-mimicker, respectively. Each bony piece was stabilized with polymerized condensation silicone so that we could not only make it firmly stabilized while applying forces through the MFTMT device but also precisely relocate the assembly on the CBCT scanner with pre-marked reference lines. Because of the average mucoperiosteal flap tension for primary wound closure known as .15~.2N [55] and the rotating radius created by urethane dimethacrylate with 1.5cm as connected with polytetrafluoroethylene string, our Straumann torquing ranch was applied with around 0.15Ncm to create a physiologically mimicking biomechanical pressure to the experimental groups of graft materials (Fig. 6-3 B).

6.3.4. Volumetric deformation quantification

Pre-CBCT scans of each bone piece with four samples of our two experimental groups (i.e. CP and GH-CP) were taken, followed by post-CBCT after applying compressive forces with approximately 0.15Ncm torque through the MFTMT device (Fig. 6-3 C). Then each cross-sectional slide of the same reference position were used to measure the deformation. Each positional grit of pre-CBCT on each image was verified for fine-tuning the position of the post-CBCT image through utilizing supplementary anatomical reference points and lines as illustrated on the figure 6-4 A and explained below.

For one-wall defect,

Anatomical reference lines = A) line, created by connecting b) to c), and C) line, created by connecting e) and f)

Then, anatomical points b) and e) were used to create a tangent line to the measuring point of a) and d) each. Pre-CT measured lines for CP and GH-CP were drawn as B) line and D) line, respectively.

For three-wall defect,

Anatomical reference points were designated at the deepest and most corner position as h) and j), followed by drawing anatomical reference lines to the most extended points as g) and i).
Pre-CT measured lines for CP and GH were drawn as E) line and F) line, respectively.

Then, Post-CT scanning was performed in the exact same position as pre-CT, followed by the same positional calibration, calculating the deformation ratio as below.
*Deformation ratio (%) = [(Pre-CT measured line) - (Post-CT measured line)] / (Pre-CT measured line) * 100%*

6.4. Results

6.4.1. Calibration of GBR mimicking defect sizes and locations

According to the pilot experiment with MFTMT device, out of four different defect lesions (socket, one-wall, two-walls, three-walls) (Fig. 6-1 E), only one wall and three wall defects demonstrated its ideal positional relation to the nylon-based plastic side of the torquing device. Further, the ideal volume necessary for the experiment, throughout the pilot experiment with different corticonomy sizes (Fig. 6-1 D), turned out to be approximately 300μL in terms of location and enough thickness to get affected by MFTMT device.

6.4.2. Calibration of CBCT

Each mandibular piece was stabilized with silicone putty fixation and pre-calibrated for its vertical and horizontal axis for repeatable positioning (Fig. 6-3 C). Final optimized radiographic set-up of CBCT was 60kV and 2.0mA, along with voxel size as 76μm.

6.4.3. Volumetric deformation ratio (%)

Two-factor ANOVA revealed a statistical significance of deformation ratio (%) on different graft materials (i.e., CP vs. CH-CP) ($p = 0.0035$) and on different bony defect walls ($p = 0.0191$) (Fig. 6-4 B).

Tukey's post-hoc test showed statistically significant differences in CP:1-wall defect vs. CP:3-wall defect ($p < 0.05$), CP:1-wall defect vs. GH-CP:1-wall defect ($p < 0.01$), and CP:1-wall

defect vs. GH-CP:3-wall defect ($p < 0.01$). The average mean values of CP:1-wall defect, CP:3-wall defect, GH-CP:1-wall defect, and GH-CP:3-wall defect was 17.72 ± 6.25%, 8.12 ± 3.53%, 6.32 ± 2.78%, and 5.05 ± 2.20%, respectively (n=4, mean ± S.D.) (Fig. 6-4 B).

6.5. Discussion

6.5.1. GH-CP presents with a more superior structural integrity under the physiologic mucoperiosteal tension of primary wound closure.

Along with our mucoperiosteal flap tension mimicking torquer (MFTMT) (Fig 6-3), a direct volumetric comparison of CP vs. GH-CP is performed under the physiologically mimicked tension application. Interestingly, GH-CP has demonstrated its superior viscoelasticity in terms of keeping its original shape in one-wall defect or onlay grafting scenario, while three-wall defect has not really shown a statistical difference (Fig. 6-4 A & B). This interesting observation potentiates its future inclusion criteria of clinical application. For example, post-extractive socket preservation may not have a structural benefit from GH-CP, while a tunneled subperiosteal pouch GBR may have its potential efficiency. Combined with our cellular (Chapter 4) and chemotactic (Chapter 5) investigative outcomes, the potential effectiveness of GH-CP becomes even greater with this translational verification of structural integrity.

6.5.2. In vivo feasibility of GH-CP in GBR environment: a complete subperiosteal pouch concept

Current GBR procedures with volumetric expansion from augmentation require a high level of complexities with several technique-sensitive steps like; 1) full-thickness mucoperiosteal flap design; 2) corticonomies for oozing bone marrows; 3) layering structurally stable bovine bone hydroxyapatites on top of osteogenic autogenous bone chips [231]; 4) internal periosteal incision to increase releasing capacity of flap tissue; 5) various types of stabilizing mattress sutures or tacking screws [232].

One of the key factors to achieve a successful periosteal wound healing with bone grafting is the structural integrity of graft-host union [3]. Therefore, clinicians utilize various GBR techniques, emphasizing the importance of stability in grafted materials, such as; 1) layering structurally stable bovine bone hydroxyapatites on top of the osteogenic autogenous bone chips with double layered barrier membranes [233]; 2) utilizing anchorage bone tacking

screws [232]; or 3) creating a tunneled subperiosteal pouch [2, 6]. The current subperiosteal pouch is created with single or double long vertical incisions where insertion of collagen barrier membrane may still be necessary to block the infiltration of epithelial cells from the open wound environment. Consequently, completely injectable bone graft particulates with the hydrogel matrix substratum, through a needle-gauge tube, enables a new paradigm of flapless GBR, where accessing the surgical site through an extremely small surgical access becomes feasible (Fig. 6-5). This conceptual flapless GBR procedure may not even necessitate technique-sensitive suturing closures because *in situ* hemorrhagic clotting may be sufficient enough to achieve primary wound closure. In a case of pre-edentulous alveolar ridges, periosteum detachment without raising any invasive flaps using a tunneling technique can successfully create a fully intact subperiosteal pouch where inserted graft materials can be stabilized through the surrounding attached anatomical mucoperiosteal architectures. This micro-invasive approach can maximize the comfort of patients, shorten the operative duration, and decrease surgical complications.

To come up with a more specific clinical guideline with GH-CP, further investigations of *in vivo* analysis to figure out the amount of new bone regeneration, epithelial tissue infiltrations, total tissue shrinkage, keratinized tissue formation, etc., are necessary to systematically categorize different thickness of necessary keratinized tissues, size of a surgical site, and the amount of necessary subperiosteal pouch volume for a certain amount of expansion. Several clinical scenarios (immediate socket preservation procedure, vertical/horizontal bone augmentation, contour GBR, etc) may also be developed for its practical application.

6.6. Summary

A translational cone beam computed tomography (CBCT) volumetric experiment of GBR in an *ex vivo* model was employed to investigate the structural integrity of the graft-host union. Our *ex vivo* volumetric CBCT analysis revealed structural integrity of GH-CP over the conventional calcium phosphate not in the three-wall but in the one-wall defect.

Chapter 7 - Limitations and future work

For the purpose of cellular investigations, this thesis has chosen a methodology of infusing the mesenchymal stem cells (MSCs) within GH-CP. This investigative method does not necessarily mean that we should incorporate MSCs in our future *in vivo* trials. Especially, since merchandising multiple components together seems realistically challenging in terms of FDA regulatory approval, GH-CP without MSCs may be initially tested on our next *in vivo* pilot trial. Goat bone marrow-derived mesenchymal stem cells (bMSCs) in our thesis experiments have been extracted from one or two animal's blood bone marrow. It would have been much more strong if multiple animals are used for this bMSCs acquisition. Later, if we decide to incorporate bMSCs infused GH-CP as *in vivo* investigations, a highly purified cell line may be necessary.

Since both of gels (Gtn-HPA and HA-Tyr) have been donated from our collaborative company (A*STAR, Singapore), and therefore limited in volume, experimental groups and sample sizes are kept as concise as possible. With the unlimited volume of gels, more groups and sample sizes may have been tested; for example, rheological (Fig. 3-9), compressive (Fig. 3-10), and swelling (Fig. 3-11) tests may have been examined with not only GH-CP but also with G and GH for testing the correlation of different CP particle sizes.

For qualitative and quantitative analysis of osteogenic differentiation and mineralization, confocal immunofluorescence (OCN/OPN and ARS staining) has been investigated with its distributional interpretations. For more robust data support, either polymerase chain reaction (PCR) or western blot test may be conducted as a supplementary *in vitro* experiment, although a thorough methodological design is first necessary to properly and precisely filter out bone matrix adhered CP particles from the gel substratum.

Prior to proceeding to *in vivo* experiment, several supplementary *in vitro* tests may be conducted such as degradation, pH, calcium/phosphate ion measurements in terms of comprehensive data collection. Plus, chemoattractant release experiment and cell tests may be combined together in a way to reveal such cellular response to the released growth factor substrates.

Although migration of bMSCs has been well demonstrated in this thesis via live cell monitoring, a different experimental approach of migration assay can be also performed to visualize the recruitment of cells from the medium attaching to the surface of gel substrate cores.

Plus, live cell monitoring may have been incorporated with fluorescent dyes for its high-grade visualization.

Highly likely, next trajectory experiment may be an *in vivo* trial, probably utilizing a simple rabbit tibial model or cranial bone model with critical size defects. For this trial, GH-CP without incorporating bMSCs can be initially tested to see its efficacy. Then, later, we can decide to incorporate chemoattractants in GH-CP. If so, incorporating method and possible option of utilizing lysate of platelet-rich plasma may be also considered.

Our ultimate goal for GH-CP is its future clinical application at GBR surgical arena, as well as other potential clinical scenarios like recession treatment, periodontal defects and/or peri-implantitis. Therefore, after the aforementioned experiments, possible collaborative work with a company may be considered, followed by patent application of both dual-syringe auto-mix device and GH-CP gel. Then, we can finally apply for FDA approval, as well as final product licensing.

Chapter 8 - Conclusions

Throughout the data from previous chapters, our thesis exhibits an encouraging level of evidence that gelatin-hyaluronan calcium phosphate (GH-CP) can render such an ideal substratum condition with structurally rigid, osteogenic, osteoconductive, and osteoinductive potentials in a realm of bio-tissue engineering. Notably, the establishment of a dual-syringe auto-mix system ensures GH-CP as a truly injectable bone graft delivering modality, which portrays a clinical favorability in translational orthopedic research, particularly, in a conceptual clinical scenario of flapless guided bone regeneration. Both pre-/post-gelated GH-CP has demonstrated microscopically well-dispersed CP particles and bMSCs. This mechanically fine-tunable GH-CP demonstrated higher storage and compressive modulus, and reduced swelling and expansion ratios, compared to gelatin (G) and gelatin-hyaluronan (GH) gels.

G and GH gels also revealed highly favorable viability, while H gel showed inferiority. Each gel illustrated different morphological traits of bMSCs on the G gel as mostly elongated; the H gel as mostly rounded; and the GH gel as half mixed. With no apparent differences among the three gel groups, α-SMA showed a prominent expression compared to Ki67 level. Interestingly, GH-CP gel, as expressed with both intra- and extra-cellularly, resulted in a greater osteogenic potential of OCN/OPN levels and ARS staining compared to G and GH gels.

Pre-soaking of CP particles with the chemoattractants, rhPDGF-BB/rhFGF-2, results in attachment of bMSCs, with the possibility of contact osteogenesis. The culture medium also exhibited notable effects on this *in vitro* differentiation capability.

Along with the aforementioned cellular outcomes, our *ex vivo* volumetric CBCT analysis also revealed structural integrity of GH-CP over the conventional calcium phosphate.

Collectively, these findings provide favorable *in vitro* physicochemical and osteogenic support for GH-CP to be utilized in such flapless GBR surgical arena with its further potentials in incorporating diverse pharmacotherapeutics, such as potential lysates derived from human platelet-rich plasma (PRP) in the future.

Our next work will be an *in vivo* test of the animal model with critical size defects to investigate the osteogenic efficacy of GH-CP.

Chapter 9 - Figures and tables

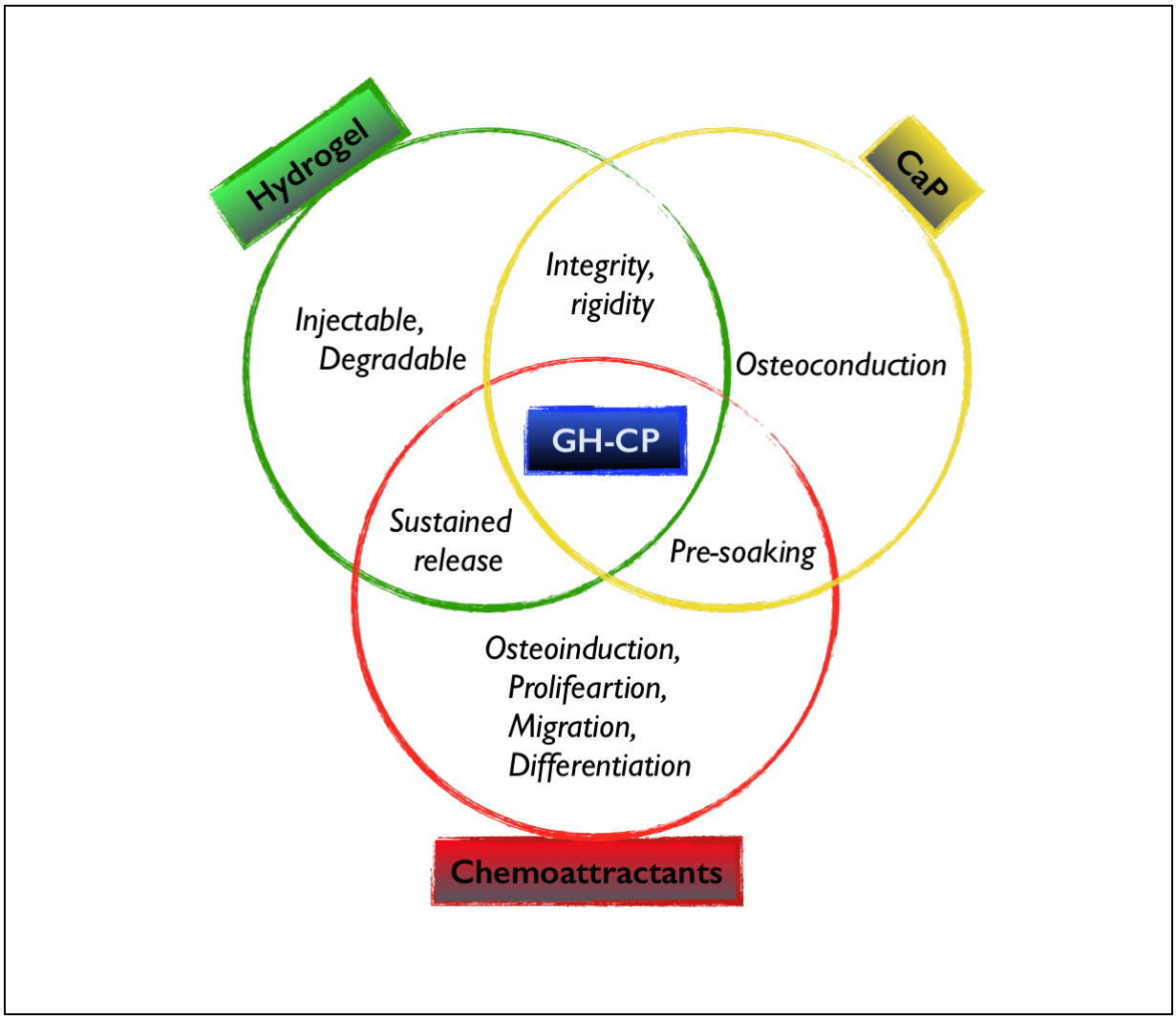

Figure 1-1 *Diagram of components in gelatin-hyaluronan calcium phosphate (GH-CP) (Image courtesy of Young K. Kim).*

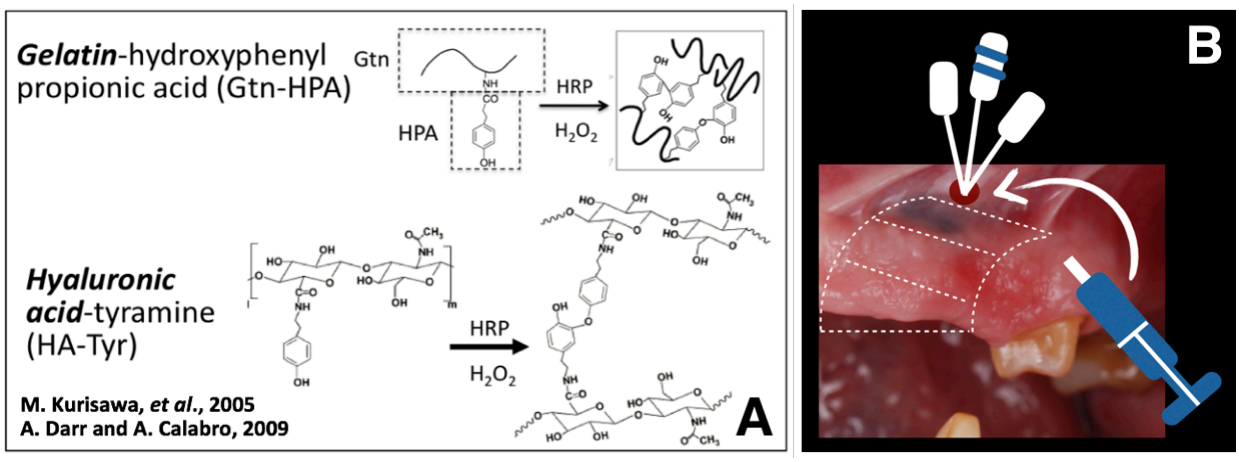

Figure 3-1 (A) *Covalent cross-linking mechanisms of Gtn-HPA and HA-Tyr;* ***(B)*** *Schematic diagram of flapless GBR (Image courtesy of Young K. Kim).*

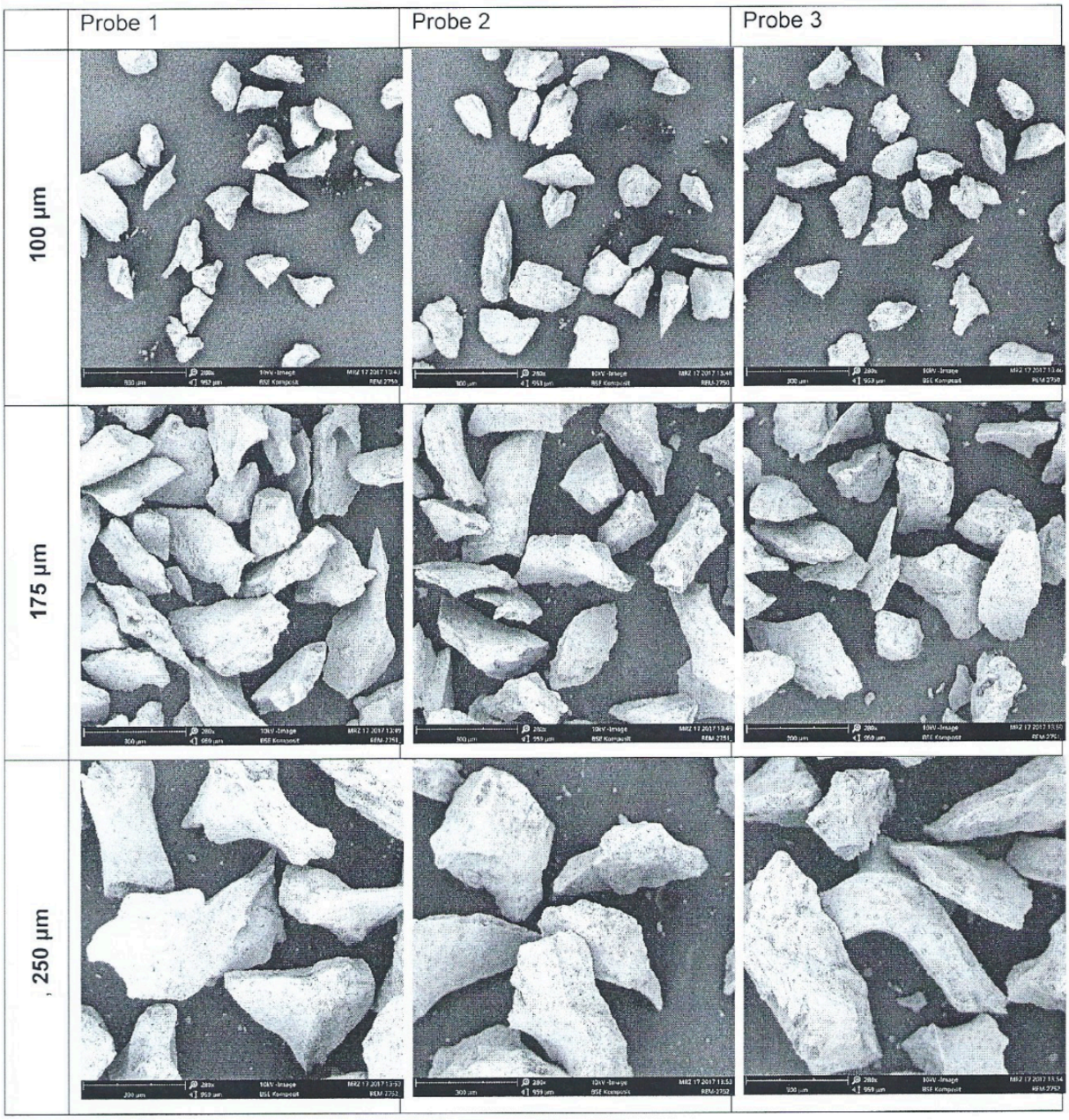

Figure 3-2 *Different sizes of CP particles (~100µm, ~175µm, and ~250µm).*

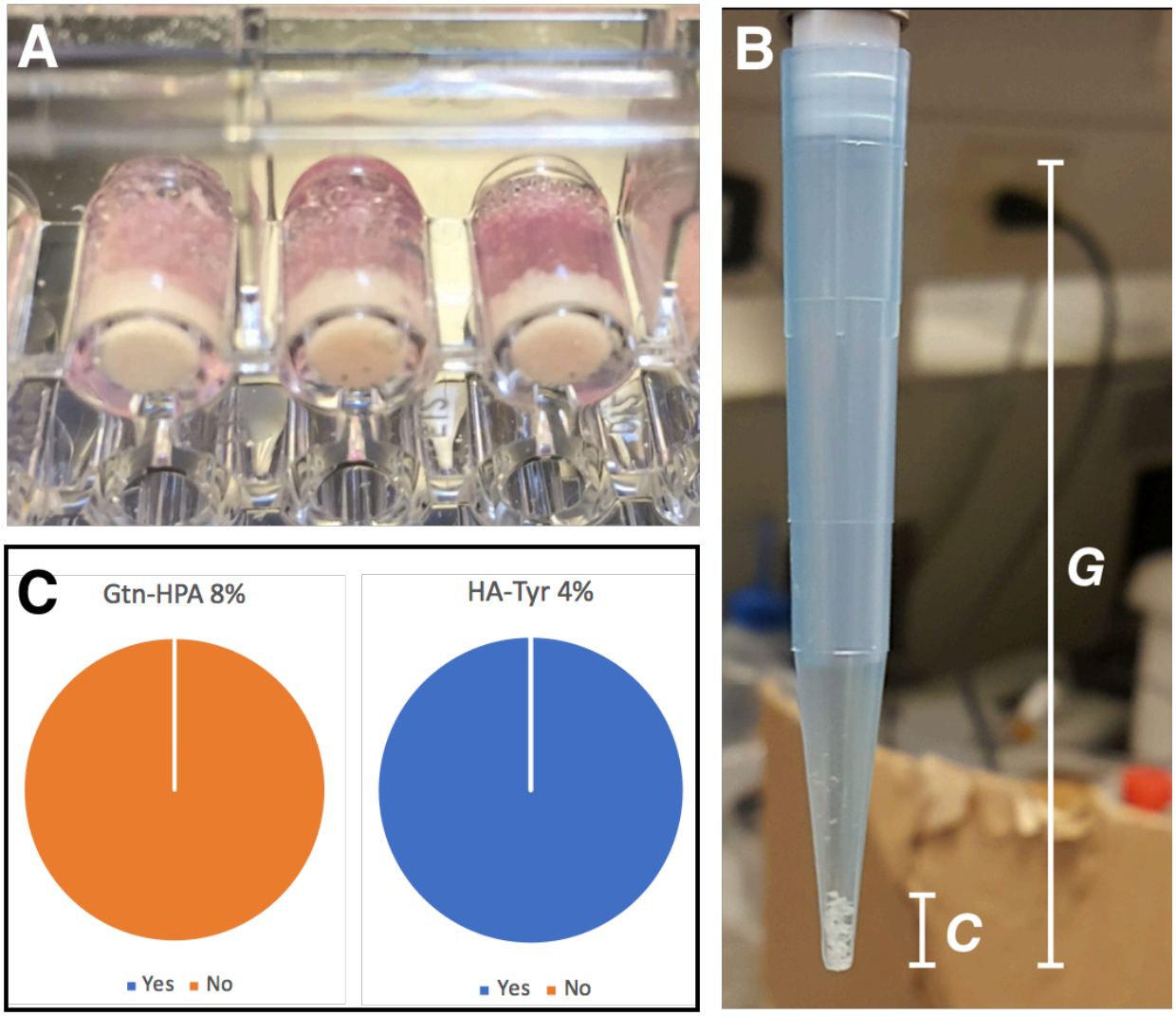

Figure 3-3 *Sedimentation phenomenon* ***(A)*** *Pre-gelation CP sinking phenomenon;* ***(B)*** *Quantitative analysis of clogging issue (C = vertical distance of sinking CP particles, G = total vertical distance of gel);* ***(C)*** *Inclusion pie graphs (n=6).*

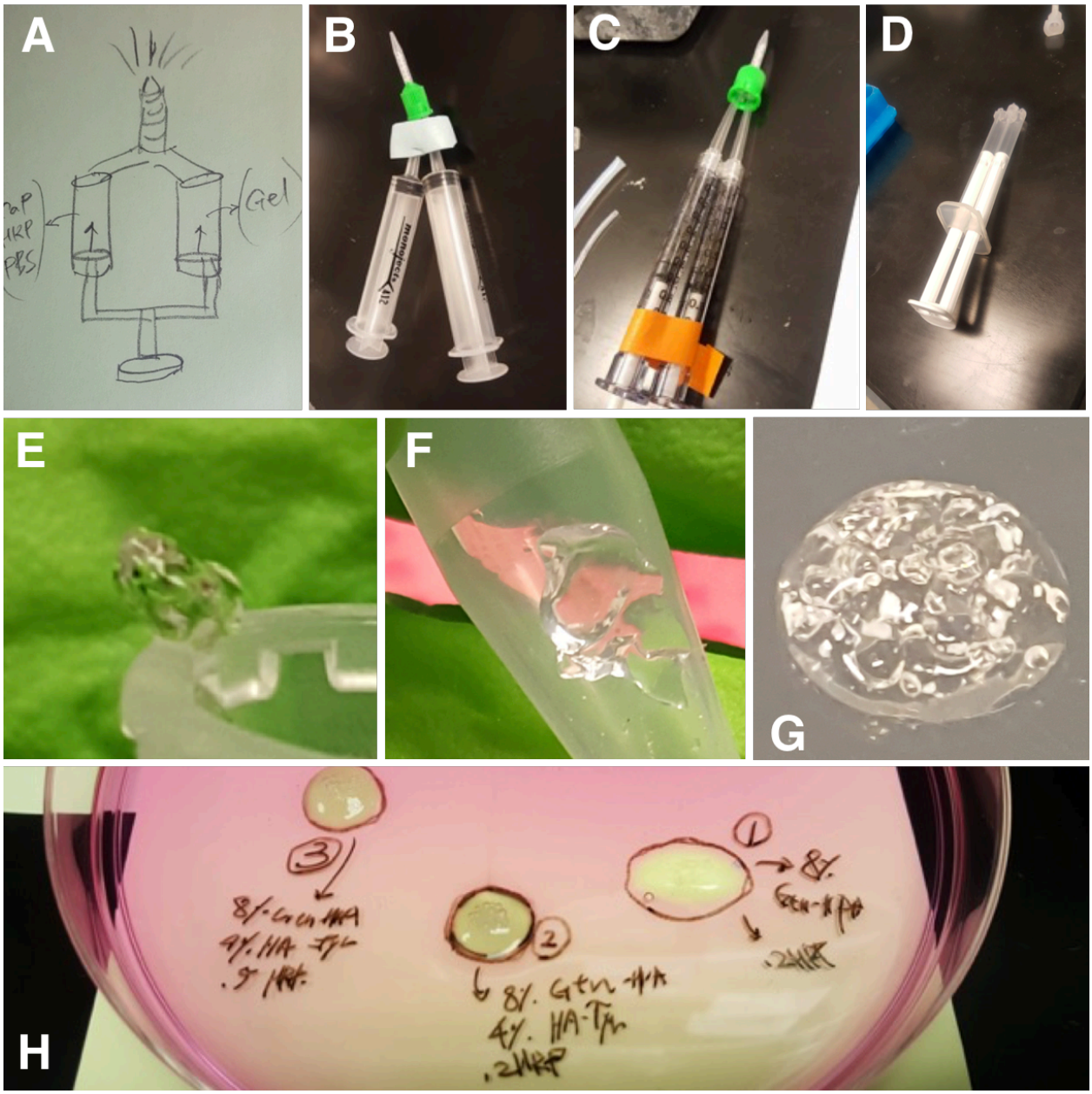

Figure 3-4 ***(A)*** *Schematic drawing of the dual syringe model****;*** ***(B)*** *First prototype;* ***(C)*** *Second prototype;* ***(D)*** *Final syringe system;* ***(E)*** *Too rigidly cross-linked GH gel;* ***(F)*** *Too weakly cross-linked GH gel;* ***(G)*** *Cross-linked GH-CP;* ***(H)*** *Fine tuning [HRP] and [*H_2O_2*].*

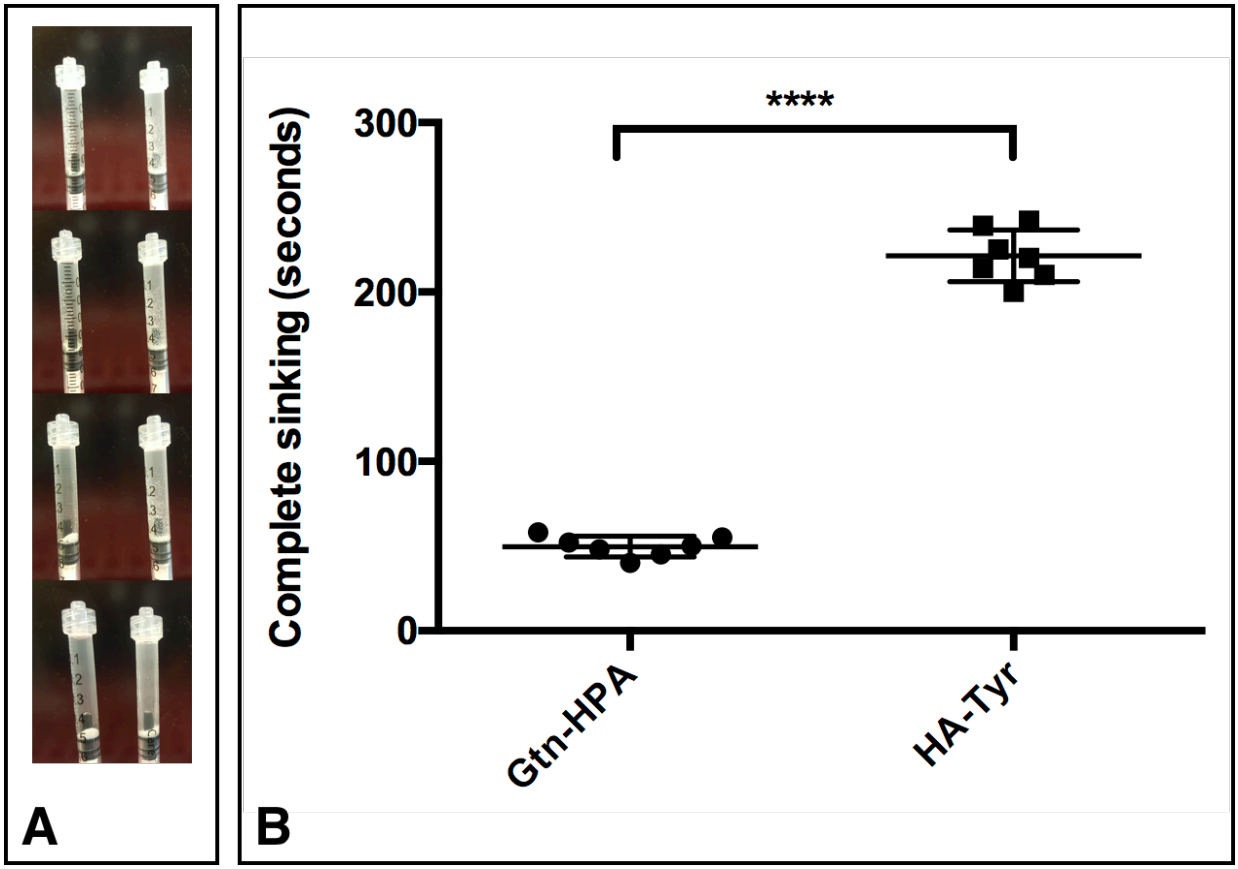

Figure 3-5 (A) *Sequential experimental photographs of pre-gelation CP sedimentation test;* ***(B)*** *Complete sinking seconds (n=7): Unpaired t-test, n=7, ****p-value < .0001.*

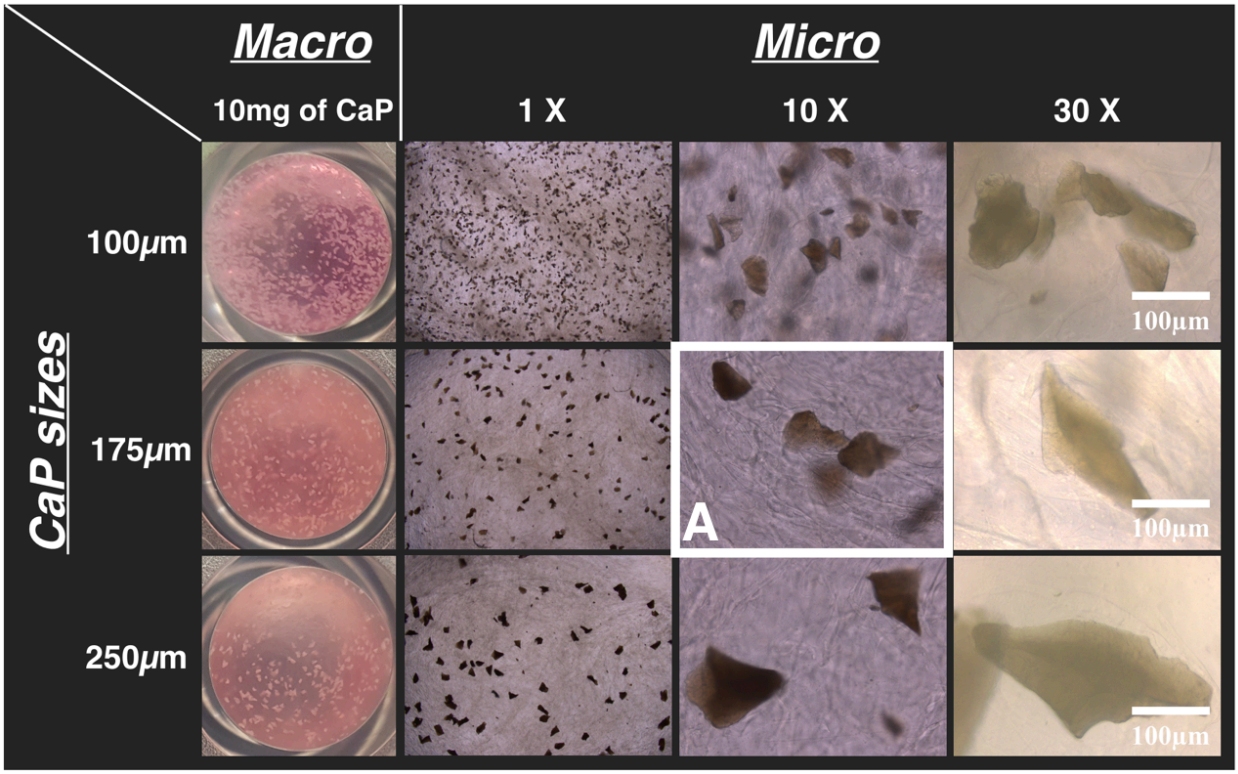

Figure 3-6 *Post-gelation gap distance:* ***(A)*** *Idealized microscopic-view of CP particles (10 w/v%) in GH gel (n=4).*

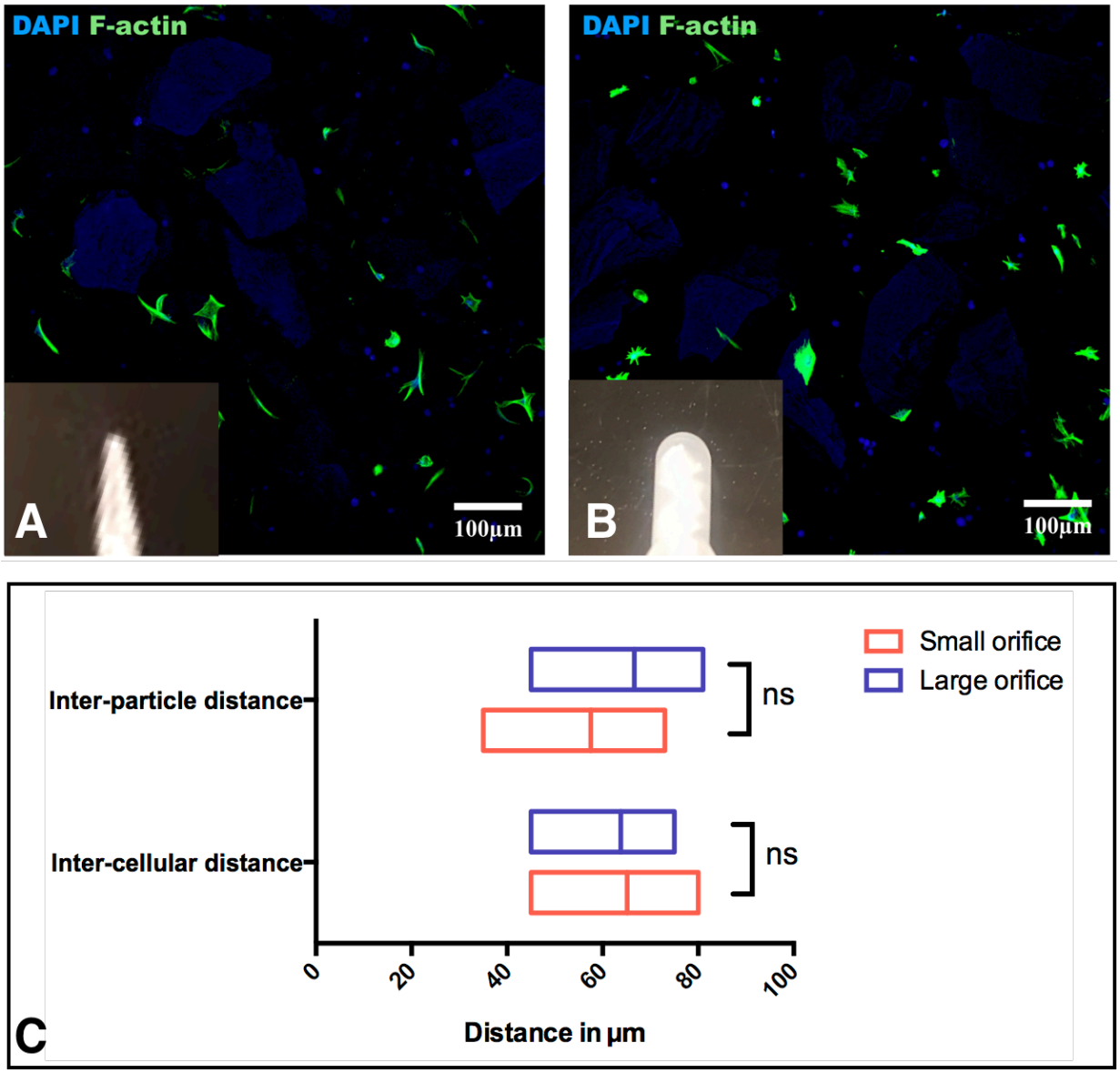

Figure 3-7 *Distribution of bMSCs and CP particles within cross-linked GH-CP through* ***(A)*** *small orifice tip and* ***(B)*** *large orifice tip. Each gel was stained with DAPI and phalloidin, F-actin staining solution (Thermo Fisher), to observe nucleus and actin cytoskeleton;* ***(C)*** *Inter-particle/cellular distance: Two-way ANOVA, n=4, mean ± min & max., ns as p-value > .05.*

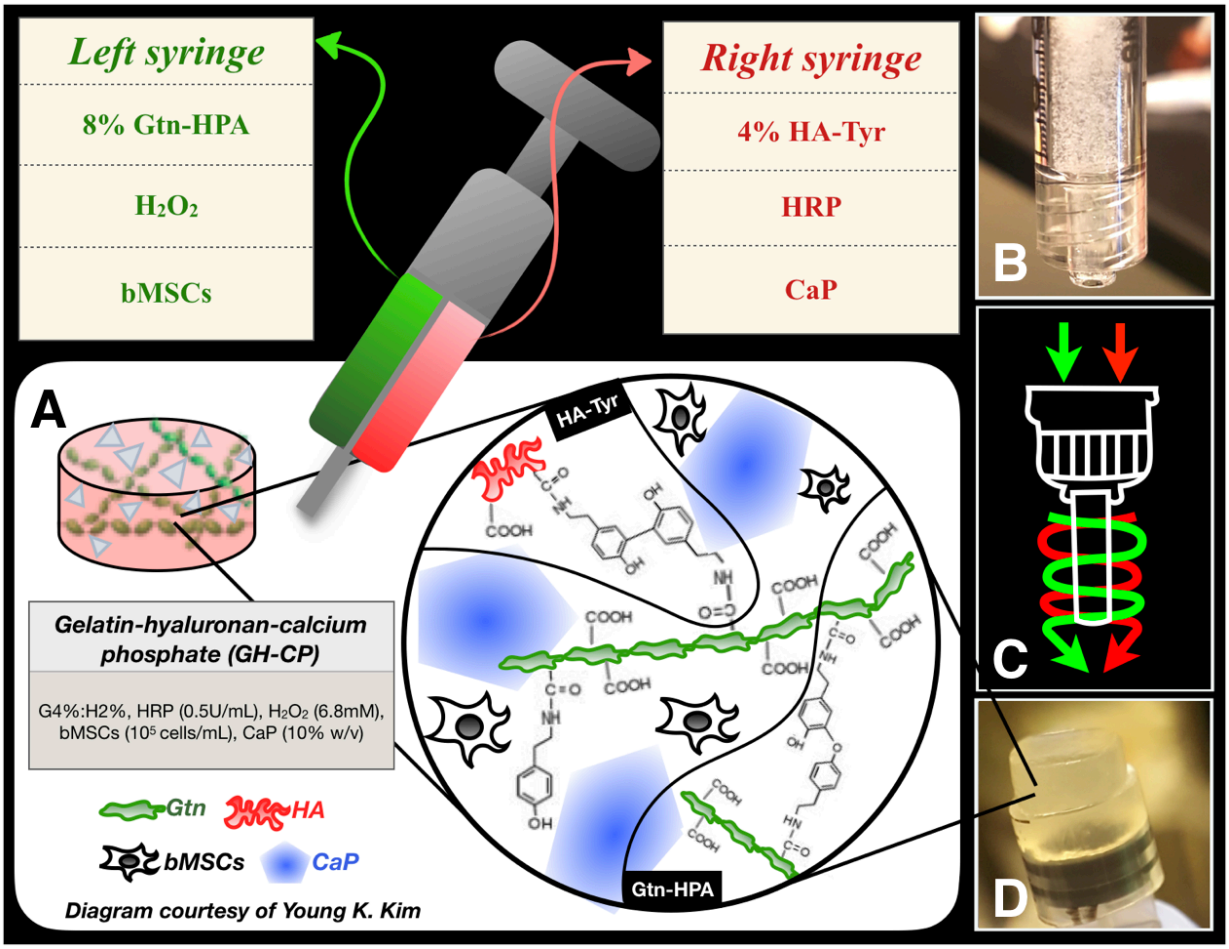

Figure 3-8 *Dual syringe system for GH-CP:* ***(A)*** *Molecular schematic diagram;* ***(B)*** *Dissipated CP particles in pre-gelated HA-Tyr;* ***(C)*** *Schematic of an auto-mix tip;* ***(D)*** *Cross-linked 3D cast sample of GH-CP (6mm in diameter and 3-4mm in thickness).*

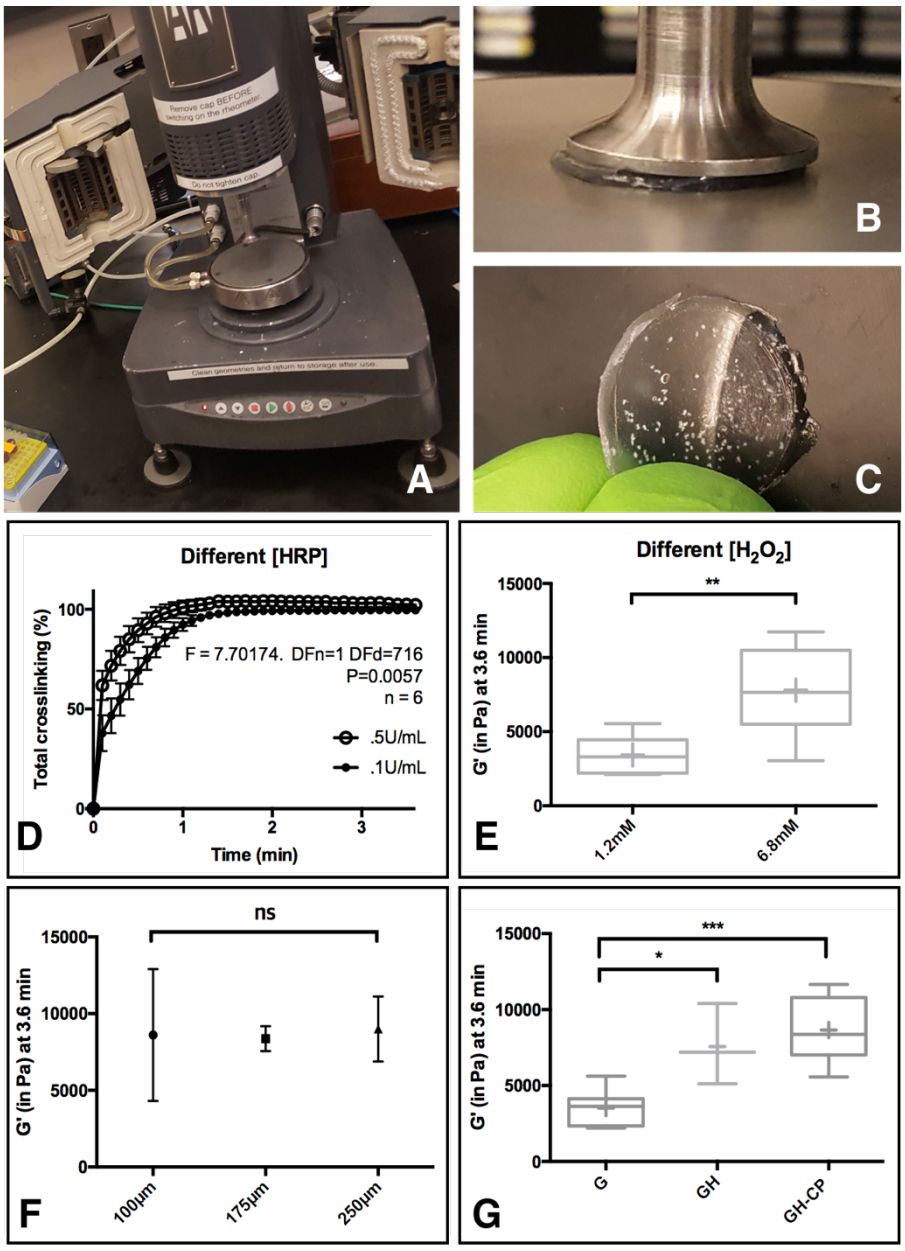

Figure 3-9 ***(A)*** *A Zwick/Roell Z2.5 static materials tester (Zwick GmbH & Co., Ulm, Germany);* ***(B)*** *Before the compression;* ***(C)*** *After the compression;* ***(D)*** *Typical nominal (red) and true stress/strain curves (blue);* ***(E)*** *Typical loading and unloading curve;* ***(F)*** *Compression modulus (E) in Pa with different particle sizes (n=3, mean ± S.D.);* ***(G)*** *E in Pa with different gel groups: One-way ANOVA, followed by Tukey's post-hoc test, n=6, a box-and-whiskers plot, + indicating the mean, *p-value < 0.05, ***p-value < .001.*

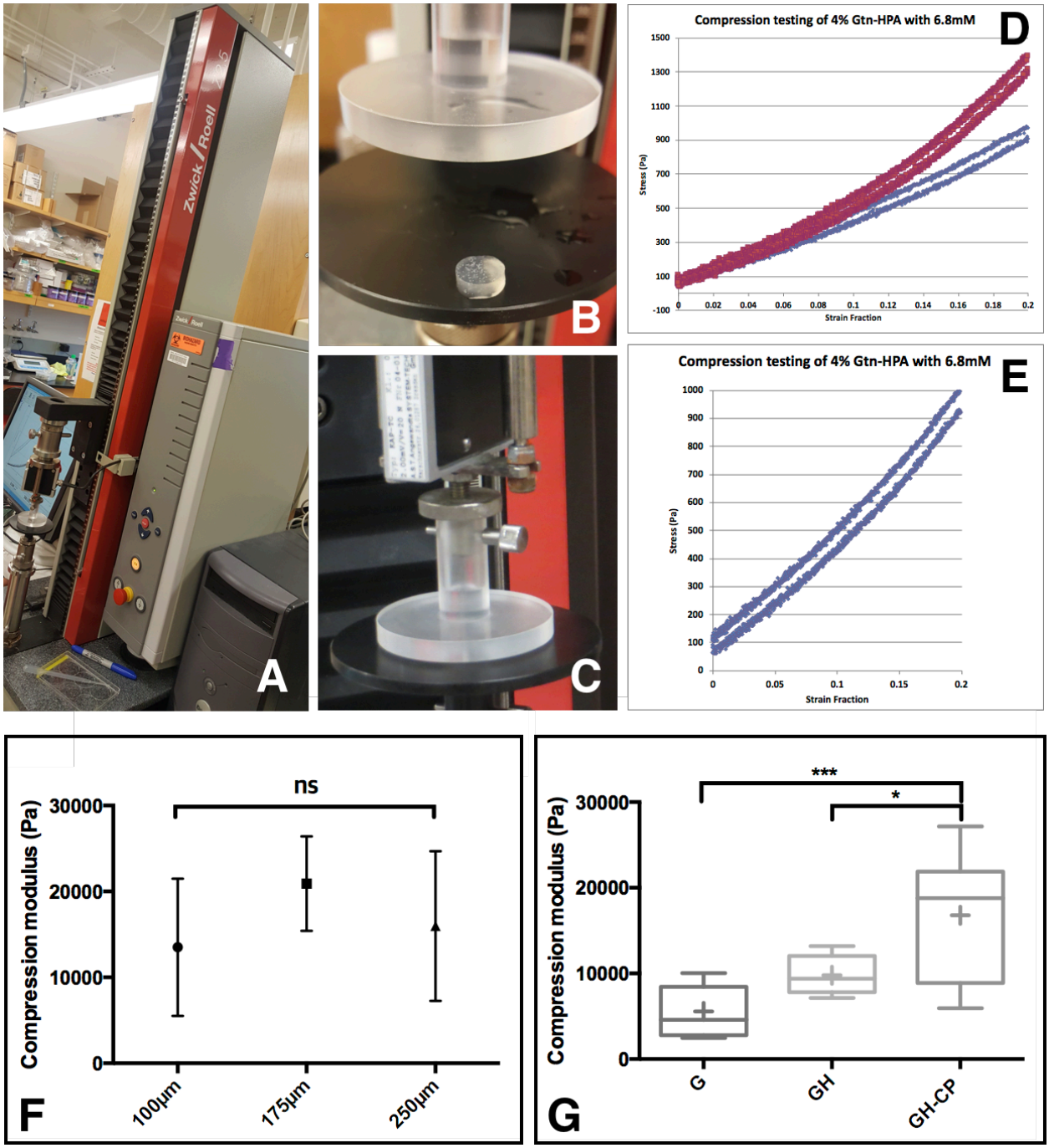

Figure 3-10 (A) *A Zwick/Roell Z2.5 static materials tester (Zwick GmbH & Co., Ulm, Germany);* ***(B)*** *Before the compression;* ***(C)*** *After the compression;* ***(D)*** *Typical nominal (red) and true stress/strain curves (blue);* ***(E)*** *Typical loading and unloading curve;* ***(F)*** *Compression modulus (E) in Pa with different particle sizes (n=3, mean ± S.D.);* ***(G)*** *E in Pa with different gel groups: One-way ANOVA, followed by Tukey's post-hoc test, n=6, a box-and-whiskers plot, + indicating the mean, *p-value < 0.05, ***p-value < .001.*

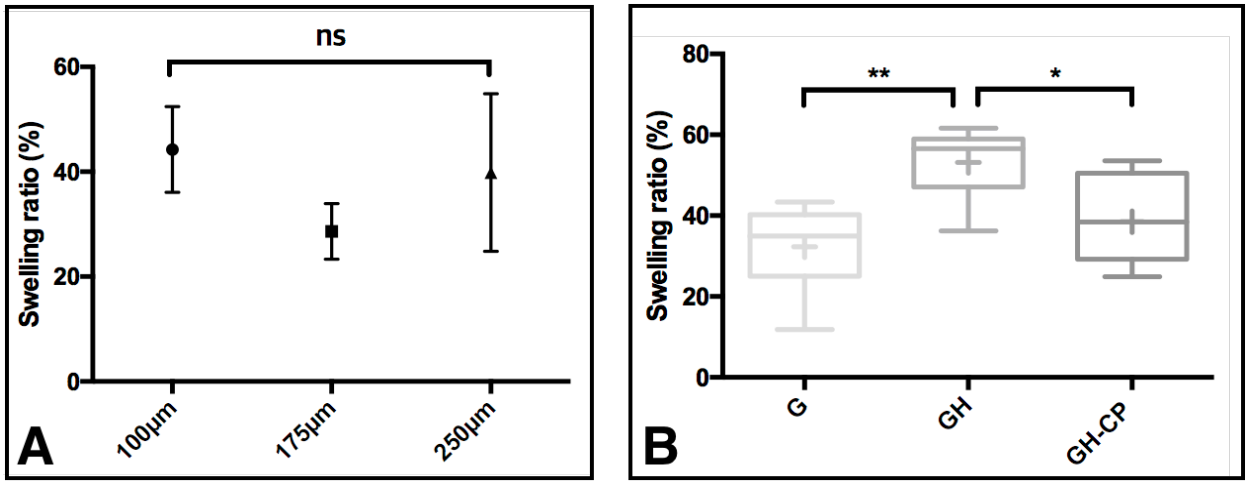

Figure 3-11 (A) *Swelling ratio (%) with different particle sizes (n=3, mean ± S.D.) after 7 days;* ***(B)*** *Swelling ratio (%) with different gel groups: One-way ANOVA, followed by Tukey's post-hoc test, n=6, a box-and-whiskers plot, + indicating the mean, *p-value < 0.05, **p-value < .01.*

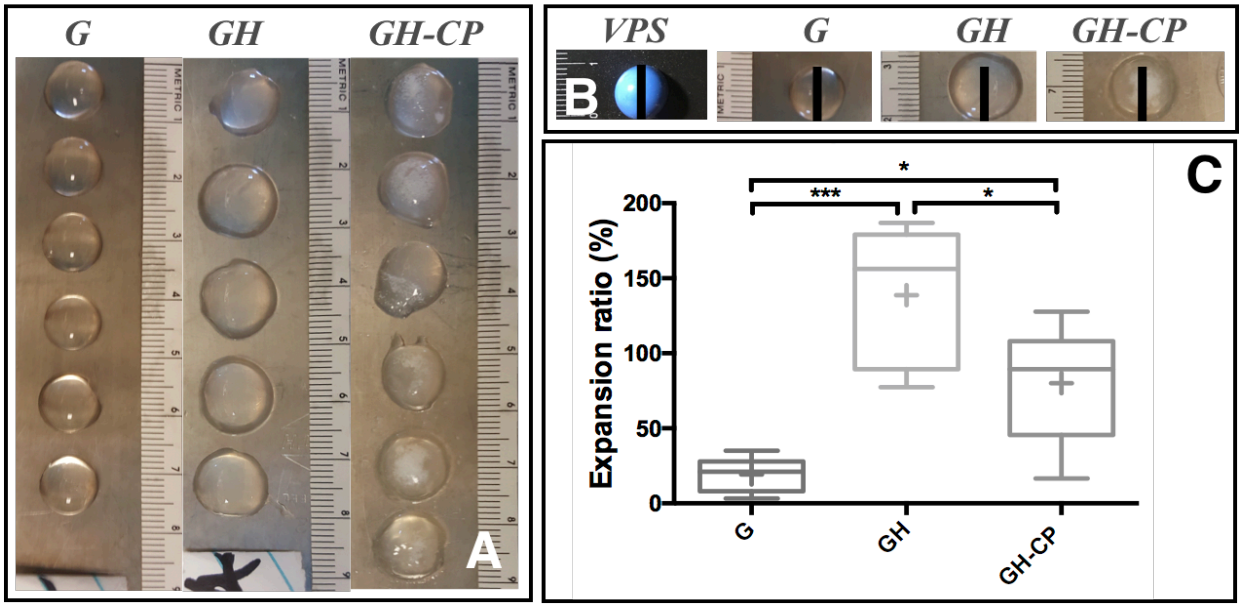

Figure 3-12 (A) *Gross photos of the expanded gel groups after 7 days;* ***(B)*** *Gels with a scaling bar (10mm);* ***(C)*** *Expansion ratio (%) with different gel groups: One-way ANOVA, followed by Tukey's post-hoc test, n=6, a box-and-whiskers plot, + indicating the mean, *p-value < 0.05, ***p-value < .001.*

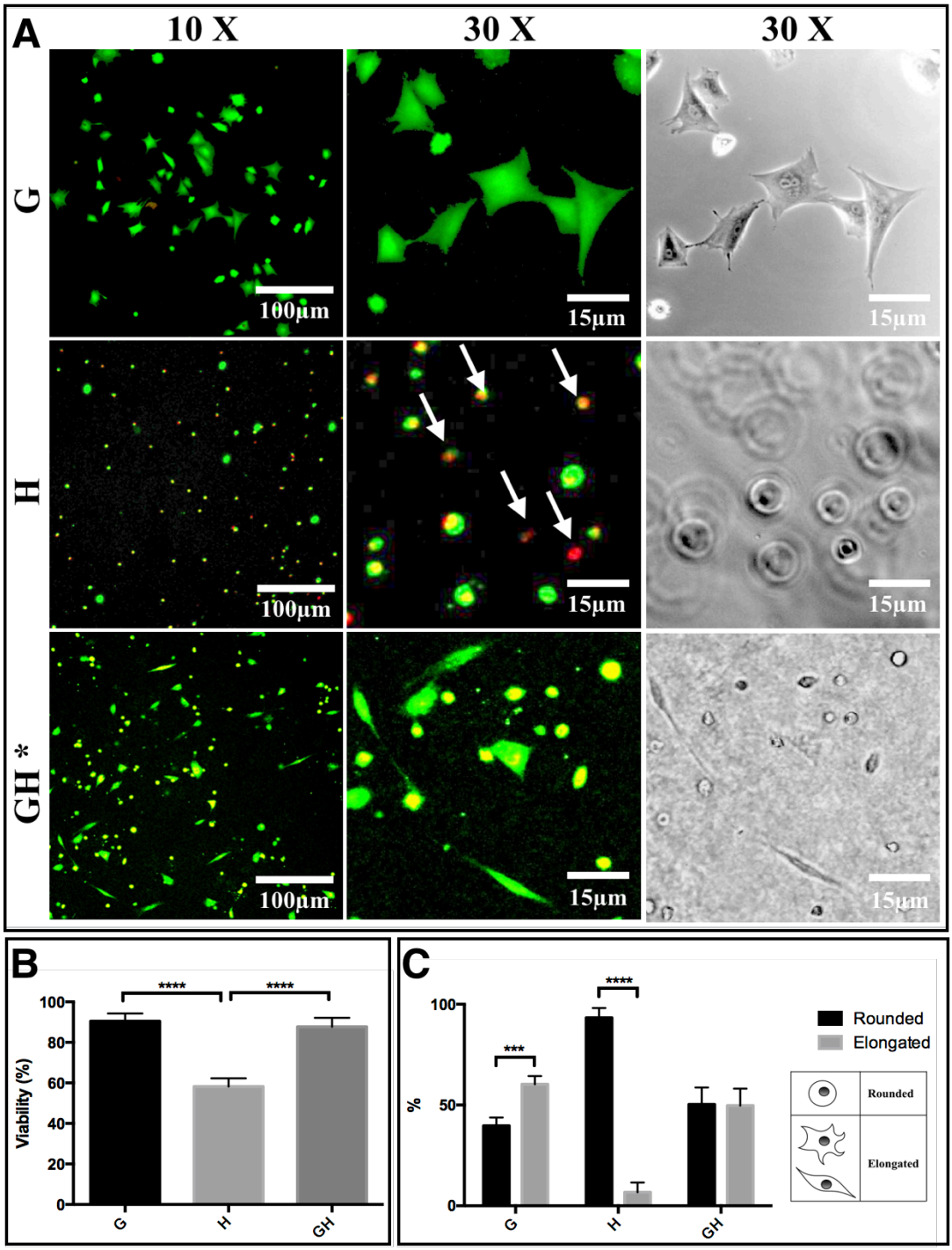

Figure 4-1 ***(A)*** *Live/dead viability cytotoxicity kit was utilized for viability test. Live cell was stained with Calcein AM, while dead cell was stained by Ethd-1 (white arrows). bMSCs in different gel groups were measured, via calculating the ratio of live cells over total cells, after 24 hours;* ***(B)*** *Cell viability for bMSCs incorporated with different gel groups: One-way ANOVA, n=6, mean ± S.D., ****p-value < .0001;* ***(C)*** *Cell morphology ratio within different gel groups: Two-way ANOVA, n=6, mean ± S.E., ***p-value < .001, ****p-value < .0001.*

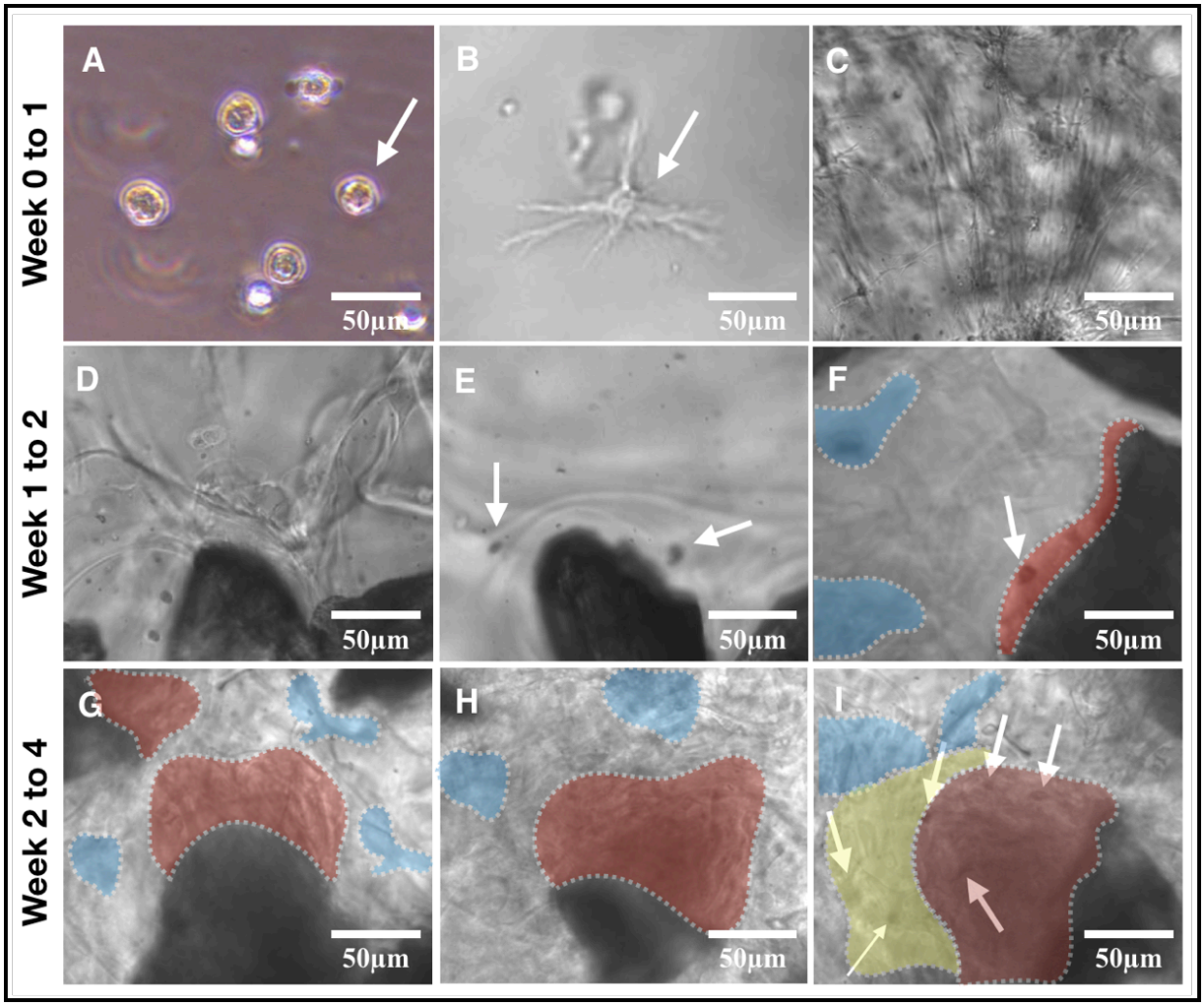

Figure 4-2 *A hypothetical cascade of de novo bone formation of bMSCs (white arrows) in GH-CP (28 days) in vitro under optical microscopy (30 X).*
(A) *bMSCs in expansion medium;* ***(B)*** *bMSCs in osteogenic medium;* ***(C)*** *Inter-connecting lines within GH-CP;* ***(D)*** *Docking MSC on the surface of CP;* ***(E)*** *Adhered MSCs;* ***(F)*** *Osteoid deposition from contact osteogenesis (red) and distance osteogenesis (blue);* ***(G)*** *Initial de novo bone formation;* ***(H)*** *Prolonged de novo bone formation;* ***(I)*** *Cling zone (yellow) from "Cling osteogenesis" theory to form osteoid/calcified-bone boundary (OCBB) (See Fig. 4-8).*

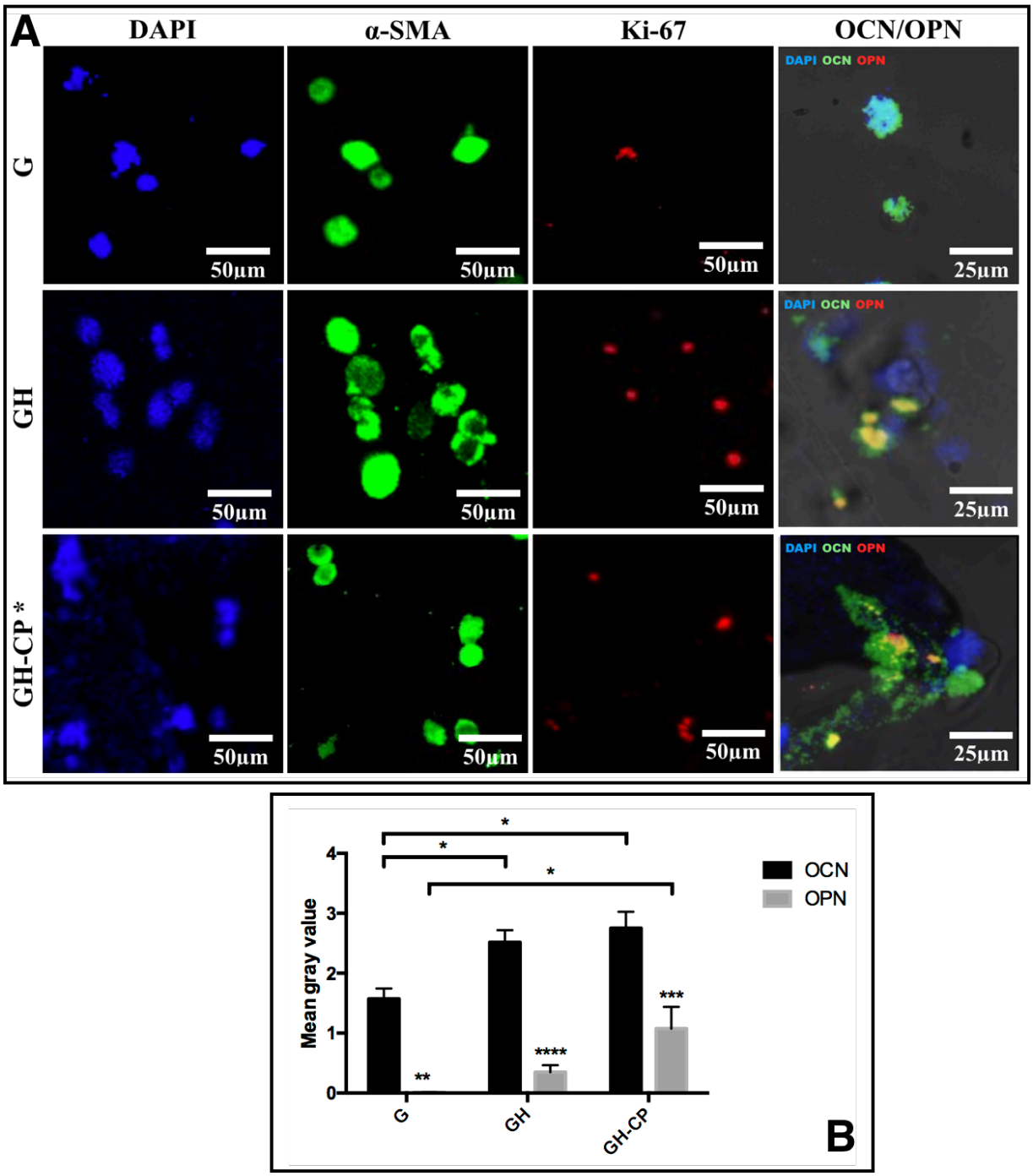

Figure 4-3 (A) *Osteogenic differentiation of bMSCs in different gel groups (28 days) with immunofluorescence staining analysis (n=6): DAPI (1/25,000), anti-alpha smooth muscle actin antibody ab5694 (α-SMA) (1/400), Anti-Ki67 antibody ab15580 (Ki-67) (1/1000), Anti-Osteocalcin antibody ab13418 (OCN) (1/200), Anti-Osteopontin antibody ab8448 (OPN) (1/1000);* ***(B)*** *Mean gray values of OCN/OPN in different gel groups: Two-way ANOVA, n=6, mean ± S.E., *p-value < .05., **p-value < .01., ***p-value < .001, ****p-value < .0001.*

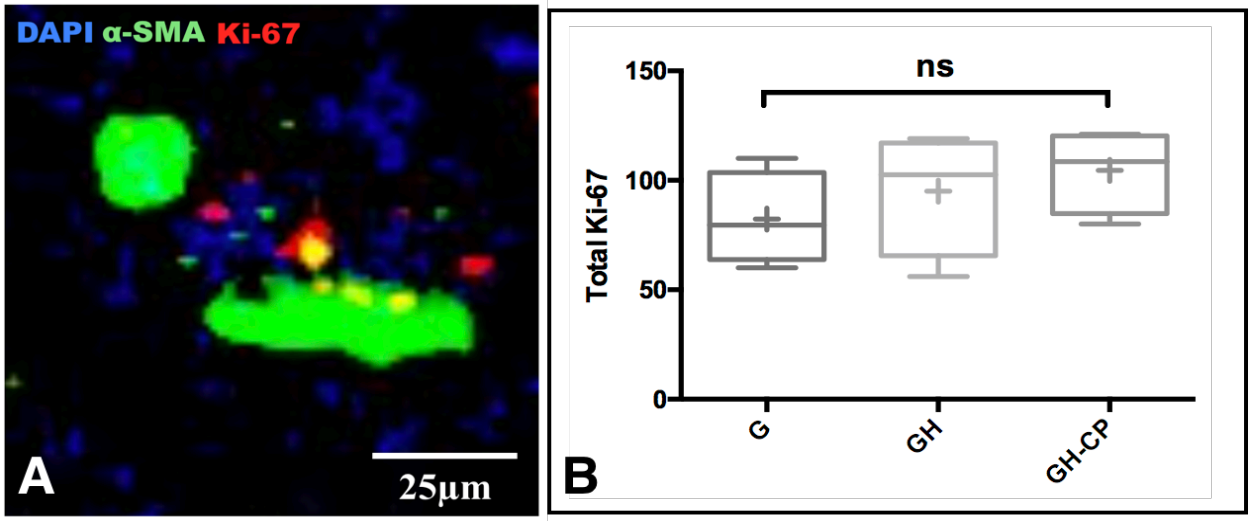

Figure 4-4 (A) *Proliferating bMSCs with immunofluorescence staining analysis: DAPI (1/25,000), anti-alpha smooth muscle actin antibody ab5694 (α-SMA) (1/400), Anti-Ki67 antibody ab15580 (Ki-67) (1/1000);* ***(B)*** *Total Ki-67 in different gel groups: One-way ANOVA, n=6, a box-and-whiskers plot, + indicating the mean, ns as p-value > .05.*

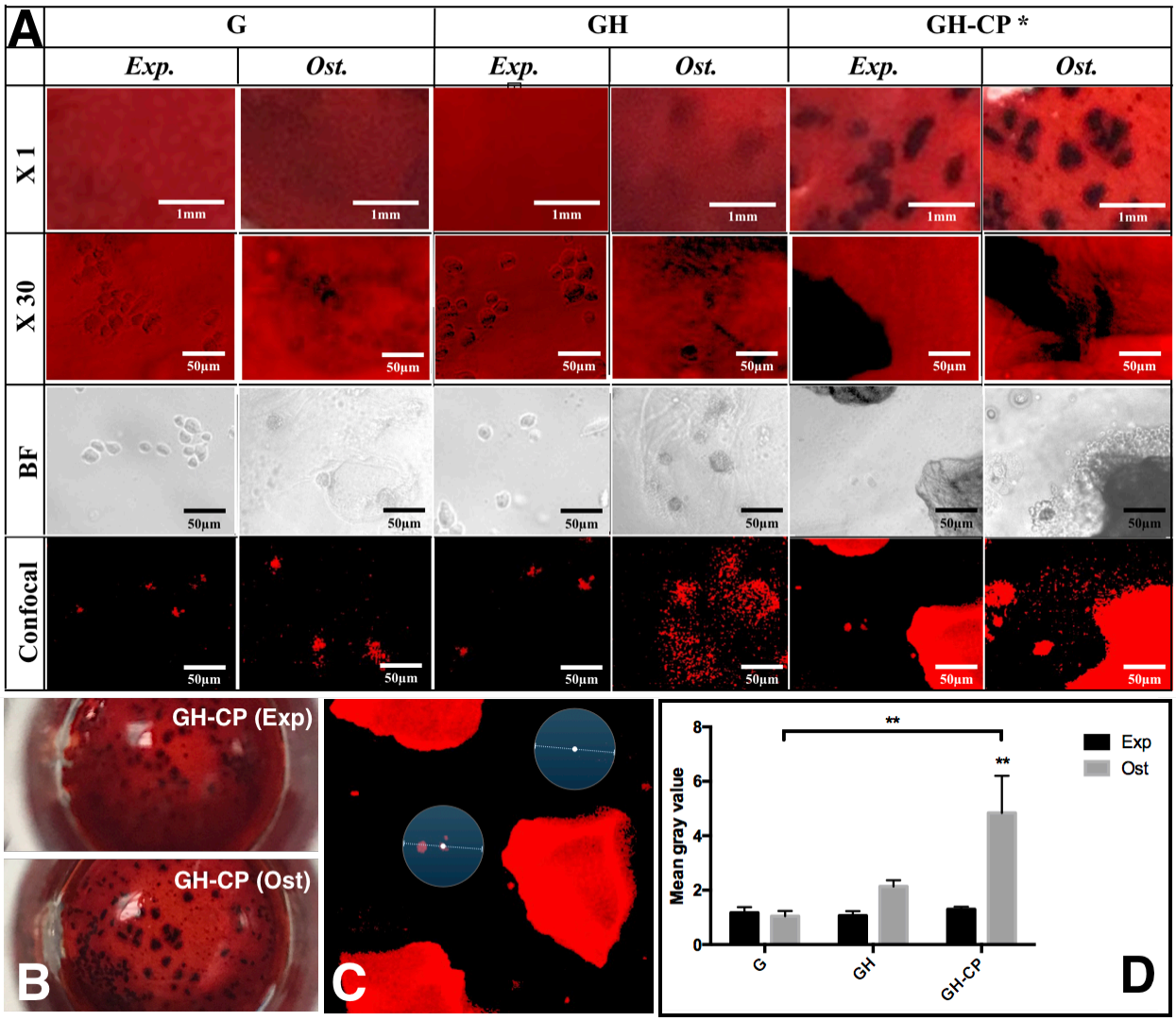

Figure 4-5 (A) *Alizarin Red S (ARS) staining for mineralization in different gel groups (28 days). Calcium deposits appearing as dark nodules under the bright field of optical microscopy and as red nodules under the confocal microscopy.;* ***(B)*** *Gross views of ARS stained and washed GH-CP gels;* ***(C)*** *Circular region of interest (ROI) with a diameter of 100µm, originating at the center of a visible cell.;* ***(D)*** *Mean gray values of ARS fluorescence in different gel groups: Two-way ANOVA, n=6, mean ± S.E., **p-value < .01.*

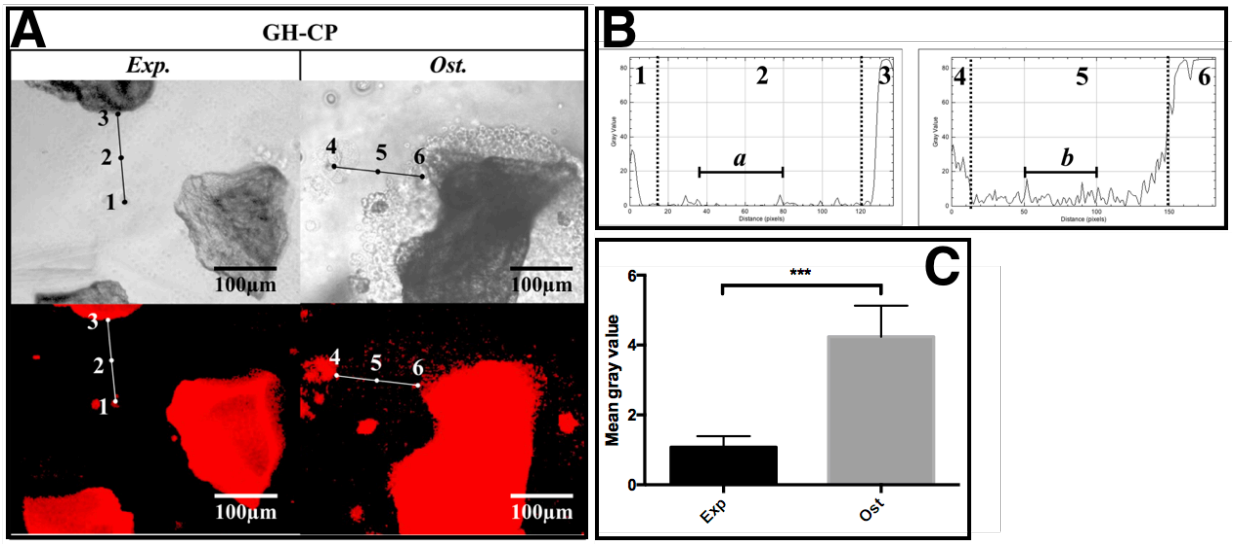

Figure 4-6 (A) *ARS fluorescence around CP particles in GH-CP with inter-distant segmentations (directed from the cell → medium → CP).;* ***(B)*** *Gray values of ARS fluorescence at the selected ROI of 50 pixels (a = ROI at the zone 2; b = ROI at the zone 5);* ***(C)*** *Mean gray values of ARS fluorescence at ROIs: Unpaired t-test, n=4, mean ± S.D., ***p-value < .001.*

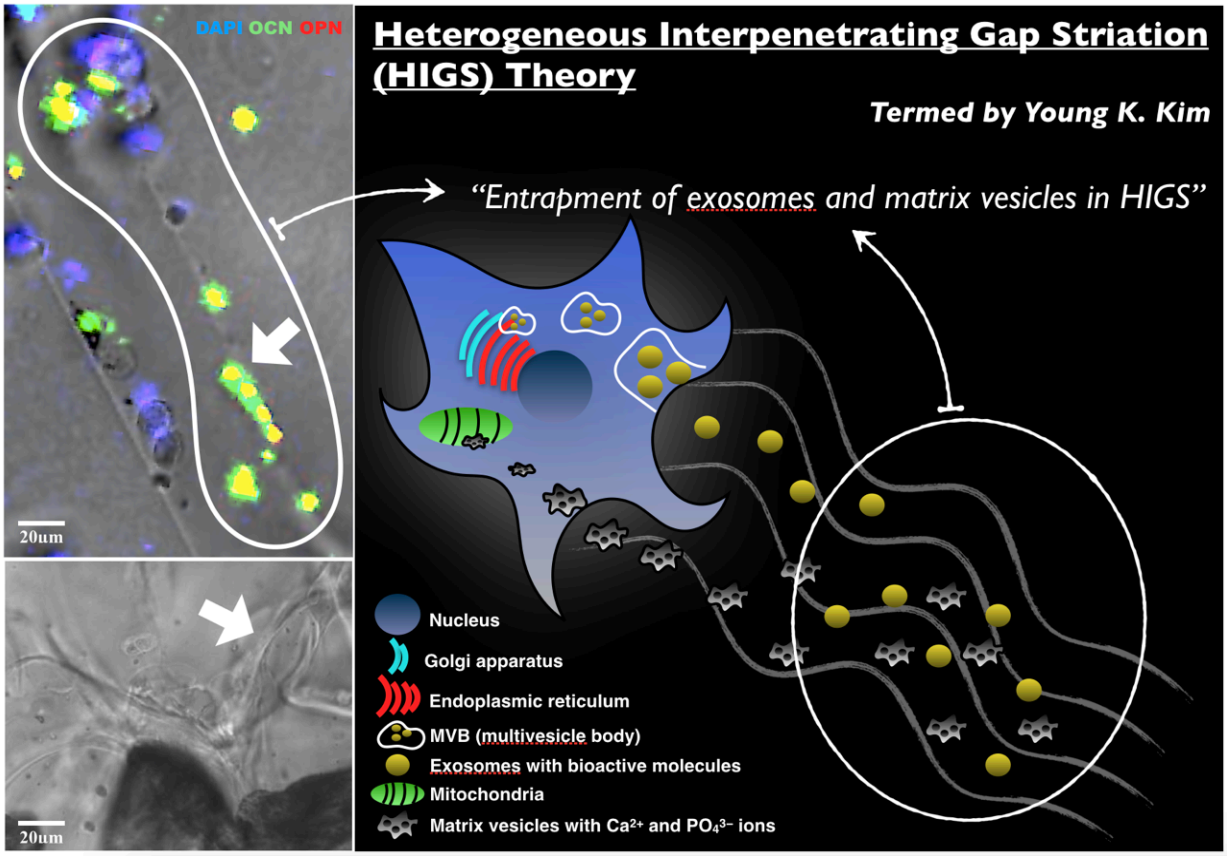

Figure 4-7 *Schematic diagram of "Heterogeneous Interpenetrating Gap Striation" (HIGS) theory - Termed by & diagram courtesy of Young. K. Kim*

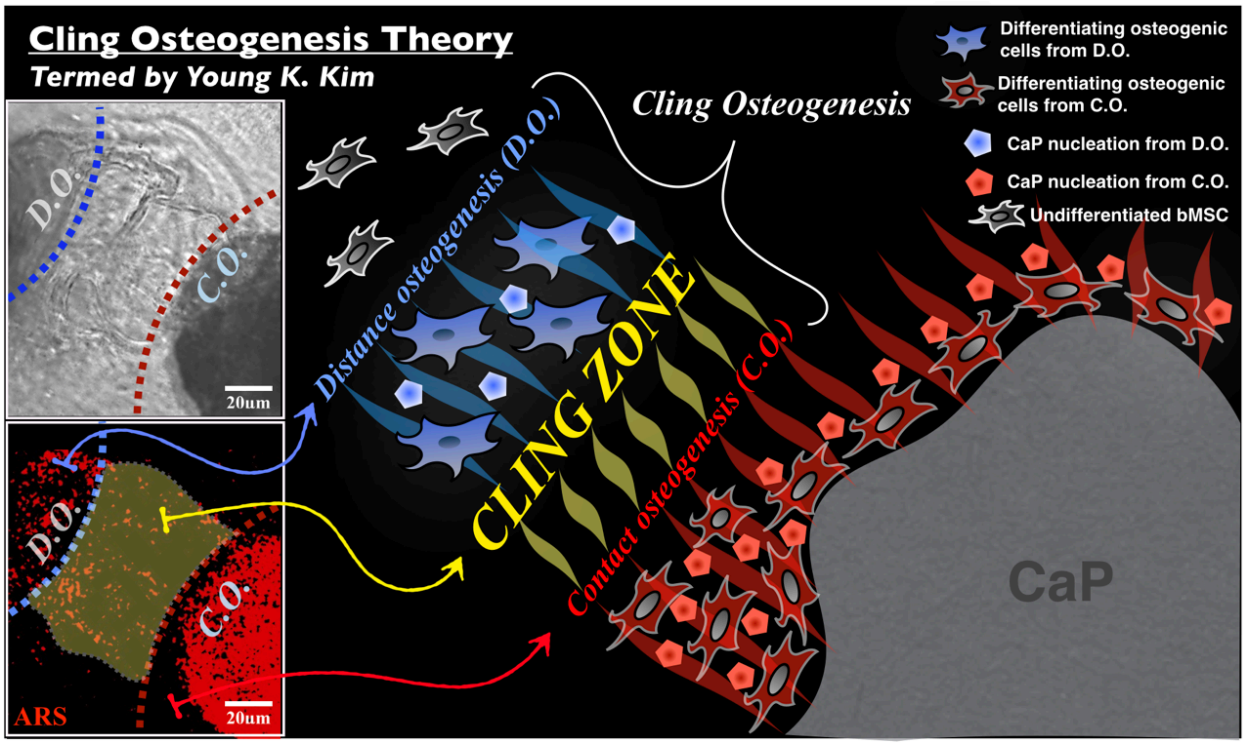

Figure 4-8 *Schematic diagram of "Cling Osteogenesis" theory - Termed by & diagram courtesy of Young. K. Kim*

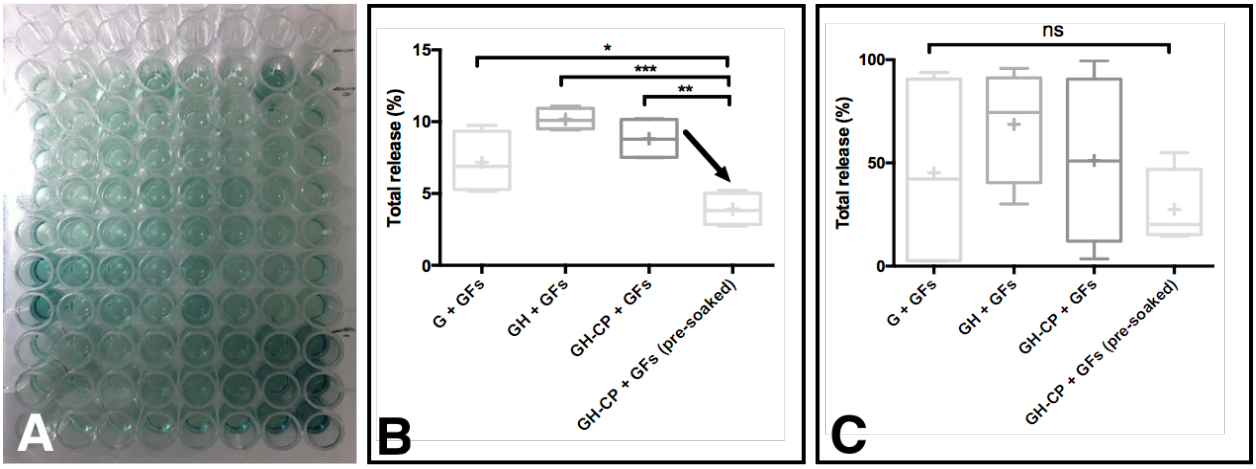

Figure 5-1 ***(A)*** *A sample plate using a human PDGF/FGF-basic standard ABTS ELISA development kits;* ***(B)*** *Total % release of PDGF-BB in different gel groups (after 7 days);* ***(C)*** *Total % release of FGF-2 in different gel groups (after 7 days) (One-way ANOVA, followed by Tukey's post-hoc test, n=6, a box-and-whiskers plot, + indicating the mean, ns as p-value > .05, *p-value < .05, **p-value < .01, ***p-value < .001).*

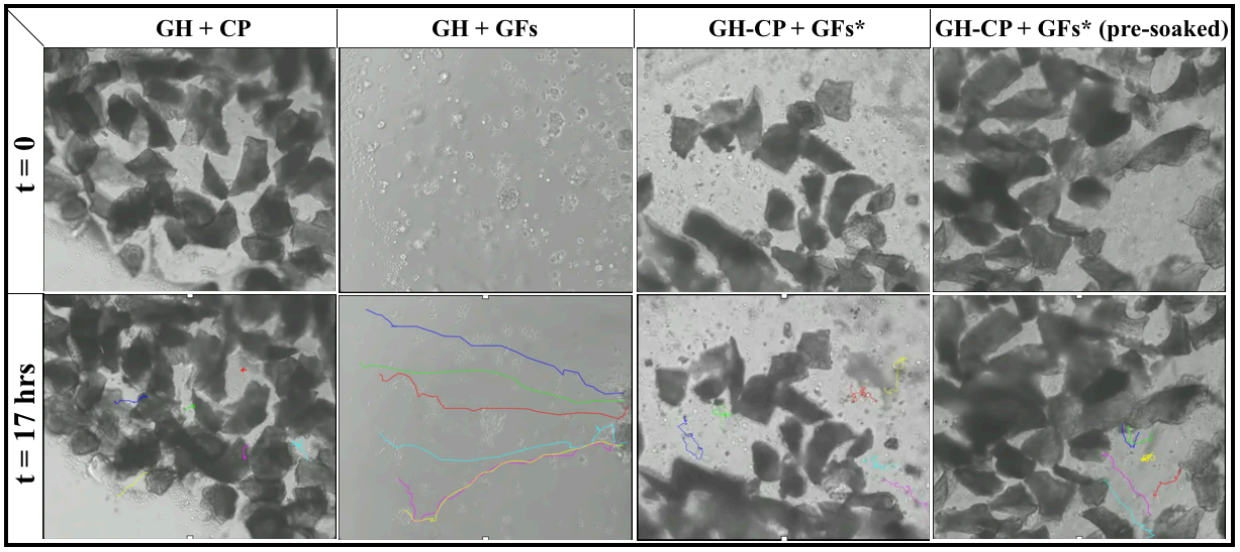

Figure 5-2 *Time-lapse images of live cell monitoring using Nikon Eclipse Ti-E with HUBC Inverted Phase Contrast Fluorescent Microscope (Cambridge Scientific Corp., MA, USA): colored lines as individual cell tracing records (n = 6).*

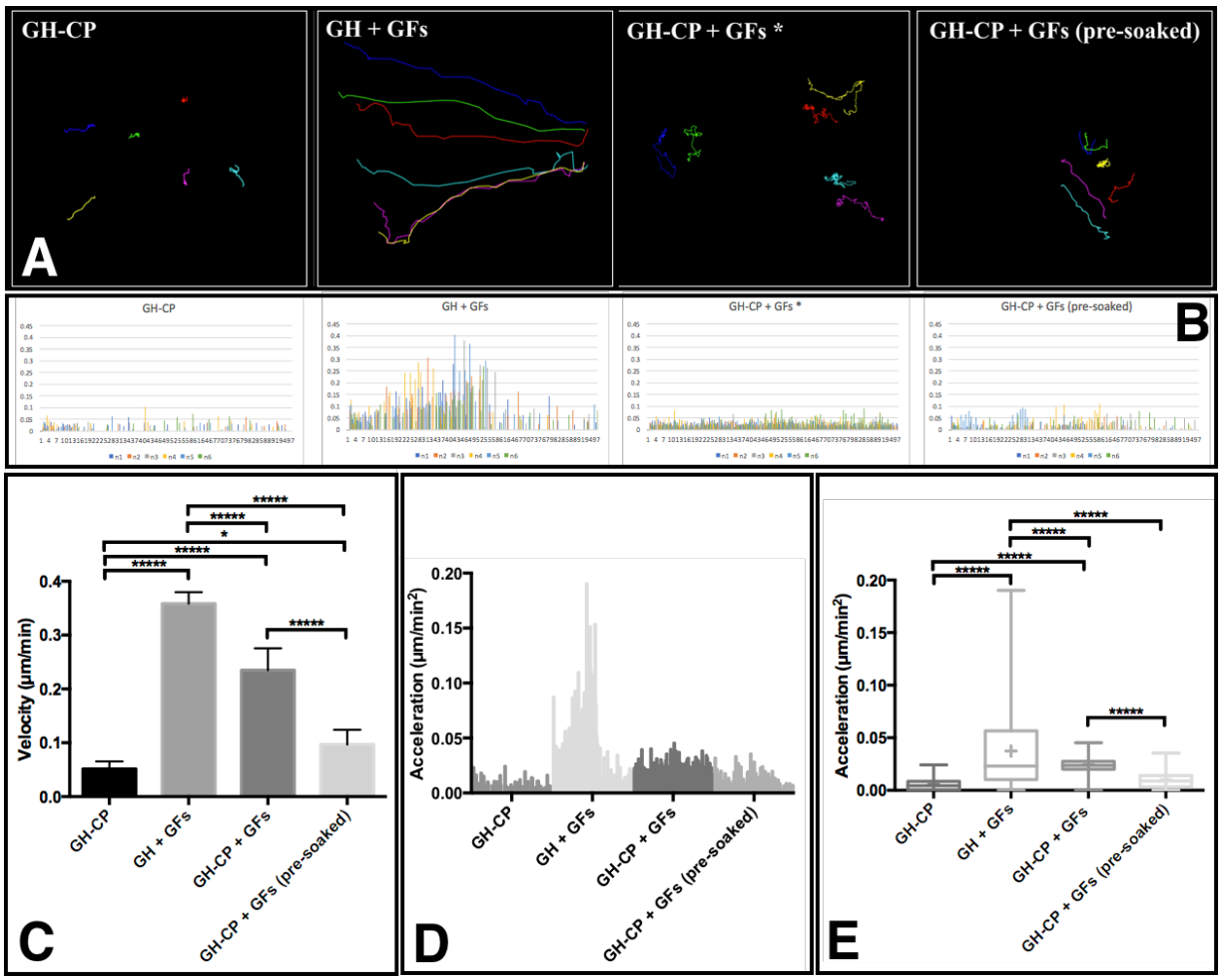

Figure 5-3 ***(A)*** *Live cell monitoring tracings (Image J software);* ***(B)*** *Raw graphs of acceleration distribution;* ***(C)*** *Mean velocity (µm/min) of proliferating bMSCs within different gel groups: One-way ANOVA, followed by Tukey's post-hoc test, n=6, mean ± S.E;* ***(D)*** *Acceleration (µm/min^2) distribution of proliferating bMSCs within different gel groups (n=6);* ***(E)*** *Mean acceleration (µm/min^2) of each gel group: One-way ANOVA, followed by Tukey's post-hoc test, n=6, a box-and-whiskers plot, + indicating the mean, ****p-value < .0001.*

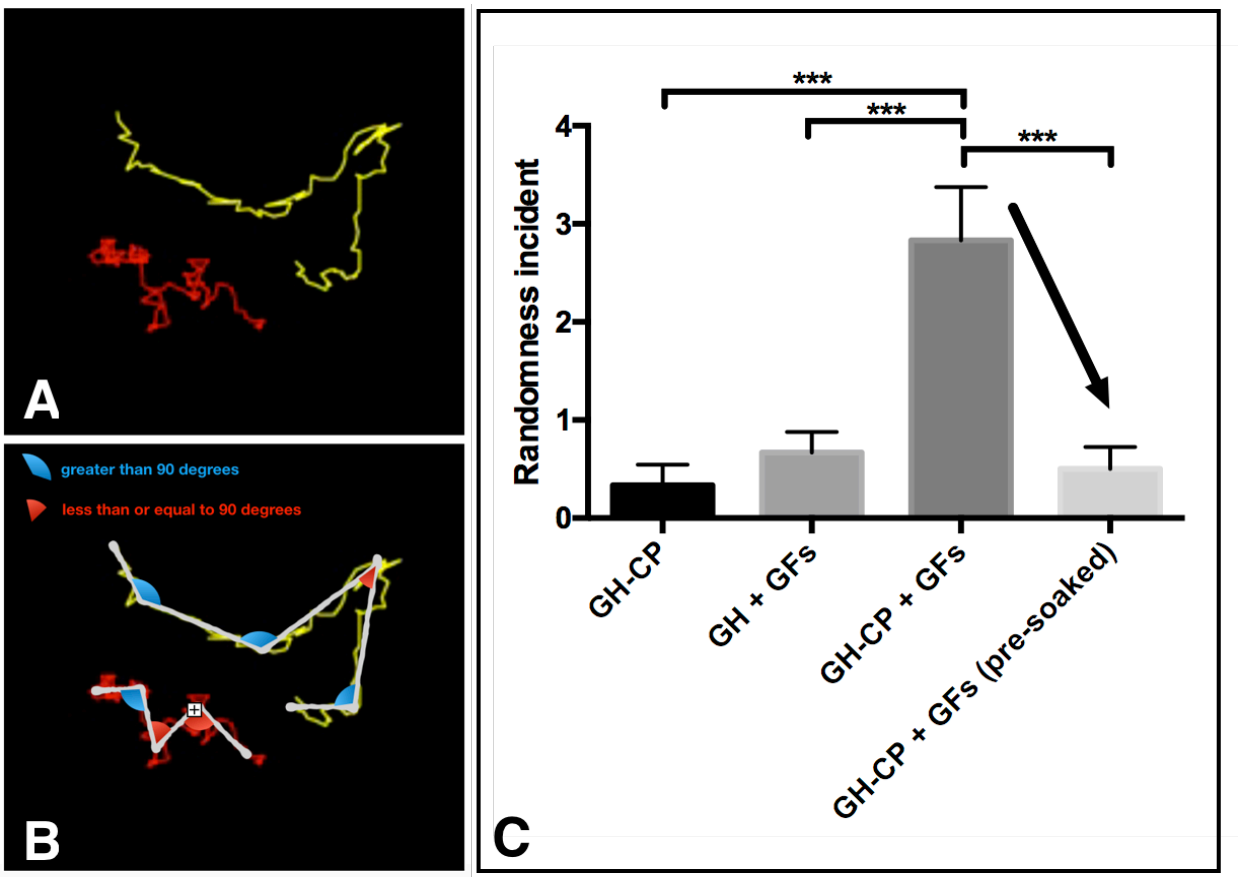

Figure 5-4 *(**A**) Sample tracings of proliferating bMSCs; **(B)** Inclusion criteria of randomness quantification; **(C)** Randomness incidents of proliferating bMSCs in different gel groups: One-way ANOVA, followed by Tukey's post-hoc test, n=6, mean ± S.E., ***p-value < .001.*

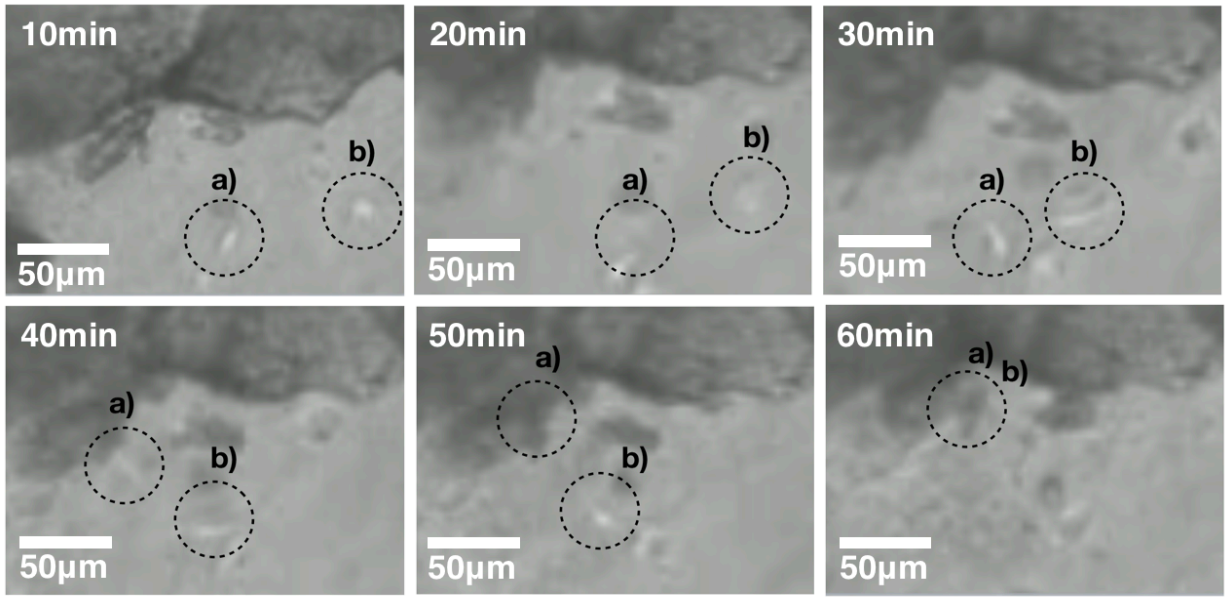

Figure 5-5 *Time-lapse optical microscopic images of accelerated bMSCs towards pre-soaked CP particles with rhPDGF-BB and rhFGF-2.*

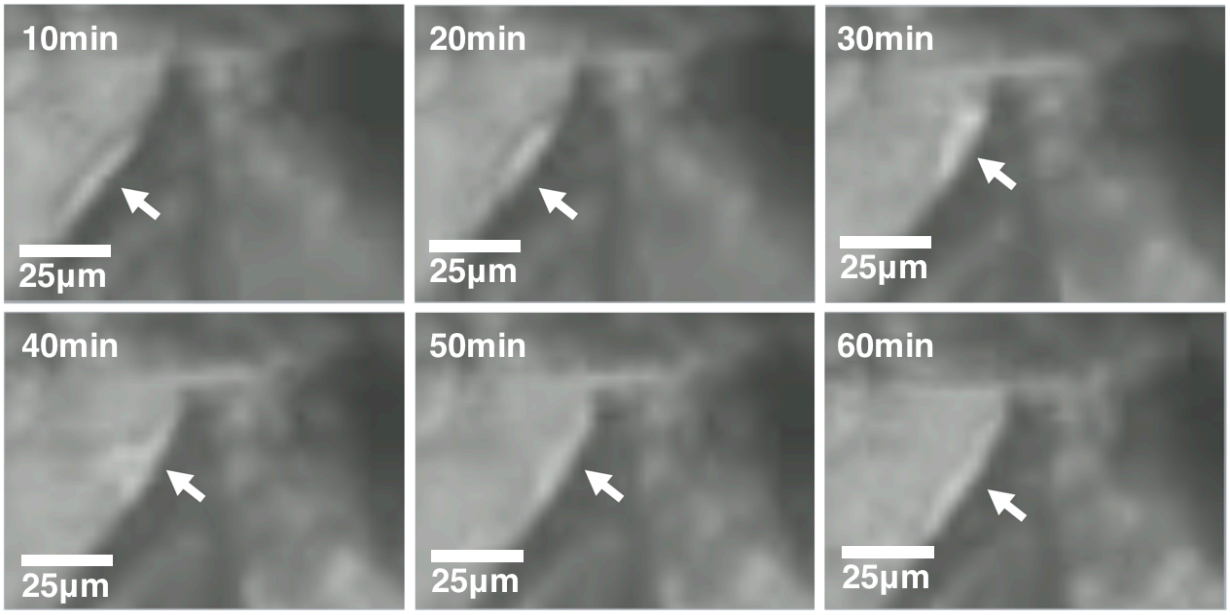

Figure 5-6 *Time-lapse optical microscopic images of contraction of bMSC attaching on the surface of CP.*

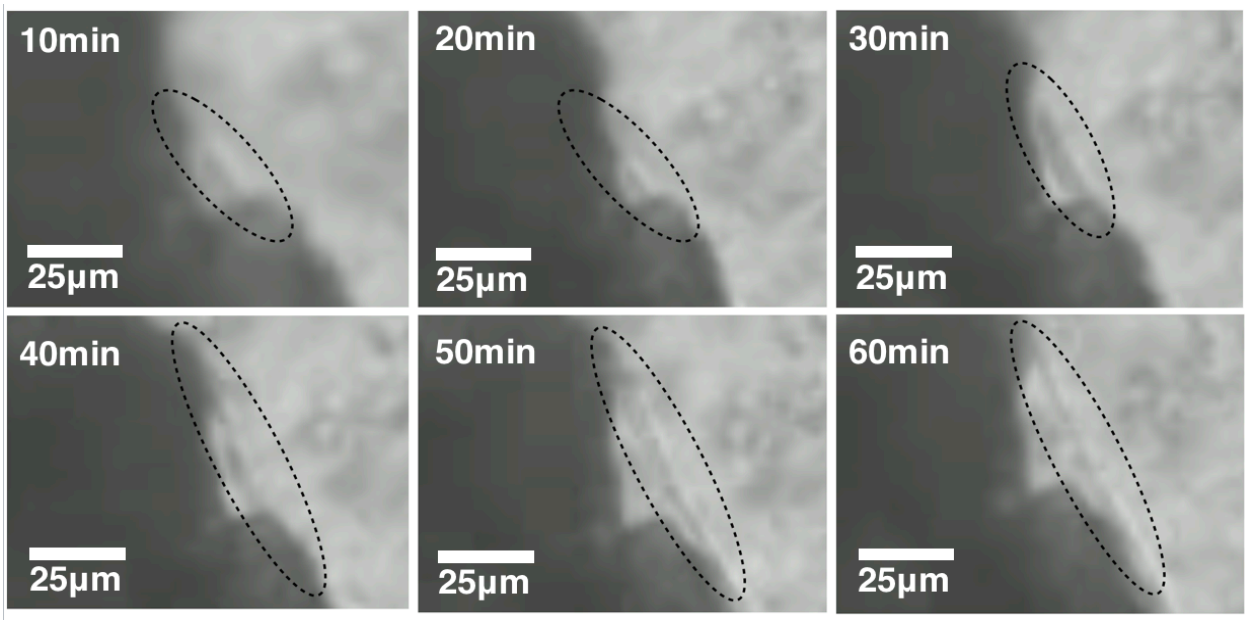

Figure 5-7 *Time-lapse optical microscopic images of elongated morphology of migrating bMSC on the surface of CP.*

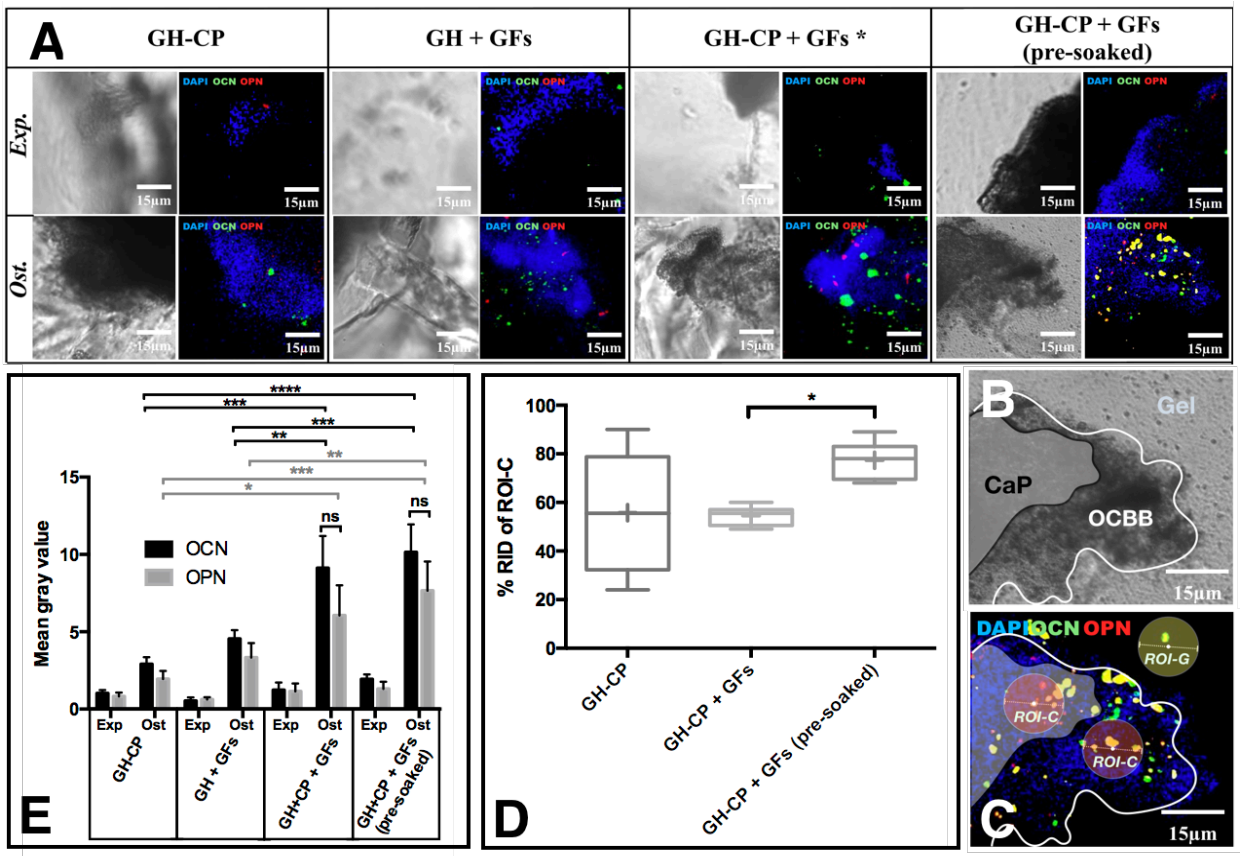

Figure 5-8 ***(A)*** *Osteogenic differentiation of bMSCs in different gel groups (28 days) with ICC/IF staining analysis (n=6) under the magnification of 30X: DAPI (1/25,000), OCN (1/200), OPN (1/1000);* ***(B)*** *Bright field view (30X);* ***(C)*** *Inclusion criteria of immunofluorescence in ROI-G or ROI-C;* ***(D)*** *% RID of ROI-C within different gel groups: One-way ANOVA, followed by Tukey's post-hoc test, n=6, a box-and-whiskers plot, + indicating the mean, *p-value < 0.05;* ***(E)*** *Mean gray values of OCN/OPN in different gel groups: Two-way ANOVA, followed by the Fisher's PLSD test, and unpaired t-test, n=6, mean ± S.E., *p-value < .05., **p-value < .01., ***p-value < .001, ****p-value < .0001.*

Abbreviations: Immunocytochemistry/immunofluorscence (IFF/IC), Anti-Osteocalcin antibody ab13418 (OCN), Anti-Osteopontin antibody ab8448 (OPN), Region of interest within gel (ROI-G), Osteoid/calcified-bone boundary (OCBB), Region of interest on the surface of CP and within OCBB (ROI-C).

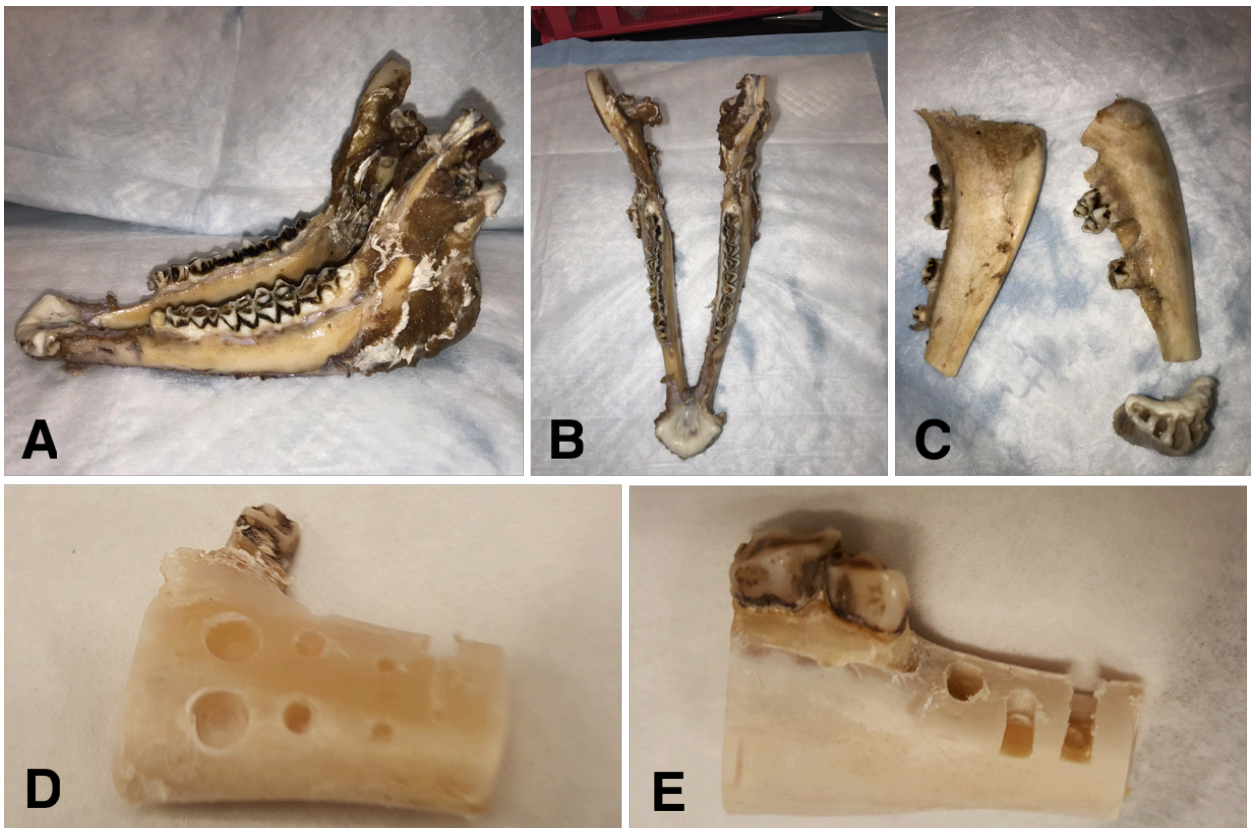

Figure 6-1 *Surgically extracted goat mandible in* ***(A)*** *lateral view;* ***(B)*** *horizontal view;* ***(C)*** *sectioned mandible pieces;* ***(D)*** *circular corticonomies in different sizes for calibration;* ***(E)*** *different GBR mimicking defects.*

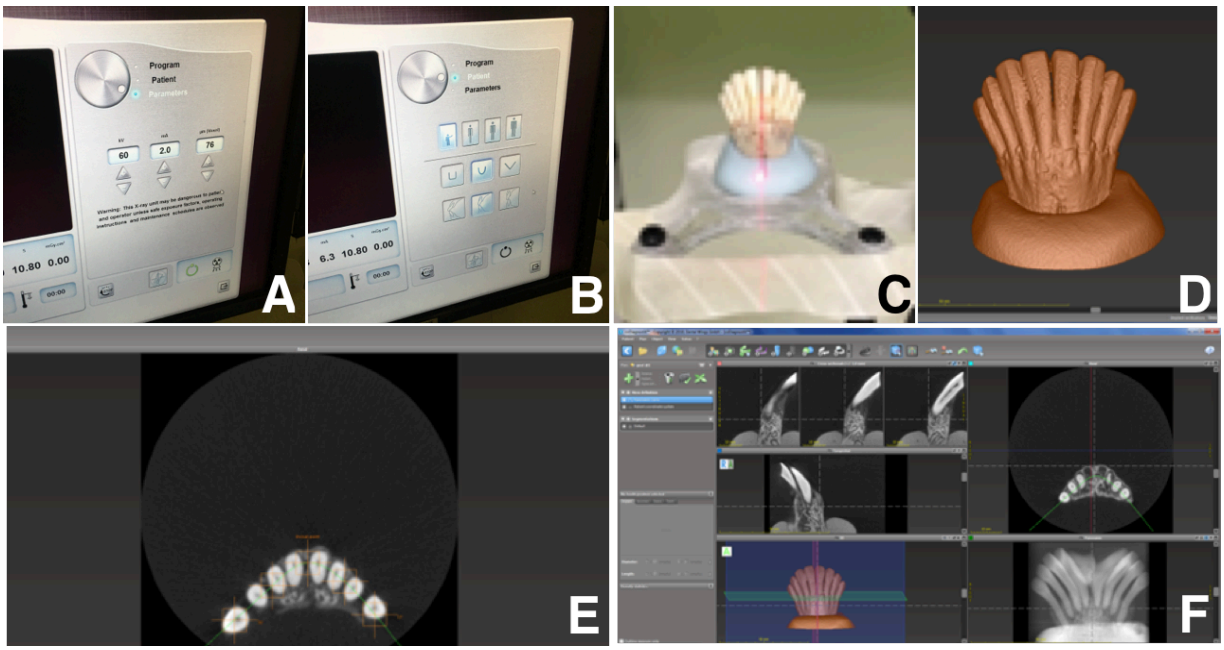

Figure 6-2 ***(A)*** *Cone beam computed topography (CBCT) exposure calibration;* ***(B)*** *CBCT locational calibration;* ***(C)*** *Stabilized sample goat mandible piece ready for imaging;* ***(D)*** *Segmented DICOM image;* ***(E)*** *Alignment calibration;* ***(F)*** *A view in the software (CoDiagnostiX™).*

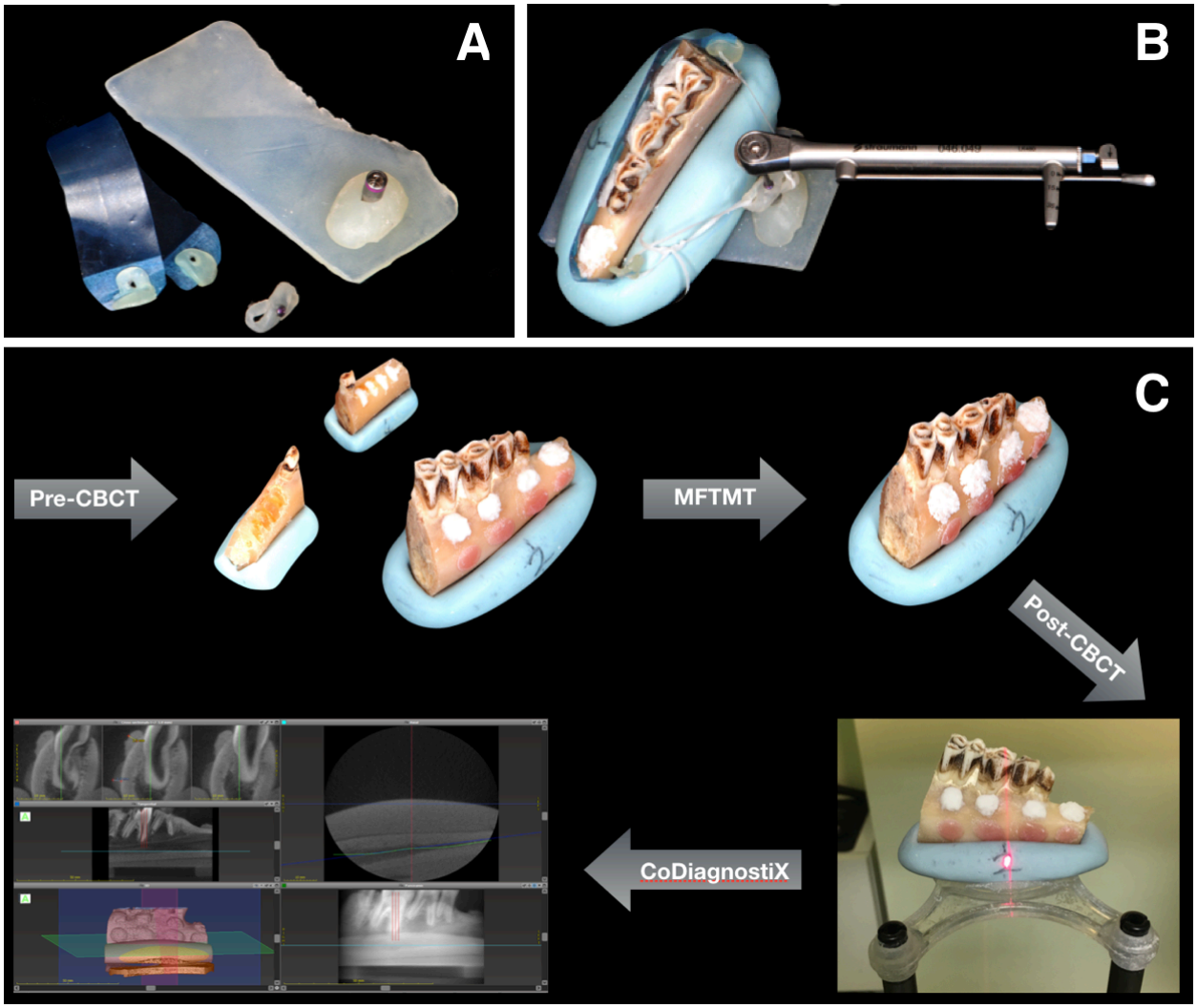

Figure 6-3 (A) *Components for mucoperiosteal flap tension mimicking torquer (MFTMT) - developed by Young K. Kim;* ***(B)*** *Assembled MFTMT ready for use;* ***(C)*** *Flowchart of ex vivo volumetric computed topography analysis.*

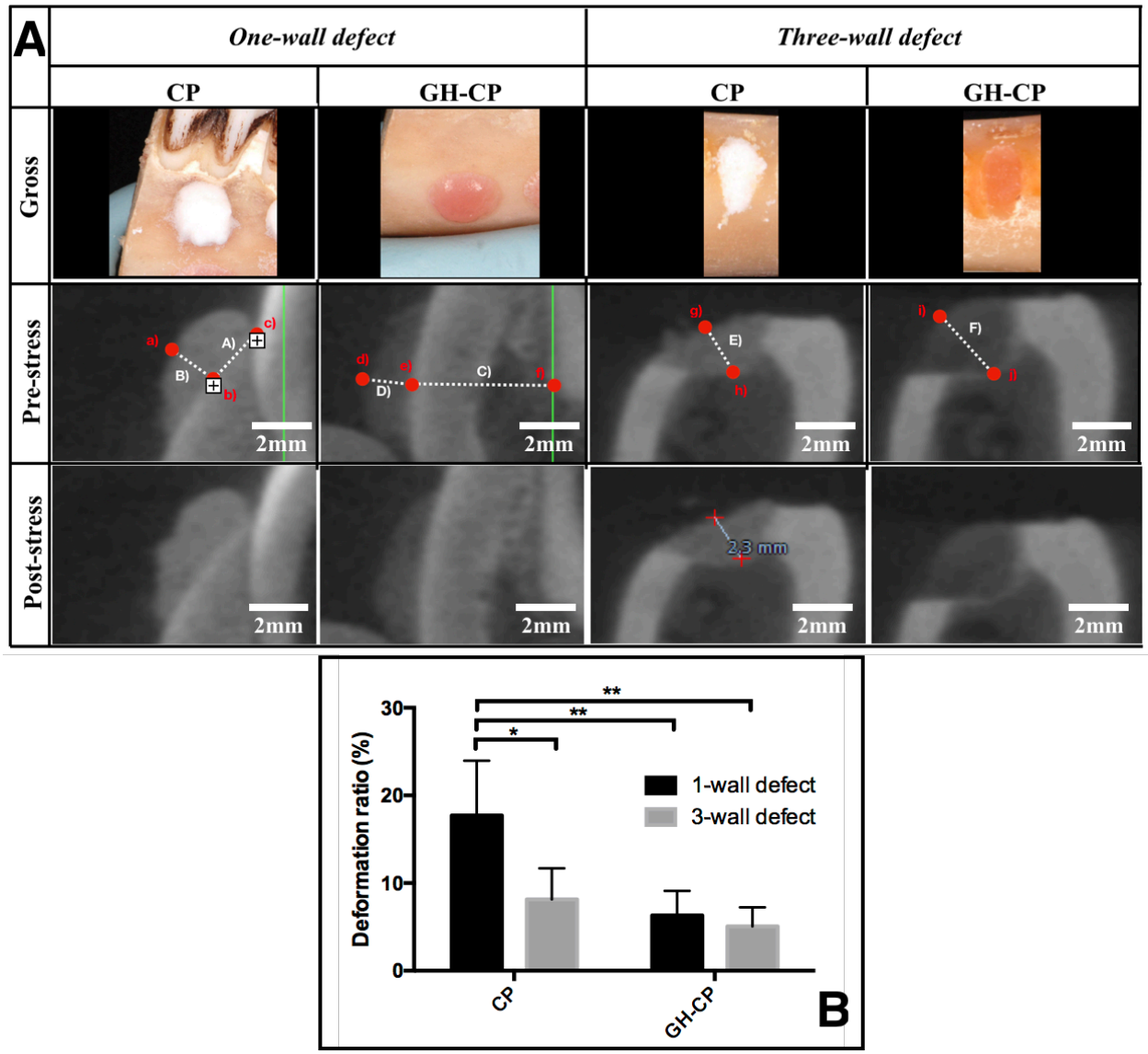

Figure 6-4 (A) *Comparative CBCT volumetric deformation images in one or three-wall defects;* ***(B)*** *Deformation ratio (%): Two-way ANOVA, followed by Tukey's post-hoc test, n=4, mean ± S.D., *p-value < .05, **p-value < .01.*

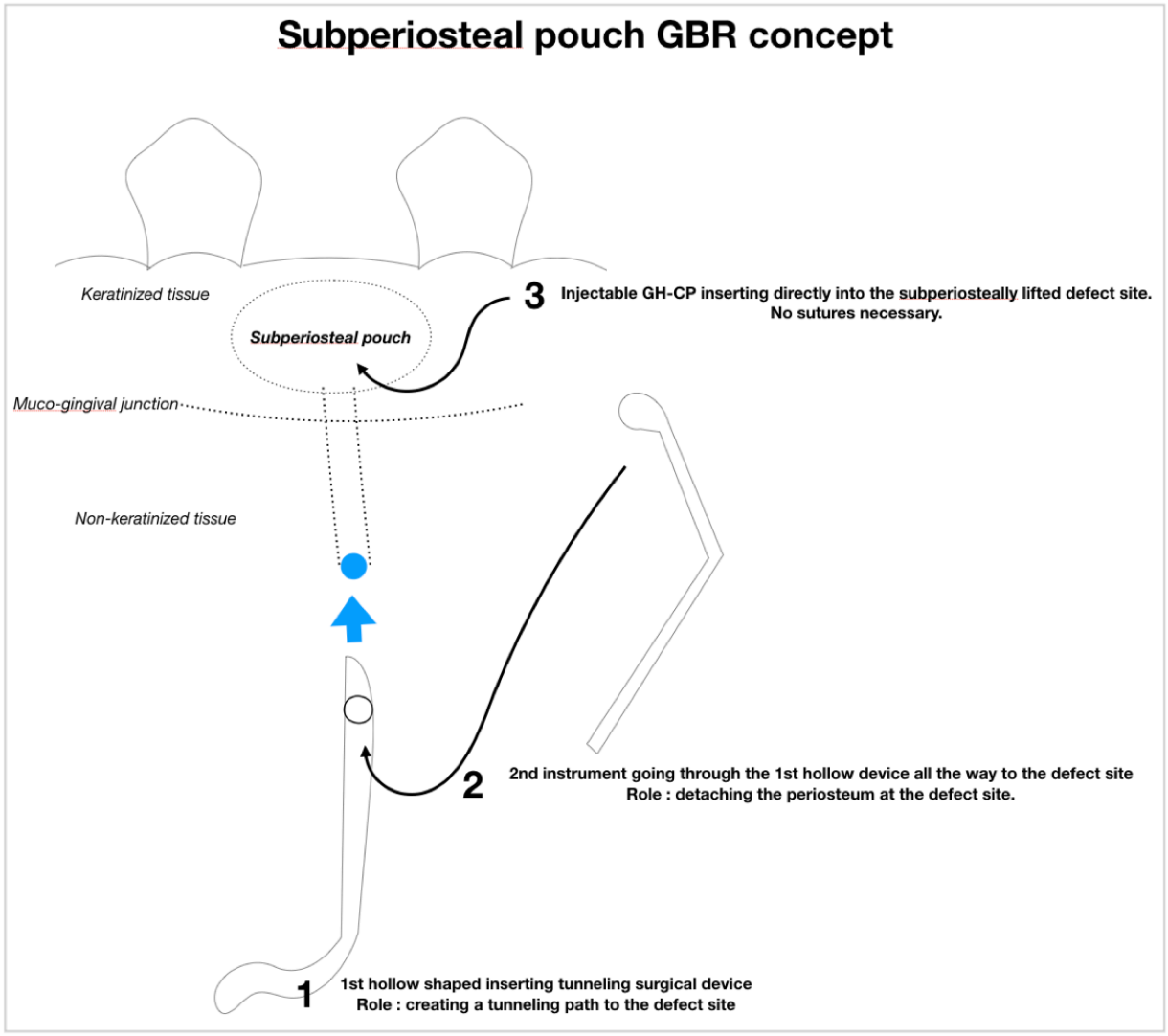

Figure 6-5 *A schematic of surgical sequence in subperiosteal pouch GBR (Courtesy of Young K. Kim)*

Chapter 10 - References

[1] Chao, J.C. (2012) A novel approach to root coverage: the pinhole surgical technique. *Int J Periodontics Restorative Dent* **32**, 521-531.

[2] Lee, E.A. (2017) Subperiosteal Minimally Invasive Aesthetic Ridge Augmentation Technique (SMART): A New Standard for Bone Reconstruction of the Jaws. *Int J Periodontics Restorative Dent* **37**, 165-173.

[3] Stevenson, S., Emery, S.E. and Goldberg, V.M. (1996) Factors Affecting Bone Graft Incorporation. *Clin Orthop Relat Res* 66-74.

[4] Urban, I.A., Nagursky, H., Lozada, J.L. and Nagy, K. (2013) Horizontal ridge augmentation with a collagen membrane and a combination of particulated autogenous bone and anorganic bovine bone-derived mineral: a prospective case series in 25 patients. *International Journal of Periodontics & Restorative Dentistry* **33**, 299-307.

[5] Von Arx, T. and Buser, D. (2006) Horizontal ridge augmentation using autogenous block grafts and the guided bone regeneration technique with collagen membranes: a clinical study with 42 patients. *Clin Oral Implants Res* **17**, 359-366.

[6] Nevins, M.L., Camelo, M., Nevins, M., Schupbach, P., Friedland, B., Camelo, J.M. and Kim, D.M. (2009) Minimally invasive alveolar ridge augmentation procedure (tunneling technique) using rhPDGF-BB in combination with three matrices: a case series. *Int J Periodontics Restorative Dent* **29**, 371-383.

[7] Asparuhova, M.B., Caballe-Serrano, J., Buser, D. and Chappuis, V. (2018) Bone-conditioned medium contributes to initiation and progression of osteogenesis by exhibiting synergistic TGF-beta1/BMP-2 activity. *Int J Oral Sci* **10**, 20.

[8] Caballe-Serrano, J., Fujioka-Kobayashi, M., Bosshardt, D.D., Gruber, R., Buser, D. and Miron, R.J. (2016) Pre-coating deproteinized bovine bone mineral (DBBM) with bone-conditioned medium (BCM) improves osteoblast migration, adhesion, and differentiation in vitro. *Clin Oral Investig* **20**, 2507-2513.

[9] Albrektsson, T. and Albrektsson, B. (1987) Osseointegration of bone implants. A review of an alternative mode of fixation. *Acta Orthop Scand* **58**, 567- 577.

[10] Barone, A. and Covani, U. (2007) Maxillary alveolar ridge reconstruction with nonvascularized autogenous block bone: clinical results. *J Oral Maxillofac Surg* **65**, 2039-2046.

[11] Keating, J.F., & McQueen, M. M. (2001) Substitutes for autologous bone graft in orthopaedic trauma. *J Bone Joint Surg Br* **83**, 3-8.
[12] Abubaker, A.O. and Benson, K.J. (2007) Oral and Maxillofacial Surgery Secrets (Second edition). *Mosby Elsevier*
[13] Weibrich, G., Kleis, W.K.G., Hafner, G. and Hitzler, W.E. (2002) Growth factor levels in platelet-rich plasma and correlations with donor age, sex, and platelet count. *Journal of Cranio-Maxillofacial Surgery* **30**, 97-102.
[14] Nevins, M., Giannobile, W.V., McGuire, M.K., Kao, R.T., Mellonig, J.T., Hinrichs, J.E., McAllister, B.S., Murphy, K.S., McClain, P.K. and Nevins, M.L. (2005) Platelet-derived growth factor stimulates bone fill and rate of attachment level gain: Results of a large multicenter randomized controlled trial. *Journal of periodontology* **76**, 2205-2215.
[15] Davies, J.E. (2003) Understanding peri-implant endosseous healing. *J Dent Educ.* **67**, 932-949.
[16] Cornell, C.N. and Lane, J.M. (1998) Current understanding of osteoconduction in bone regeneration. *Clin Orthop Relat Res* 267-273.
[17] Davies, J.E. (1998) Mechanisms of endosseous integration. *Int J Prosthodont.* **11**, 391-401.
[18] Davies, J.E. (2003) Understanding peri-implant endosseous healing. *J Dent Educ.* **67**, 932-949.
[19] Borstlap, W.A., Heidbuchel, K.L., Freihofer, H.P. and Kuijpers-Jagtman, A.M. (1990) Early secondary bone grafting of alveolar cleft defects. A comparison between chin and rib grafts. *J Craniomaxillofac Surg* **18**, 201-205.
[20] Eppley, B.L., Pietrzak, W. S., & Blanton, M. W. (2005) Allograft and alloplastic bone substitutes: a review of science and technology for the craniomaxillofacial surgeon. *J Craniofac Surg* **16**, 981-989.
[21] Perrott, D.H., Smith, R.A. and Kaban, L.B. (1992) The use of fresh frozen allogeneic bone for maxillary and mandibular reconstruction. *Int J Oral Maxillofac Surg* **21**, 260-265.
[22] Franco, M., Viscioni, A., Rigo, L., Guidi, R., Brunelli, G. and Carinci, F. (2009) Iliac crest fresh frozen homografts used in pre-prosthetic surgery: a retrospective study. *Cell Tissue Bank* **10**, 227-233.
[23] Buck, B.E., Malinin, T.I. and Brown, M.D. (1989) Bone transplantation and human immunodeficiency virus. An estimate of risk of acquired immunodeficiency syndrome (AIDS). *Clin Orthop Relat Res* **240**, 129- 136.

[24] Bauer, T.W. and Muschler, G.F. (2000) Bone graft materials. An overview of the basic science. *Clin Orthop Relat Res* **371**, 10-27.
[25] Urist, M.R. (1965) Bone: Formation by Autoinduction. *Science* **150**, 893-899.
[26] Froum, S.J., Wallace, S.S., Elian, N., Cho, S.C. and Tarnow, D.P. (2006) Comparison of mineralized cancellous bone allograft (Puros) and anorganic bovine bone matrix (Bio-Oss) for sinus augmentation: histomorphometry at 26 to 32 weeks after grafting. *Int J Periodontics Restorative Dent* **26**, 543-551.
[27] Becker, W., Becker, B.E. and Caffesse, R. (1994) A comparison of demineralized freeze-dried bone and autologous bone to induce bone formation in human extraction sockets. *J Periodontol* **65**, 1128-1133.
[28] Jensen, O.T., Shulman, L.B., Block, M.S. and Iacono, V.J. (1998) Report of the Sinus Consensus Conference of 1996. *Int J Oral Maxillofac Implants* **13 suppl**, 11-45.
[29] Zhang, G. (2006) Maxillofacial Bone Augmentation and Replacement. *Polymers for Dental and Orthopedic Applications*
[30] Norton, M.R., Odell, E.W., Thompson, I.D. and Cook, R.J. (2003) Efficacy of bovine bone mineral for alveolar augmentation: a human histologic study. *Clin Oral Implants Res* **14**, 775-783.
[31] LeGeros, R.Z. (2002) Properties of osteoconductive biomaterials: calcium phosphates. *Clin Orthop Relat Res* **395**, 81-98.
[32] Cohen, R.E., Mullarky, R.H., Noble, B., Comeau, R.L. and Neiders, M.E. (1994) Phenotypic characterization of mononuclear cells following anorganic bovine bone implantation in rats. *J Periodontol* **65**, 1008-1015.
[33] Pinholt, E.M., Bang, G. and Haanaes, H.R. (1991) Alveolar ridge augmentation in rats by Bio-Oss. *Scand J Dent Res* **99**, 154-161.
[34] Carmagnola, D., Adriaens, P. and Berglundh, T. (2003) Healing of human extraction sockets filled with Bio-Oss. *Clin Oral Implants Res* **14**, 137-143.
[35] Stavropoulos, A., Kostopoulos, L., Mardas, N., Nyengaard, J.R. and Karring, T. (2001) Deproteinized bovine bone used as an adjunct to guided bone augmentation: an experimental study in the rat. *Clin Implant Dent Relat Res* **3**, 156-165.
[36] Schlegel, A.K. and Donath, K. (1998) Bio-Oss - a resorbable bone substitute? *J Long Term Eff Med Implants.* **3-4**, 201-209.

[37] Valentini, P., Abensur, D., Densari, D., Graziani, J. N., & Hammerle, C. (1998) Histological evaluation of Bio-Oss in a 2-stage sinus floor elevation and implantation procedure. A human case report. *Clin Oral Implants Res* **9**, 59-64.
[38] Zerbo, I.R., Zijderveld, S.A., de Boer, A., Bronckers, A.L., de Lange, G., ten Bruggenkate, C.M. and Burger, E.H. (2004) Histomorphometry of human sinus floor augmentation using a porous beta-tricalcium phosphate: a prospective study. *Clin Oral Implants Res* **15**, 724-732.
[39] Hirota, M., Matsui, Y., Mizuki, N., Kishi, T., Watanuki, K., Ozawa, T., et al. (2009) Combination with allogenic bone reduces early absorption of β-tricalcium phosphate (β-TCP) and enhances the role as a bone regeneration scaffold. Experimental animal study in rat mandibular bone defects. *Dent Mater J* **28**, 153-161.
[40] Becker, W. and BE, B. (1990) Guided tissue regeneration for implants placed into extraction sockets and for implant dehiscences: surgical techniques and case report. *Int J Periodontics Restorative Dent.* **10**, 376-391.
[41] Simion, M.B., M, Rossi, P. and Zaffe, D. (1994) A comparative study of the effectiveness of e-PTFE membranes with and without early exposure during the healing period. *Int J Periodontics Restorative Dent.* **14**, 166-180.
[42] Carmagnola, D. and Berglundh, T.L., J (2002) The effect of a fibrin glue on the integration of Bio-Oss with bone tissue. A experimental study in labrador dogs. *J Clin Periodontol.* **29**, 377-383.
[43] Ceccarelli, G., Graziano, A., Benedetti, L., Imbriani, M., Romano, F., Ferrarotti, F., Aimetti, M. and Cusella de Angelis, G.M. (2016) Osteogenic Potential of Human Oral-Periosteal Cells (PCs) Isolated From Different Oral Origin: An In Vitro Study. *J Cell Physiol* **231**, 607-612.
[44] Ferretti, C. and Mattioli-Belmonte, M. (2014) Periosteum derived stem cells for regenerative medicine proposals: Boosting current knowledge. *World J Stem Cells* **6**, 266-277.
[45] Clokie, C.M., Moghadam, H., Jackson, M. T. and Sandor, G.K. (2002) Closure of critical sized defects with allogenic and alloplastic bone substitutes. *J Craniofac Surg* **13**, 111-121.
[46] Vo, T.N., Shah, S.R., Lu, S., Tatara, A.M., Lee, E.J., Roh, T.T., Tabata, Y. and Mikos, A.G. (2016) Injectable dual-gelling cell-laden composite hydrogels for bone tissue engineering. *Biomaterials* **83**, 1-11.
[47] Fu, S., Guo, G., Gong, C., Zeng, S., Liang, H., Luo, F., Zhang, X., Zhao, X., Wei, Y. and Qian, Z. (2009) Injectable biodegradable thermosensitive hydrogel composite for orthopedic tissue engineering. 1. preparation and characterization of nanohydroxyapatite/poly (ethylene

glycol)− poly (ε-caprolactone)− poly (ethylene glycol) hydrogel nanocomposites. *The Journal of Physical Chemistry B* **113**, 16518-16525.
[48] Fu, S., Ni, P., Wang, B., Chu, B., Zheng, L., Luo, F., Luo, J. and Qian, Z. (2012) Injectable and thermo-sensitive PEG-PCL-PEG copolymer/collagen/n-HA hydrogel composite for guided bone regeneration. *Biomaterials* **33**, 4801-4809.
[49] Matsuno, T., Hashimoto, Y., Adachi, S., Omata, K., Yoshitaka, Y., Ozeki, Y., Umezu, Y., Tabata, Y., Nakamura, M. and Satoh, T. (2008) Preparation of injectable 3D-formed β-tricalcium phosphate bead/alginate composite for bone tissue engineering. *Dental materials journal* **27**, 827-834.
[50] Jiao, Y., Gyawali, D., Stark, J.M., Akcora, P., Nair, P., Tran, R.T. and Yang, J. (2012) A rheological study of biodegradable injectable PEGMC/HA composite scaffolds. *Soft Matter* **8**, 1499-1507.
[51] Huang, Y., Zhang, X., Wu, A. and Xu, H. (2016) An injectable nano-hydroxyapatite (n-HA)/glycol chitosan (G-CS)/hyaluronic acid (HyA) composite hydrogel for bone tissue engineering. *RSC Advances* **6**, 33529-33536.
[52] Han, Y., Zeng, Q., Li, H. and Chang, J. (2013) The calcium silicate/alginate composite: Preparation and evaluation of its behavior as bioactive injectable hydrogels. *Acta biomaterialia* **9**, 9107-9117.
[53] Dessì, M., Borzacchiello, A., Mohamed, T.H., Abdel-Fattah, W.I. and Ambrosio, L. (2013) Novel biomimetic thermosensitive β-tricalcium phosphate/chitosan-based hydrogels for bone tissue engineering. *J Biomed Mater Res A* **101**, 2984-2993.
[54] Yan, J., Miao, Y., Tan, H., Zhou, T., Ling, Z., Chen, Y., Xing, X. and Hu, X. (2016) Injectable alginate/hydroxyapatite gel scaffold combined with gelatin microspheres for drug delivery and bone tissue engineering. *Mater Sci Eng C Mater Biol Appl* **63**, 274-284.
[55] Burkhardt, R. and Lang, N.P. (2010) Role of flap tension in primary wound closure of mucoperiosteal flaps: a prospective cohort study. *Clin Oral Implants Res* **21**, 50-54.
[56] Hu, M., Kurisawa, M., Deng, R., Teo, C.M., Schumacher, A., Thong, Y.X., Wang, L., Schumacher, K.M. and Ying, J.Y. (2009) Cell immobilization in gelatin-hydroxyphenylpropionic acid hydrogel fibers. *Biomaterials* **30**, 3523-3531.
[57] Wang, L.S., Boulaire, J., Chan, P.P., Chung, J.E. and Kurisawa, M. (2010) The role of stiffness of gelatin-hydroxyphenylpropionic acid hydrogels formed by enzyme-mediated crosslinking on the differentiation of human mesenchymal stem cell. *Biomaterials* **31**, 8608-8616.

[58] Snyder, S.L. and Sobocinski, P.Z. (1975) An improved 2,4,6-trinitrobenzenesulfonic acid method for the determination of amines. *Anal Biochem* **64**, 284-288.
[59] Kurisawa, M., Chung, J.E., Yang, Y.Y., Gao, S.J. and Uyama, H. (2005) Injectable biodegradable hydrogels composed of hyaluronic acid-tyramine conjugates for drug delivery and tissue engineering. *Chem Commun (Camb)* 4312-4314.
[60] Lee, F., Chung, J.E. and Kurisawa, M. (2008) An injectable enzymatically crosslinked hyaluronic acid,Äìtyramine hydrogel system with independent tuning of mechanical strength and gelation rate. *Soft Matter* **4**, 880-887.
[61] Chun, Y.Y., Wang, J.K., Tan, N.S., Chan, P.P.Y., Tan, T.T.Y. and Choong, C. (2016) A Periosteum-Inspired 3D Hydrogel-Bioceramic Composite for Enhanced Bone Regeneration. *Macromol Biosci* **16**, 276-287.
[62] Lim, T.C., Rokkappanavar, S., Toh, W.S., Wang, L.S., Kurisawa, M. and Spector, M. (2013) Chemotactic recruitment of adult neural progenitor cells into multifunctional hydrogels providing sustained SDF-1alpha release and compatible structural support. *FASEB J* **27**, 1023-1033.
[63] Bystroňová, J., Sˇcˇigalkova, I., Wolfova´, L., Pravda, M., Vrana, N.E. and Velebny´, V. (2018) Creating a 3D microenvironment for monocyte cultivation: ECM-mimicking hydrogels based on gelatine and hyaluronic acid derivatives. *RSC Advances* **8**, 7606-7614.
[64] Lee, F., Chung, J.E. and Kurisawa, M. (2009) An injectable hyaluronic acid-tyramine hydrogel system for protein delivery. *J Control Release* **134**, 186-193.
[65] Ma, L., Gao, C., Mao, Z., Zhou, J. and Shen, J. (2004) Enhanced biological stability of collagen porous scaffolds by using amino acids as novel cross-linking bridges. *Biomaterials* **25**, 2997-3004.
[66] Ihalin, R., Tenovuo, J. and Pöllänen, M. (2003) Determination of safety levels of horseradish peroxidase-iodide system tohuman gingival keratinocytes and ¬¢broblastsinvitro. *Cell Biology and Toxicology* **19**, 339-353.
[67] Sakai, S., Hirose, K., Taguchi, K., Ogushi, Y. and Kawakami, K. (2009) An injectable, in situ enzymatically gellable, gelatin derivative for drug delivery and tissue engineering. *Biomaterials* **30**, 3371-3377.
[68] Oudgenoeg, G., Hilhorst, R., Piersma, S.R., Boeriu, C.G., Gruppen, H., Hessing, M., Voragen, A.G.J. and Laane, A.C. (2001) Peroxidase-Mediated Cross-Linking of a Tyrosine-Containing Peptide with Ferulic Acid. *J. Agric. Food Chem* **49**, 2503-2510.

[69] Koshy, S.T., Ferrante, T.C., Lewin, S.A. and Mooney, D.J. (2014) Injectable, porous, and cell-responsive gelatin cryogels. *Biomaterials* **35**, 2477-2487.
[70] Gómez-Guillén, M.C., Giménez, B., López-Caballero, M.E. and Montero, M.P. (2011) Functional and bioactive properties of collagen and gelatin from alternative sources: A review. *Food Hydrocolloids* **25**, 1813-1827.
[71] Matos, S., Guerra, F., Krauser, J.T., Figueiredo, H., Marcelino, J.P. and Sanz, M. (2012) Evaluation of an anorganic bovine-derived mineral with P-15 hydrogel bone graft: preliminary study in a rabbit cranial bone model. *Clin Oral Implants Res* **23**, 698-705.
[72] Hoogendoorn, H.A., Renooij, W., Akkermans, L.M., Visser, W. and Wittebol, P. (1984) Long-Term Study of Large Ceramic Implants (Porous Hydroxyapatite) in Dog Femora. *Clinical orthopaedics and related research* **187**, 281-288.
[73] Fatimi, A., Tassin, J.F., Axelos, M.A. and Weiss, P. (2010) The stability mechanisms of an injectable calcium phosphate ceramic suspension. *J Mater Sci Mater Med* **21**, 1799-1809.
[74] Yu, H., VandeVord, P.J., Mao, L., Matthew, H.W., Wooley, P.H. and Yang, S.Y. (2009) Improved tissue-engineered bone regeneration by endothelial cell mediated vascularization. *Biomaterials* **30**, 508-517.
[75] Salinas, A.J. and Vallet-Regi, M. (2013) Bioactive ceramics: from bone grafts to tissue engineering. *RSC Advances* **3**, 11116-11131.
[76] Toh, W.S., Lim, T.C., Kurisawa, M. and Spector, M. (2012) Modulation of mesenchymal stem cell chondrogenesis in a tunable hyaluronic acid hydrogel microenvironment. *Biomaterials* **33**, 3835-3845.
[77] Fitton Jackson, S. (1970) Environmental Control of Macromolecular Synthesis in Cartilage and Bone: Morphogenetic Response to Hyaluronidase. *Proceedings of the Royal Society of London. Series B, Containing papers of a Biological character. Royal Society (Great Britain)* **175**, 405-453.
[78] Shur, B.D., Vogler, M. and Kosher, R.A. (1982) Changes in endogenous cell surface galactosyltransferase activity during in vitro limb bud chondrogenesis. **137**, 229-237.
[79] Elbert, D.L. (2011) Liquid-liquid two-phase systems for the production of porous hydrogels and hydrogel microspheres for biomedical applications: A tutorial review. *Acta Biomater* **7**, 31-56.
[80] Loh, Q.L. and Choong, C. (2013) Three-dimensional scaffolds for tissue engineering applications: role of porosity and pore size. *Tissue Eng Part B Rev* **19**, 485-502.

[81] Kloxin, A.M., Kloxin, C.J., Bowman, C.N. and Anseth, K.S. (2010) Mechanical Properties of Cellularly Responsive Hydrogels and Their Experimental Determination. *Advanced Materials* **22**, 3484-3494.
[82] Salinas, C.N. and Anseth, K.S. (2009) Mesenchymal stem cells for craniofacial tissue regeneration: designing hydrogel delivery vehicles. *J Dent Res* **88**, 681-692.
[83] Jin, R., Hiemstra, C., Zhong, Z. and Feijen, J. (2007) Enzyme-mediated fast in situ formation of hydrogels from dextran,Äìtyramine conjugates. *Biomaterials* **28**, 2791-2800.
[84] Park, K.M., Ko, K.S., Joung, Y.K., Shin, H. and Park, K.D. (2011) In situ cross-linkable gelatin–poly(ethylene glycol)–tyramine hydrogel via enzyme-mediated reaction for tissue regenerative medicine. *Journal of Materials Chemistry* **21**, 13180-13187.
[85] Lee, F., Chung, J.E. and Kurisawa, M. (2009) An injectable hyaluronic acid-tyramine hydrogel system for protein delivery. *J Control Release* **134**, 186-193.
[86] Shi, N., Yin, G., Han, M. and Xu, Z. (2008) Anions bonded on the supramolecular hydrogel surface as the growth center of biominerals. *Colloids Surf B Biointerfaces* **66**, 84-89.
[87] Yun, Y.R., Won, J.E., Jeon, E., Lee, S., Kang, W., Jo, H., Jang, J.H., Shin, U.S. and Kim, H.W. (2010) Fibroblast growth factors: biology, function, and application for tissue regeneration. *J Tissue Eng* **2010**, 218142.
[88] Hunter, G.K. and Goldberg, H.A. (1994) Modulation of crystal formation by bone phosphoproteins: role of glutamic acid-rich sequences in the nucleation of hydroxyapatite by bone sialoprotein. **302**, 175-179.
[89] Song, J., Malathong, V. and Bertozzi, C.R. (2005) Mineralization of synthetic polymer scaffolds: a bottom-up approach for the development of artificial bone. *J Am Chem Soc* **127**, 3366-3372.
[90] Shih, Y.R., Hwang, Y., Phadke, A., Kang, H., Hwang, N.S., Caro, E.J., Nguyen, S., Siu, M., Theodorakis, E.A., Gianneschi, N.C., Vecchio, K.S., Chien, S., Lee, O.K. and Varghese, S. (2014) Calcium phosphate-bearing matrices induce osteogenic differentiation of stem cells through adenosine signaling. *Proc Natl Acad Sci U S A* **111**, 990-995.
[91] Xu, D., Bhatnagar, D., Gersappe, D., Sokolov, J.C., Rafailovich, M.H. and Lombardi, J. (2015) Rheology of Poly(N-isopropylacrylamide),ÄìClay Nanocomposite Hydrogels. *Macromolecules* **48**, 840-846.

[92] Piskounova, S., Rojas, R., Bergman, K. and Hilborn, J. (2011) The Effect of Mixing on the Mechanical Properties of Hyaluronan-Based Injectable Hydrogels. *Macromolecular Materials and Engineering* **296**, 944-951.
[93] Cohen, D.L., Lo, W., Tsavaris, A., Peng, D., Lipson, H. and Bonassar, L.J. (2011) Increased Mixing Improves Hydrogel Homogeneity and Quality of Three-Dimensional Printed Constructs. *Tissue Engineering Part C: Methods* **17**, 239-248.
[94] Hozumi, T., Ohta, S. and Ito, T. (2015) Analysis of the Calcium Alginate Gelation Process Using a Kenics Static Mixer. *Industrial & Engineering Chemistry Research* **54**, 2099-2107.
[95] Norris, S.C.P., Tseng, P. and Kasko, A.M. (2016) Direct Gradient Photolithography of Photodegradable Hydrogels with Patterned Stiffness Control with Submicrometer Resolution. *ACS Biomaterials Science & Engineering* **2**, 1309-1318.
[96] Gruschwitz, R., Friedrichs, J., Valtink, M., Franz, C.M., Muller, D.J., Funk, R.H. and Engelmann, K. (2010) Alignment and cell-matrix interactions of human corneal endothelial cells on nanostructured collagen type I matrices. *Invest Ophthalmol Vis Sci* **51**, 6303-6310.
[97] Wang, L.-S., Chung, J.E., Chan, P.P.-Y. and Kurisawa, M. (2010) Injectable biodegradable hydrogels with tunable mechanical properties for the stimulation of neurogenesic differentiation of human mesenchymal stem cells in 3D culture. *Biomaterials* **31**, 1148-1157.
[98] Wang, L.S., Du, C., Chung, J.E. and Kurisawa, M. (2012) Enzymatically cross-linked gelatin-phenol hydrogels with a broader stiffness range for osteogenic differentiation of human mesenchymal stem cells. *Acta Biomater* **8**, 1826-1837.
[99] Hutmacher, D.W. (2000) Sca!olds in tissue engineering bone and cartilage. *Biomaterials 21* **21**, 2529-2543.
[100] Bohner, M., Loosli, Y., Baroud, G. and Lacroix, D. (2011) Commentary: Deciphering the link between architecture and biological response of a bone graft substitute. *Acta Biomater* **7**, 478-484.
[101] Schlichting, K., Schell, H., Kleemann, R.U., Schill, A., Weiler, A., Duda, G.N. and Epari, D.R. (2008) Influence of scaffold stiffness on subchondral bone and subsequent cartilage regeneration in an ovine model of osteochondral defect healing. *Am J Sports Med* **36**, 2379-2391.
[102] Hu, H., Huang, B.W., Lee, Y.T., Hu, J., Wong, S.W., Ko, C.C. and You, W. (2018) Dramatic Improvement of the Mechanical Strength of Silane-Modified Hydroxyapatite-Gelatin Composites via Processing with Cosolvent. *ACS Omega* **3**, 3592-3598.

[103] van Oosten, A.S., Vahabi, M., Licup, A.J., Sharma, A., Galie, P.A., MacKintosh, F.C. and Janmey, P.A. (2016) Uncoupling shear and uniaxial elastic moduli of semiflexible biopolymer networks: compression-softening and stretch-stiffening. *Sci Rep* **6**, 19270.
[104] Reddy, A.S. and Sastry, G.N. (2005) Cation [M = H+, Li+, Na+, K+, Ca2+, Mg2+, NH4+, and NMe4+] interactions with the aromatic motifs of naturally occurring amino acids: a theoretical study. *J Phys Chem A* **109**, 8893-8903.
[105] Neffe, A.T., Loebus, A., Zaupa, A., Stoetzel, C., Muller, F.A. and Lendlein, A. (2011) Gelatin functionalization with tyrosine derived moieties to increase the interaction with hydroxyapatite fillers. *Acta Biomater* **7**, 1693-1701.
[106] Aspenberg, P. and Sandberg, O. (2013) Distal radial fractures heal by direct woven bone formation. *Acta Orthop* **84**, 297-300.
[107] Yan, L.P., Wang, Y.J., Ren, L., Wu, G., Caridade, S.G., Fan, J.B., Wang, L.Y., Ji, P.H., Oliveira, J.M., Oliveira, J.T., Mano, J.F. and Reis, R.L. (2010) Genipin-cross-linked collagen/chitosan biomimetic scaffolds for articular cartilage tissue engineering applications. *J Biomed Mater Res A* **95**, 465-475.
[108] Friedenstein, A.J., Deriglasova, U.F., Kulagina, N.N., Panasuk, A.F., Rudakowa, S.F., Luri√°, E.A. and Ruadkow, I.A. (1974) Precursors for fibroblasts in different populations of hematopoietic cells as detected by the in vitro colony assay method. *Exp Hematol* **2**, 83-92.
[109] Kinner, B. and Spector, M. (2000) Smooth muscle actin expression by human articular chondrocytes and their contraction of a collagen-glycosaminoglycan matrix in vitro. *Journal of Orthopaedic Researc* **19**, 233-241.
[110] Bruder, S.P., Jaiswal, N. and Haynesworth, S.E. (1997) Growth kinetics, self-renewal, and the osteogenic potential of purified human mesenchymal stem cells during extensive subcultivation and following cryopreservation. *Journal of Cellular Biochemistry* **64**, 278-294.
[111] Puchtler, H., Meloan, S.N. and Terry, M.S. (1969) On the history and mechanism of alizarin and alizarin red S stains for calcium. *J Histochem Cytochem.* **17**, 110-124.
[112] Vengrenyuk, Y., Carlier, S., Xanthos, S., Cardoso, L., Ganatos, P., Virmani, R., Einav, S., Gilchrist, L. and Weinbaum, S. (2006) A hypothesis for vulnerable plaque rupture due to stress-induced debonding around cellular microcalcifications in thin fibrous caps. *Proceedings of the National Academy of Sciences* **103**, 14678-14683.

[113] Bensimon-Brito, A., Cardeira, J., Dionisio, G., Huysseune, A., Cancela, M.L. and Witten, P.E. (2016) Revisiting in vivo staining with alizarin red S--a valuable approach to analyse zebrafish skeletal mineralization during development and regeneration. *BMC Dev Biol* **16**, 2.
[114] Talele, N.P., Fradette, J., Davies, J.E., Kapus, A. and Hinz, B. (2015) Expression of alpha-Smooth Muscle Actin Determines the Fate of Mesenchymal Stromal Cells. *Stem Cell Reports* **4**, 1016-1030.
[115] Sun, X. and Kaufman, P.D. (2018) Ki-67: more than a proliferation marker. *Chromosoma* **127**, 175-186.
[116] Price, P.A. (1985) Vitamin K-Dependent Formation of Bone Gla Protein (Osteocalcin) and Its Function. *Vitamins & Hormones* **42**, 65-108.
[117] Wians, P.V.H.F. (1989) Osteocalcin-Hydroxyapatite Interaction in the Extracellular Organic Matrix of Bone. *The Anatomical Record* 180-188.
[118] Chavassieux, P., Portero-Muzy, N., Roux, J.-P., Garnero, P. and Chapurlat, R. (2015) Are Biochemical Markers of Bone Turnover Representative of Bone Histomorphometry in 370 Postmenopausal Women. **100**, 4662-4668.
[119] Weaver, C.M., Peacock, M., Martin, B.R., Mccabe, G.P., Zhao, J., Smith, D.L. and Wastney, M.E. (1997) Quantification of Biochemical Markers of Bone Turnover by Kinetic Measures of Bone Formation and Resorption in Young Healthy Females. **12**, 1714-1720.
[120] Reinholt, F.P., Hultenby, K., Oldberg, A. and Heinegård, D. (1990) Osteopontin--a possible anchor of osteoclasts to bone. *Proceedings of the National Academy of Sciences of the United States of America* **87**, 4473.
[121] Sodek, J., Ganss, B. and McKee, M.D. (2000) Osteopontin. *Critical Reviews in Oral Biology & Medicine* **11**, 279-303.
[122] Urban, I.A., Monje, A., Lozada, J.L. and Wang, H.L. (2017) Long-term Evaluation of Peri-implant Bone Level after Reconstruction of Severely Atrophic Edentulous Maxilla via Vertical and Horizontal Guided Bone Regeneration in Combination with Sinus Augmentation: A Case Series with 1 to 15 Years of Loading. *Clin Implant Dent Relat Res* **19**, 46-55.
[123] Lee, E.A. (2017) Subperiosteal Minimally Invasive Aesthetic Ridge Augmentation Technique (SMART): A New Standard for Bone Reconstruction of the Jaws. *Int J Periodontics Restorative Dent* **37**, 165-173.

[124] Rehfeldt, F., Brown, A.E., Raab, M., Cai, S., Zajac, A.L., Zemel, A. and Discher, D.E. (2012) Hyaluronic acid matrices show matrix stiffness in 2D and 3D dictates cytoskeletal order and myosin-II phosphorylation within stem cells. *Integr Biol (Camb)* **4**, 422-430.
[125] Boontheekul, T., Hill, E.E., Kong, H.-J. and Mooney, D.J. (2007) Regulating myoblast phenotype through controlled gel stiffness and degradation. *Tissue engineering* **13**, 1431-1442.
[126] Cao, X., Pettit, M.E., Conlan, S.L., Wagner, W., Ho, A.D., Clare, A.S., Callow, J.A., Callow, M.E., Grunze, M. and Rosenhahn, A. (2009) Resistance of polysaccharide coatings to proteins, hematopoietic cells, and marine organisms. *Biomacromolecules* **10**, 907-915.
[127] Evanko, S.P., Tammi, M.I., Tammi, R.H. and Wight, T.N. (2007) Hyaluronan-dependent pericellular matrix. *Adv Drug Deliv Rev* **59**, 1351-1365.
[128] Reichert, D., Friedrichs, J., Ritter, S., Käubler, T., Werner, C., Bornhäuser, M. and Corbeil, D. (2015) Phenotypic, morphological and adhesive differences of human hematopoietic progenitor cells cultured on murine versus human mesenchymal stromal cells. *Scientific reports* **5**, 15680.
[129] Bachir, A., Horwitz, A.R., Nelson, W.J. and Bianchini, J.M. (2017) Cell Adhesions: Actin-Based Modules that Mediate Cell-Extracellular Matrix and Cell-Cell Interactions. *Cold Spring Harbor perspectives in biology* **9**. doi:10.1101/cshperspect.a023234.
[130] Rahmany, M.B. and Van Dyke, M. (2013) Biomimetic approaches to modulate cellular adhesion in biomaterials: A review. *Acta Biomater* **9**, 5431-5437.
[131] Gruschwitz, R., Friedrichs, J., Valtink, M., Franz, C.M., Muller, D.J., Funk, R.H. and Engelmann, K. (2010) Alignment and cell-matrix interactions of human corneal endothelial cells on nanostructured collagen type I matrices. *Invest Ophthalmol Vis Sci* **51**, 6303-6310.
[132] Carvalho, R.S., Kostenuik, P.J., Salih, E., Bumann, A. and Gerstenfeld, L.C. (2003) Selective adhesion of osteoblastic cells to different integrin ligands induces osteopontin gene expression. *Matrix Biology* **22**, 241-249.
[133] Schor, S.L. and Court, J. (1979) Different mechanisms in the attachment of cells to native and denatured collagen. *J Cell Sci* **38**, 267-281.
[134] Geiger, B., Spatz, J.P. and Bershadsky, A.D. (2009) Environmental sensing through focal adhesions. *Nature reviews Molecular cell biology* **10**, 21.
[135] Davidenko, N., Schuster, C.F., Bax, D.V., Farndale, R.W., Hamaia, S., Best, S.M. and Cameron, R.E. (2016) Evaluation of cell binding to collagen and gelatin: a study of the effect of 2D and 3D architecture and surface chemistry. *J Mater Sci Mater Med* **27**, 148.

[136] Ivanovska, I.L., Shin, J.W., Swift, J. and Discher, D.E. (2015) Stem cell mechanobiology: diverse lessons from bone marrow. *Trends Cell Biol* **25**, 523-532.
[137] Chaudhuri, O., Gu, L., Darnell, M., Klumpers, D., Bencherif, S.A., Weaver, J.C., Huebsch, N. and Mooney, D.J. (2015) Substrate stress relaxation regulates cell spreading. *Nature communications* **6**, 6365.
[138] Xue, R., Li, J.Y., Yeh, Y., Yang, L. and Chien, S. (2013) Effects of matrix elasticity and cell density on human mesenchymal stem cells differentiation. *J Orthop Res* **31**, 1360-1365.
[139] Yim, E.K., Darling, E.M., Kulangara, K., Guilak, F. and Leong, K.W. (2010) Nanotopography-induced changes in focal adhesions, cytoskeletal organization, and mechanical properties of human mesenchymal stem cells. *Biomaterials* **31**, 1299-1306.
[140] Kilian, K.A., Bugarija, B., Lahn, B.T. and Mrksich, M. (2010) Geometric cues for directing the differentiation of mesenchymal stem cells. *Proc Natl Acad Sci U S A* **107**, 4872-4877.
[141] Vicente-Manzanares, M., Ma, X., Adelstein, R.S. and Horwitz, A.R. (2009) Non-muscle myosin II takes centre stage in cell adhesion and migration. *Nature reviews Molecular cell biology* **10**, 778.
[142] Peyton, S.R., Kim, P.D., Ghajar, C.M., Seliktar, D. and Putnam, A.J. (2008) The effects of matrix stiffness and RhoA on the phenotypic plasticity of smooth muscle cells in a 3-D biosynthetic hydrogel system. *Biomaterials* **29**, 2597-2607.
[143] Boontheekul, T., Hill, E.E., Kong, H.-J. and Mooney, D.J. (2007) Regulating myoblast phenotype through controlled gel stiffness and degradation. *Tissue engineering* **13**, 1431-1442.
[144] Boguslawski, G., Hale, L.V., Yu, X.-P., Miles, R.R., Onyia, J.E., Santerre, R.F. and Chandrasekhar, S. (2000) Activation of osteocalcin transcription involves interaction of protein kinase A-and protein kinase C-dependent pathways. *Journal of Biological Chemistry* **275**, 999-1006.
[145] Zohar, R., Cheifetz, S., McCulloch, C.A. and Sodek, J. (1998) Analysis of intracellular osteopontin as a marker of osteoblastic cell differentiation and mesenchymal cell migration. *Eur J Oral Sci* **106 Suppl 1**, 401-407.
[146] Denhardt, D.T., Noda, M., O'Regan, A.W., Pavlin, D. and Berman, J.S. (2001) Osteopontin as a means to cope with environmental insults: regulation of inflammation, tissue remodeling, and cell survival. *The Journal of clinical investigation* **107**, 1055-1061.

[147] Matsuo, K. and Irie, N. (2008) Osteoclast–osteoblast communication. *Archives of biochemistry and biophysics* **473**, 201-209.
[148] Gordon, J.A., Tye, C.E., Sampaio, A.V., Underhill, T.M., Hunter, G.K. and Goldberg, H.A. (2007) Bone sialoprotein expression enhances osteoblast differentiation and matrix mineralization in vitro. *Bone* **41**, 462-473.
[149] Dong, M., Yu, X., Chen, W., Guo, Z., Sui, L., Xu, Y., Shang, Y., Niu, W. and Kong, Y. (2018) Osteopontin Promotes Bone Destruction in Periapical Periodontitis by Activating the NF-κB Pathway. *Cell Physiol Biochem* **49**, 884-898.
[150] Zheng, H., Guo, Z., Ma, Q., Jia, H. and Dang, G. (2004) Cbfa1/osf2 Transduced Bone Marrow Stromal Cells Facilitate Bone Formation In Vitro and In Vivo. **74**, 194-203.
[151] Ritter, N.M., Farach-Carson, M.C. and Butler, W.T. (1992) Evidence for the Formation of a Complex Between Osteopontin and Osteocalcin. *Journal of Bone and Mineral Research* **7**, 877-884.
[152] Carvalho, M.S., Cabral, J.M., da Silva, C.L. and Vashishth, D. (2019) Synergistic effect of extracellularly supplemented osteopontin and osteocalcin on stem cell proliferation, osteogenic differentiation, and angiogenic properties. *J Cell Biochem* **120**, 6555-6569.
[153] Han, F., Zhu, C., Guo, Q., Yang, H. and Li, B. (2016) Cellular modulation by the elasticity of biomaterials. *Journal of Materials Chemistry B* **4**, 9-26.
[154] Ivanovska, I.L., Shin, J.W., Swift, J. and Discher, D.E. (2015) Stem cell mechanobiology: diverse lessons from bone marrow. *Trends Cell Biol* **25**, 523-532.
[155] Kilian, K.A. and Mrksich, M. (2012) Directing stem cell fate by controlling the affinity and density of ligand-receptor interactions at the biomaterials interface. *Angew Chem Int Ed Engl* **51**, 4891-4895.
[156] Engler, A.J., Sen, S., Sweeney, H.L. and Discher, D.E. (2006) Matrix elasticity directs stem cell lineage specification. *Cell* **126**, 677-689.
[157] Zemel, A., Rehfeldt, F., Brown, A.E.X., Discher, D.E. and Safran, S.A. (2010) Optimal matrix rigidity for stress-fibre polarization in stem cells. *Nature physics* **6**, 468.
[158] Sun, H., Zhu, F., Hu, Q. and Krebsbach, P.H. (2014) Controlling stem cell-mediated bone regeneration through tailored mechanical properties of collagen scaffolds. *Biomaterials* **35**, 1176-1184.

[159] Zhao, W., Li, X., Liu, X., Zhang, N. and Wen, X. (2014) Effects of substrate stiffness on adipogenic and osteogenic differentiation of human mesenchymal stem cells. *Mater Sci Eng C Mater Biol Appl* **40**, 316-323.
[160] Phadke, A., Zhang, C., Hwang, Y., Vecchio, K. and Varghese, S. (2010) Templated mineralization of synthetic hydrogels for bone-like composite materials: Role of matrix hydrophobicity. *Biomacromolecules* **11**, 2060-2068.
[161] Phadke, A., Shih, Y.V. and Varghese, S. (2012) Mineralized synthetic matrices as an instructive microenvironment for osteogenic differentiation of human mesenchymal stem cells. *Macromolecular bioscience* **12**, 1022-1032.
[162] Chen, Y.C., Lin, R.Z., Qi, H., Yang, Y., Bae, H., Melero-Martin, J.M. and Khademhosseini, A. (2012) Functional Human Vascular Network Generated in Photocrosslinkable Gelatin Methacrylate Hydrogels. *Adv Funct Mater* **22**, 2027-2039.
[163] Guerreiro, S.G., Oliveira, M.J., Barbosa, M.A., Soares, R. and Granja, P.L. (2014) Neonatal human dermal fibroblasts immobilized in RGD-alginate induce angiogenesis. *Cell Transplant* **23**, 945-957.
[164] Hozumi, T., Kageyama, T., Ohta, S., Fukuda, J. and Ito, T. (2018) Injectable Hydrogel with Slow Degradability Composed of Gelatin and Hyaluronic Acid Cross-Linked by Schiff‚Äôs Base Formation. *Biomacromolecules* **19**, 288-297.
[165] Boonrungsiman, S., Gentleman, E., Carzaniga, R., Evans, N.D., McComb, D.W., Porter, A.E. and Stevens, M.M. (2012) The role of intracellular calcium phosphate in osteoblast-mediated bone apatite formation. *Proceedings of the National Academy of Sciences* **109**, 14170-14175.
[166] Qin, Y., Sun, R., Wu, C., Wang, L. and Zhang, C. (2016) Exosome: A Novel Approach to Stimulate Bone Regeneration through Regulation of Osteogenesis and Angiogenesis. *Int J Mol Sci* **17**, doi: 10.3390/ijms17050712.
[167] Farquhar, M.G. (1985) Progress in Unraveling Pathways of Golgi Traffic. *Ann. Rev. Cell Bioi.* **1**, 447-488.
[168] Théry, C., Zitvogel, L. and Amigorena, S. (2002) Exosomes: composition, biogenesis and function. *Nature reviews immunology* **2**, 569.
[169] Anderson, H.C. (1967) Electron microscopic studies of induced cartilage development and calcification. *The Journal of cell biology* **35**, 81-101.

[170] Kirsch, T., Harrison, G., Golub, E.E. and Nah, H.-D. (2000) The roles of annexins and types II and X collagen in matrix vesicle-mediated mineralization of growth plate cartilage. *Journal of Biological Chemistry* **275**, 35577-35583.
[171] Golub, E.E. (2009) Role of matrix vesicles in biomineralization. *Biochimica et Biophysica Acta (BBA)-General Subjects* **1790**, 1592-1598.
[172] Arispe, N., Rojas, E., Genge, B.R., Wu, L.N. and Wuthier, R.E. (1996) Similarity in calcium channel activity of annexin V and matrix vesicles in planar lipid bilayers. *Biophysical journal* **71**, 1764-1775.
[173] Wu, L.N., Genge, B.R., Lloyd, G.C. and Wuthier, R.E. (1991) Collagen-binding proteins in collagenase-released matrix vesicles from cartilage. Interaction between matrix vesicle proteins and different types of collagen. *Journal of Biological Chemistry* **266**, 1195-1203.
[174] Tenenbaum, H.C. and Heersche, J.N.M. (1986) Differentiation of osteoid-producing cellsin vitro: Possible evidence for the requirement of a microenvironment. **38**, 262-267.
[175] Gkioni, K., Leeuwenburgh, S.C., Douglas, T.E., Mikos, A.G. and Jansen, J.A. (2010) Mineralization of hydrogels for bone regeneration. *Tissue Eng Part B Rev* **16**, 577-585.
[176] Thyberg, J. and Moskalewski, S. (1979) Bone formation in cartilage produced by transplanted epiphyseal chondrocytes. *Cell Tissue Res.* **204**, 77-94.
[177] Osborn, J.F. (1980) Dynamic aspects of the implant-bone-interface, Heimke, G. Dental implants. Materials and systems. *Carl Hanser Verlag, Munchen* 111-123.
[178] Davies, J.E. (2003) Understanding peri-implant endosseous healing. *J Dent Educ.* **67**, 932-949.
[179] Bukka, P., McKee, M.D. and Karaplis, A.C. (2004) Molecular regulation of osteoblast differentiation. *Bone Formation* 1-17.
[180] Cölfen, H. (2010) Biomineralization: a crystal-clear view. *Nature materials* **9**, 960.
[181] McKee, M.D., Addison, W.N. and Kaartinen, M.T. (2005) Hierarchies of extracellular matrix and mineral organization in bone of the craniofacial complex and skeleton. *Cells Tissues Organs* **181**, 176-188.
[182] Ishimoto, T., Nakano, T., Umakoshi, Y., Yamamoto, M. and Tabata, Y. (2013) Degree of biological apatite c-axis orientation rather than bone mineral density controls mechanical function in bone regenerated using recombinant bone morphogenetic protein-2. *Journal of Bone and Mineral Research* **28**, 1170-1179.

[183] Caballe-Serrano, J., Fujioka-Kobayashi, M., Bosshardt, D.D., Gruber, R., Buser, D. and Miron, R.J. (2016) Pre-coating deproteinized bovine bone mineral (DBBM) with bone-conditioned medium (BCM) improves osteoblast migration, adhesion, and differentiation in vitro. *Clin Oral Investig* **20**, 2507-2513.
[184] Nugent, M.A. and Iozzo, R.V. (2000) Fibroblast growth factor-2. *The international journal of biochemistry & cell biology* **32**, 115-120.
[185] Cao, R., Bråkenhielm, E., Pawliuk, R., Wariaro, D., Post, M.J., Wahlberg, E., Leboulch, P. and Cao, Y. (2003) Angiogenic synergism, vascular stability and improvement of hind-limb ischemia by a combination of PDGF-BB and FGF-2. *Nature medicine* **9**, 604.
[186] Kim, S.J., Kim, S.Y., Kwon, C.H. and Kim, Y.K. (2007) Differential effect of FGF and PDGF on cell proliferation and migration in osteoblastic cells. *Growth factors* **25**, 77-86.
[187] Ng, F., Boucher, S., Koh, S., Sastry, K.S.R., Chase, L., Lakshmipathy, U., Choong, C., Yang, Z., Vemuri, M.C. and Rao, M.S. (2008) PDGF, TGF-β, and FGF signaling is important for differentiation and growth of mesenchymal stem cells (MSCs): transcriptional profiling can identify markers and signaling pathways important in differentiation of MSCs into adipogenic, chondrogenic, and osteogenic lineages. *Blood* **112**, 295-307.
[188] Virakul, S., Heutz, J.W., Dalm, V.A., Peeters, R.P., Paridaens, D., van den Bosch, W.A., Hirankarn, N., van Hagen, P.M. and Dik, W.A. (2016) Basic FGF and PDGF-BB synergistically stimulate hyaluronan and IL-6 production by orbital fibroblasts. *Mol Cell Endocrinol* **433**, 94-104.
[189] Aspenberg, P. and Sandberg, O. (2013) Distal radial fractures heal by direct woven bone formation. *Acta orthopaedica* **84**, 297-300.
[190] Kratchmarova, I., Blagoev, B., Haack-Sorensen, M., Kassem, M. and Mann, M. (2005) Mechanism of divergent growth factor effects in mesenchymal stem cell differentiation. *Science* **308**, 1472-1477.
[191] Baron, R., Saffar, J.L. and Duflot-Vignery, A. (1976) Alveolar bone remodelling in the rat: Normal status and effects of PTX and PTH on the remodelling sequence and the osteoclastic pool. **22**, 502-504.
[192] Urist, M.R., DeLange, R. and Finerman, G. (1983) Bone Cell Differentiation and Growth Factors. *Science (New York, N.Y.)* **220**, 680-686.
[193] Genco, R.J., Marx, R.E. and Lynch, S.E. (1999) *Tissue engineering: applications in maxillofacial surgery and periodontics*, Quintessence Publishing Company

[194] Barnes, G.L., Kostenuik, P.J., Gerstenfeld, L.C. and Einhorn, T.A. (1999) Growth Factor Regulation of Fracture Repair. **14**, 1805-1815.
[195] Gerhardt, H. and Betsholtz, C. (2003) Endothelial-pericyte interactions in angiogenesis. *Cell Tissue Res* **314**, 15-23.
[196] Pechak, D.G., Kujawa, M.J. and Caplan, A.I. (1986) Morphology of bone development and bone remodeling in embryonic chick limbs. *Bone* **7**, 459-472.
[197] Caplan, A.I. (2009) New Era of Cell-Based Orthopedic Therapies. *TISSUE ENGINEERING: Part B* **15**, 195-200.
[198] Hollinger, J.O., Hart, C.E., Hirsch, SN and al., E. (2008) Recombinant Human Platelet-Derived Growth Factor: Biology and Clinical Applications. *J Bone Joint Surg Am* **90**, 48-54.
[199] Pereira, R.C., Economides, A.N. and Canalis, E. (2000) Bone Morphogenetic Proteins Induce Gremlin, a Protein That Limits Their Activity in Osteoblasts 1. *Endocrinology* **141**, 4558-4563.
[200] Canalis, E., Centrella, M. and Mccarthy, T. (1988) Effects of basic fibroblast growth factor on bone formation in vitro. *J Clin Invest.* **81**, 1572-1577.
[201] Power, R.A., Iwaniec, U.T. and Wronski, T.J. (2002) Changes in gene expression associated with the bone anabolic effects of basic fibroblast growth factor in aged ovariectomized rats. **31**, 143-148.
[202] Javerzat, S., Auguste, P. and Bikfalvi, A. (2002) The role of fibroblast growth factors in vascular development. *Trends in Molecular Medicine* **8**, 483-489.
[203] Jeong, I., Yu, H.S., Kim, M.K., Jang, J.H. and Kim, H.W. (2010) FGF2-adsorbed macroporous hydroxyapatite bone granules stimulate in vitro osteoblastic gene expression and differentiation. *J Mater Sci Mater Med* **21**, 1335-1342.
[204] Kawaguchi, H., Nakamura, K., Tabata, Y., Ikada, Y., Aoyama, I., Anzai, J., Nakamura, T., Hiyama, Y. and Tamura, M. (2001) Acceleration of Fracture Healing in Nonhuman Primates by Fibroblast Growth Factor-2. *J Clin Endocrinol Metab.* **86**, 875-880.
[205] Tabata, Y., Nagano, A., Muniruzzaman, M. and Ikada, Y. (1998) In vitro sorption and desorption of basic fibroblast growth factor from biodegradable hydrogels. *Biomaterials* **19**, 1781-1789.
[206] Okazaki, H., Kurokawa, T., Nakamura, K., Matsushita, T., Mamada, K. and Kawaguchi, H. (1999) Stimulation of Bone Formation by Recombinant Fibroblast Growth Factor-2 in Callotasis Bone Lengthening of Rabbits. **64**, 542-546.

[207] Kuhn, L.T., Ou, G., Charles, L., Hurley, M.M., Rodner, C.M. and Gronowicz, G. (2013) Fibroblast growth factor-2 and bone morphogenetic protein-2 have a synergistic stimulatory effect on bone formation in cell cultures from elderly mouse and human bone. *J Gerontol A Biol Sci Med Sci* **68**, 1170-1180.
[208] Presta, M., Dell'Era, P., Mitola, S., Moroni, E., Ronca, R. and Rusnati, M. (2005) Fibroblast growth factor/fibroblast growth factor receptor system in angiogenesis. *Cytokine and Growth Factor Reviews* **16**, 159-178.
[209] Andreopoulos, F.M. and Persaud, I. (2006) Delivery of basic fibroblast growth factor (bFGF) from photoresponsive hydrogel scaffolds. *Biomaterials* **27**, 2468-2476.
[210] Gao, Y., Zhu, S., Luo, E., Li, J., Feng, G. and Hu, J. (2009) Basic fibroblast growth factor suspended in Matrigel improves titanium implant fixation in ovariectomized rats. *Journal of Controlled Release* **139**, 15-21.
[211] Noshi, T., Yoshikawa, T., Ikeuchi, M., Dohi, Y., Ohgushi, H., Horiuchi, K., Sugimura, M., Ichijima, K. and Yonemasu, K. (2000) Enhancement of the in vivo osteogenic potential of marrow/hydroxyapatite composites by bovine bone morphogenetic protein. *Journal of Biomedical Materials Research* **52**, 621-630.
[212] Lindahl, U. and Li, J.P. (2009) Interactions between heparan sulfate and proteins-design and functional implications. *International review of cell and molecular biology* **276**, 105-159.
[213] Midy, V., Rey, C., Bres, E. and Dard, M. (1998) Basic fibroblast growth factor adsorption and release properties of calcium phosphate. *J Biomed Mater Res* **41**, 405-411.
[214] Tabata, Y. and Ikada, Y. (1999) Vascularization effect of basic fibroblast growth factor released from gelatin hydrogels with different biodegradabilities. *Biomaterials.* **20**, 2169-2175.
[215] Russo, K., Ragone, R., Facchiano, A.M., Capogrossi, M.C. and Facchiano, A. (2002) Platelet-derived growth factor-BB and basic fibroblast growth factor directly interact in vitro with high affinity. *J Biol Chem* **277**, 1284-1291.
[216] Zhu, J., Lin, F., Brown, D.A. and Clark, R.A.F. (2014) A Fibronectin Peptide Redirects PDGF-BB/PDGFR Complexes to Macropinocytosis-Like Internalization and Augments PDGF-BB Survival Signals. *Journal of Investigative Dermatology(***134**, 921-929.
[217] Raab, M., Swift, J., Dingal, P.C., Shah, P., Shin, J.W. and Discher, D.E. (2012) Crawling from soft to stiff matrix polarizes the cytoskeleton and phosphoregulates myosin-II heavy chain. *J Cell Biol* **199**, 669-683.

[218] Isenberg, B.C., Dimilla, P.A., Walker, M., Kim, S. and Wong, J.Y. (2009) Vascular smooth muscle cell durotaxis depends on substrate stiffness gradient strength. *Biophys J* **97**, 1313-1322.
[219] Tse, J.R. and Engler, A.J. (2011) Stiffness gradients mimicking in vivo tissue variation regulate mesenchymal stem cell fate. *PLoS One* **6**, e15978.
[220] Banks, J.M., Mozdzen, L.C., Harley, B.A.C. and Bailey, R.C. (2014) The combined effects of matrix stiffness and growth factor immobilization on the bioactivity and differentiation capabilities of adipose-derived stem cells. *Biomaterials* **35**, 8951-8959.
[221] Ichida, M., Yui, Y., Yoshioka, K., Tanaka, T., Wakamatsu, T., Yoshikawa, H. and Itoh, K. (2011) Changes in cell migration of mesenchymal cells during osteogenic differentiation. *FEBS Lett* **585**, 4018-4024.
[222] Kevy, S.V. and Jacobson, M.S. (2004) Comparison of methods for point of care preparation of autologous platelet gel. *Journal of Extracorporeal Technology* **36**, 28-35.
[223] Sawada, K., Caballé-Serrano, J., Schuldt Filho, G., Bosshardt, D.D., Schaller, B., Buser, D. and Gruber, R. (2015) Thermal processing of bone: in vitro response of mesenchymal cells to bone-conditioned medium. *Int J Oral Maxillofac Surg* **44**, 1060-1066.
[224] Fujioka-Kobayashi, M., Caballé-Serrano, J., Bosshardt, D.D., Gruber, R., Buser, D. and Miron, R.J. (2016) Bone conditioned media (BCM) improves osteoblast adhesion and differentiation on collagen barrier membranes. *BMC Oral Health* **17**, 7.
[225] Asparuhova, M.B., Caballe-Serrano, J., Buser, D. and Chappuis, V. (2018) Bone-conditioned medium contributes to initiation and progression of osteogenesis by exhibiting synergistic TGF-beta1/BMP-2 activity. *Int J Oral Sci* **10**, 20.
[226] Tenenbaum, H. and Heersche, J. (1982) Differentiation of osteoblasts and formation of mineralized bone In Vitro Calcif. *Calcified tissue international* **34**, 76-79.
[227] Roberts, W.E., Mozsary, P.G. and Klingler, E. (1982) Nuclear size as a cell-kinetic marker for osteoblast differentiation. **165**, 373-384.
[228] Zallone, A.Z. (1977) Relationships between shape and size of the osteoblasts and the accretion rate of trabecular bone surfaces. *Anatomy and embryology* **152**, 65-72.
[229] Stanka, P. (1975) Occurrence of cell junctions and microfilaments in osteoblasts. *Cell Tissue Res.* **159**, 413-22.
[230] Jeansonne, B.G., Feagin, F.F., McMinn, R., Shoemaker, R. and Rehm, W. (1979) Cell-to-Cell Communication of Osteoblasts. *Journal of dental research* **58**, 1415-1423.

[231] Von Arx, T. and Buser, D. (2006) Horizontal ridge augmentation using autogenous block grafts and the guided bone regeneration technique with collagen membranes: a clinical study with 42 patients. *Clin Oral Implants Res* **17**, 359-366.
[232] Urban, I.A., Monje, A., Lozada, J.L. and Wang, H.L. (2017) Long-term Evaluation of Peri-implant Bone Level after Reconstruction of Severely Atrophic Edentulous Maxilla via Vertical and Horizontal Guided Bone Regeneration in Combination with Sinus Augmentation: A Case Series with 1 to 15 Years of Loading. *Clin Implant Dent Relat Res* **19**, 46-55.
[233] Buser, D., Dahlin, C. and Schenk, R.K. (1994) Guided bone regeneration. *Chicago: Quintessence.*